10-3-2011 12:00 AM

Time-Domain Macromodeling of High Speed Distributed Networks

Amir Beygi
The University of Western Ontario

Supervisor
Dr. Anestis Dounavis
The University of Western Ontario

Graduate Program in Electrical and Computer Engineering
A thesis submitted in partial fulfillment of the requirements for the degree in Doctor of Philosophy

Time-Domain Macromodeling of High Speed Distributed Networks

(Thesis format: Monograph)

by

Amir Beygi

Graduate Program in Engineering Science
Department of Electrical and Computer Engineering

A THESIS SUBMITTED IN PARTIAL FULFILLMENT OF THE REQUIREMENTS FOR THE DEGREE OF DOCTOR OF PHILOSOPHY

The School of Graduate and Postdoctoral Studies
The University of Western Ontario
London, Ontario, Canada

THE UNIVERSITY OF WESTERN ONTARIO
School of Graduate and Postdoctoral Studies

CERTIFICATE OF EXAMINATION

Supervisor

Dr. Anestis Dounavis

Supervisory Committee

Examiners

Dr. Pavan Gunupudi

Dr. Anand V. Singh

Dr. Robert Sobot

Dr. Xianbin Wang

The thesis by

Amir Beygi

entitled:

Time-Domain Macromodeling of High Speed Distributed Networks

is accepted in partial fulfillment of the
requirements for the degree of
Doctor of Philosophy

Date

Chair of the Thesis Examination Board

Abstract

With the rapid growth in density, operating speeds and complexity of modern very-large-scale integration (VLSI) circuits, there is a growing demand on efficient and accurate modeling and simulation of high speed interconnects and packages in order to ensure the signal integrity, reliability and performance of electronic systems. Such models can be derived from the knowledge of the physical characteristics of the structure or based on the measured port-to-port response.

In the first part of this thesis, a passive macromodeling technique based on Method of Characteristics (referred as Passive Method of Characteristics or PMoC) is described which is applicable for modeling of electrically long high-speed interconnect networks. This algorithm is based on extracting the propagation delay of the interconnect followed by a low order rational approximation to capture the attenuation effects. The key advantage of the algorithm is that the curve fitting to realize the macromodel depends only on per-unit-length (p.u.l.) parameters and not on the length of the transmission line. In this work, the PMoC is developed to model multiconductor transmission lines.

Next, an efficient approach for time domain sensitivity analysis of lossy high speed interconnects in the presence of nonlinear terminations is presented based on PMoC. An important feature of the proposed method is that the sensitivities are obtained from the solution of the original network, leading to significant computational advantages. The sensitivity analysis is also used to optimize the physical parameters of the network to satisfy the required design constraints.

A time-domain macromodel for lossy multiconductor transmission lines exposed to electromagnetic interference is also described in this thesis based on PMoC. The algorithm provides an efficient mechanism to ensure the passivity of the macromodel for different line lengths. Numerical examples illustrate that when compared to other passive incident field coupling algorithms, the proposed method is efficient in modeling electrically long interconnects since delay extraction without segmentation is used to capture the frequency response.

In addition, this thesis discusses macromodeling techniques for complex packaging structures based on the frequency-domain behavior of the system obtained from measurements or electromagnetic simulators. Such techniques approximate the transfer function of the interconnect network as a rational function which can be embedded with modern circuit simulators with integrated circuit emphasis (SPICE). One of the most popular tools for rational approximations of measured or simulated data is based on vector fitting (VF) algorithms. Nonetheless, the vector fitting algorithms usually suffer convergence issues and lack of accuracy when dealing with noisy measured data. As a part of this thesis, a methodology is presented to improve the convergence and accuracy issues of vector fitting algorithm based on instrumental variable technique. This methodology is based on obtaining the "instruments" in an iterative manner and do not increase the complexity of vector fitting to capture the frequency response and minimize the biasing.

Keywords: Multiconductor Transmission Lines, High Speed Circuits, Interconnects, Macromodeling, Method of Characteristics, Passivity, Vector fitting, Noise, Instrumental Variable, Electromagnetic Interference, Incident Fields.

Acknowledgments

This thesis would not have been accomplished without the invaluable guidance and the help of Dr. Anestis Dounavis of the Department of Electrical and Computer Engineering, University of Western Ontario. I would like to extent my appreciation and gratitude toward him for introducing me to the area of high-speed interconnect modeling. His encouragement, helpful ideas, keen supervision and friendly approach made the work of this thesis less difficult.

I am thankful towards the faculty and staff members the Department of Electrical and Computer Engineering, University of Western Ontario for their support and help. I would like to specially mention my colleagues and friends Majid Ahmadloo, Somil Bansil, Morteza Haydari, Ehsan Rasekh, Sourajeet Roy and Shamsol Arefin Seddiqi for their inspiration and for sharing their experience and knowledge with me.

I cannot express my appreciation too emphatically to my parents, Fereshteh and Hamidreza. Without their encouragement and endless support, I would not have had the opportunity to complete this study thousands of miles away from home.

Table of Contents

List of Tables

List of Figures

List of Appendices

Abbreviations

CMOS	Complementary Metal Oxide Semiconductor.
DEPACT	Delay extraction-based passive compact transmission-line macromodel.
IFFT	Inverse fast Fourier transform.
IV	Instrumental variable.
LU	Lower-upper matrix decomposition.
MNA	Modified nodal analysis.
MoC	Method of characteristics.
MRA	Matrix rational approximation.
MTL	Multi-conductor transmission line.
ODE	Ordinary differential equation.
PCB	Printed circuit board.
PDE	Partial differential equation.
PMoC	Passive method of characteristics.
PRIMA	Passive reduced-order interconnect macromodeling algorithm.
p.u.l	Per-unit-length.
RVF	Relaxed vector fitting.
SNR	Signal-to-noise ratio.
TEM	Transverse electromagnetic.
VF	Vector fitting.
VF-AS	Vector fitting with adding and skimming.
VWVF	Variance weighted vector fitting.

Chapter 1

1 Introduction

1.1 Background and Motivation

The rapid growth in density, operating speeds and complexity of modern integrated circuits has made electrical interconnects a critical part for determining signal integrity and speed performance of electronic systems. Improperly designed interconnects can increase signal delay, distortion, attenuation, ringing and crosstalk which can severely degrade system performance [1]-[3]. In addition, interconnect networks can be susceptible to electromagnetic fields. Electromagnetic interference can induce undesired voltages and currents in the circuit which may degrade the signal integrity or even damage the circuit [1],[4]-[7].

These effects are observed at the chip, multi-chip, packaging and board levels. Furthermore, skin effect losses in the conductors and shunt losses in the dielectrics also become prominent at higher frequencies and distributed multiconductor transmission line (MTL) models with frequency-dependent parameters are required. However, the analysis of distributed transmission lines in the presence of nonlinear elements suffers from the mixed

frequency/time problem as well as CPU inefficiency. The mixed frequency/time problem arises from the fact that transmission lines are described by partial differential equations (PDE) which are traditionally solved in the frequency domain, whereas the transient responses of nonlinear elements are described in the time domain by nonlinear differential equations. In order to link transmission lines into nonlinear circuit simulators, macromodeling algorithms are required to convert these equations into ordinary differential equations (ODE) [1]-[3].

Macromodeling can be roughly categorized into two classes of algorithms. The first class of algorithms are performed with the knowledge of the physical characteristics of the interconnect structure. The majority of these algorithms are based on quasi-TEM mode of propagation. For the case, when the physical properties of the interconnect structure is not known, or an analytic solution is not easy to derive, macromodeling can be performed based on rational approximation of the port-port measured or full-wave electromagnetic simulated data.

In addition, macromodeling algorithms of a network with known physical characteristics can be either based on sectioning/rational approximation or delay extraction techniques. Algorithms that use sectioning/rational approximation are lumped RLGC macromodel [1], PRIMA [8], matrix rational approximation (MRA) [9]-[10], compact difference [11] and integral congruent transformation [12]-[13]. The advantage of these algorithms is that they can be made to be passive by construction. However, these algorithms approximate the propagation delay implicitly without using delay extraction. Consequently, to model long

lines with significant delay these algorithms require high order approximations to accurately capture the delay of the signal leading to inefficient transient simulation [14].

In contrast, delay extraction methods like MoC [15], traditionally are not passive by construction. However they are very efficient for modeling of electrically long lines. With a sectioning/rational approximation approach, many poles have to be used to capture the transfer function of a long line and subsequently it increases the simulation time. With a Method of Characteristic (MoC) macromodel, the delay of the transfer function is extracted, and as a result, its "left-over" is approximated with a low order rational function which significantly reduces the computational complexity.

Although, MoC provides fast solutions for long low loss transmission lines, there are major challenges in the implementation of the algorithm. One disadvantage is the potential loss of passivity that can occur in the constructed macromodel. Since transmission lines are passive elements, passivity of the macromodel is important since nonpassive but stable macromodels when connected to arbitrary nonlinear and even passive elements can lead to an unstable overall system [8]. This leads to erroneous artificial oscillations in the time domain simulation due to the instability of the entire network.

In [16], a passive delay extraction macromodel (DEPACT algorithm) based on the modified Lie product has been proposed to efficiently model long low-loss lines. Nonetheless, the efficiency of the DEPACT macromodel depends on the losses of the transmission line. As the losses of the line increase, a higher order Lie product approximation is required to capture the frequency characteristics of the line. Recently, methodologies have been developed to

verify and identify the location of passivity violations of MoC-based macromodels and to restore the passivity of these models using perturbation techniques [17]-[19].

Another difficulty with MoC-based algorithms is the numerical curve fitting required to realize the macromodel. For the case of MTLs eigen-mode analysis is required to decouple the transmission line equations. The numerical curve fitting required to capture the eigen-characteristics can present many challenges in terms of computational expense and accuracy. These challenges become greater as the number of coupled lines increase, the losses of the line become more significant and the length of the line becomes longer.

An additional important aspect of a macromodel is the ability to extract gradient information of a network referred as sensitivity analysis. An efficient and accurate sensitivity analysis with respect to physical/electrical interconnect parameters is very helpful for identifying the critical components in the design particularly when combined with optimization tools to increase the reliability and performance of the system. It is also very important for the macromodel to calculate the effect of an incident electromagnetic field coupling to transmission lines in the framework of nonlinear circuit simulators.

Another useful class of algorithms is based on tabulated data [20]. Tabulated data can be obtained either from simulations or from measurements. The behavior of high speed interconnect networks such as chip interconnects, connections on multichip modules, micro-strip printed circuit board traces, and cable connections can be represented by frequency-dependent admittance [21]-[29], impedance, or scattering parameters [30], Green's functions [31], transfer functions [32], etc.. These parameters can be obtained using a port-port measurement, or using a full-wave electromagnetic analysis or simulation.

1.2 Objectives and Contributions

The objective of this thesis is to develop efficient macromodeling algorithms for distributed high-speed interconnect networks. For the case where the physical characteristics of the interconnect structure is known and the electrical model can be derived from Telegrapher's equations, the following contribution are made.

The passive method of characteristics (PMoC) macromodel is developed for distributed lossy multiconductor transmission lines. A theorem is provided that specifies sufficient conditions to guarantee the passivity of the MoC by construction. A key feature of the proposed algorithm is that the curve fitting to realize the MoC depends only on the per-unit-length parameters and not on the discretization of the macromodel. Thus, with the knowledge of the rational functions derived by the per unit length parameters, the MoC is formulated in a closed form manner for any line length while ensuring passivity. PMoC macromodel extracts the propagation delay of transmission line, and hence, it requires lower order of rational approximation compared to segmentation algorithms. Numerical examples are provided to illustrate the accuracy and efficiency of the PMoC.

The PMoC macromodel is extended to efficiently calculate sensitivities of high speed interconnects in the presence of nonlinear terminations. An important feature of the proposed method is that the sensitivities are analytically obtained from the solution of the original network, leading to significant computational advantages. The sensitivity analysis is also used in an optimization process of the physical parameters of a network to obtain the constrained design requirements.

Time-domain analysis of lossy multiconductor transmission lines in the presence of electromagnetic incident fields is obtained. The equivalent sources due to the incident fields coupling are formulated to take advantages of the PMoC macromodel, which provides an efficient mechanism to ensure the passivity of the macromodel for different line lengths. Numerical examples illustrate that when compared to other passive incident field coupling algorithms, the proposed method is efficient in modeling electrically long interconnects since delay extraction without segmentation is used to capture the frequency response.

For the case where the macromodeling is derived from measurement, a methodology is presented to improve the convergence and accuracy issues of vector fitting algorithm for the noisy frequency-domain measured data. The proposed technique which is based on an instrumental variable approach, does not increase the computational complexity of vector fitting algorithm.

1.3 Organization of the Thesis

The thesis is organized as follows. Chapter 2 reviews the challenges of macromodeling high speed interconnects. The chapter addresses the issues of macromodeling techniques based on quasi-TEM mode of propagation when the physical structure of the interconnect network is known as well as the ones based on port-port tabulated data and when the physical structure is unknown. Chapter 3 develops a passive method of characteristics (PMoC) macromodel for the case of lossy multiconductor transmission lines. Numerical examples are also given in this chapter to demonstrate the efficiency of the macromodel. Chapter 4 expands the PMoC

macromodel to support sensitivity analysis followed by a few numerical examples. Chapter 5 develops the PMoC macromodel in order to evaluate the effect of external electromagnetic fields. Chapter 6 discusses a new vector fitting algorithm based on an instrumental variable technique to characterize distributed electromagnetic systems described by noisy data. Finally, Chapter 7 summarizes the proposed work and also presents some suggestions for future related work.

Chapter 2

2 Background and Literature Review

2.1 Introduction

Interconnects are the physical links between electrical devices in chips, electrical packages, printed circuit boards (PCB), backplanes, etc. Interconnects at low frequencies behave as short circuits, however, as the frequency increases, they behave as transmission lines and become responsible for majority of signal degradation such as signal delay, distortion, attenuation, ringing and crosstalk. The subject of this chapter is to review some of the interconnect macromodels and numerical techniques that are used for interconnect analysis. Section 2.2 explains macromodeling of high speed interconnect networks derived from quasi-TEM mode of propagation. Section 2.3 provides several transmission line macromodels for nonlinear circuit simulators. Section 2.4 describes least square curve fitting algorithms to derive rational macromodels of distributed systems characterized from tabulated data. From this discussion, section 2.5 talks about the methodologies for improving the accuracy and convergence issues of least-squares fitting algorithm when dealing with noisy data.

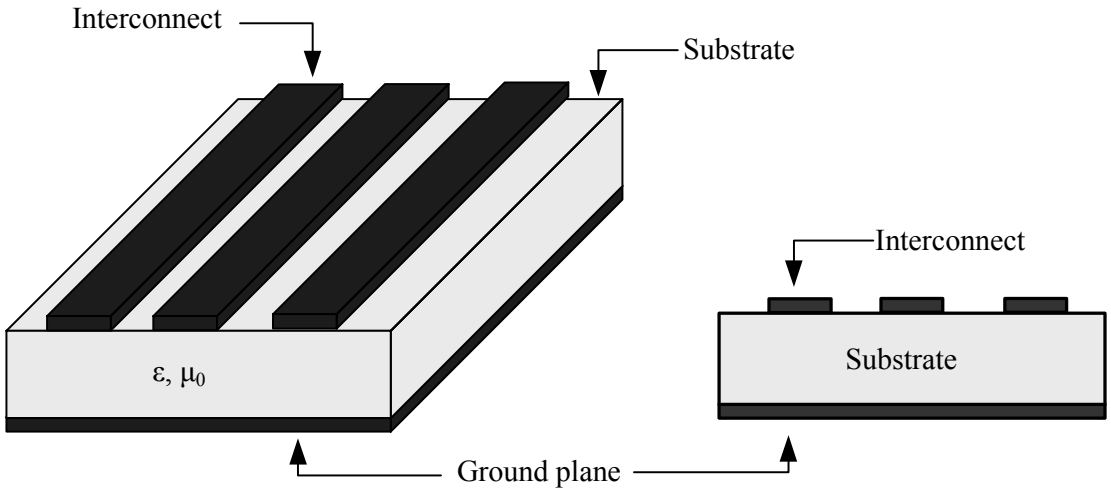

Figure 2-1: Three-dimensional and cross sectional views of an interconnect structure.

2.2 High Speed Interconnect Models

Figure 2-1 shows the three-dimensional and cross sectional views of an interconnect network. The complexity of the interconnect macromodel depends on the physical dimensions and operating frequency of the circuit. These two factors determine whether the modeling of interconnects is based on quasi-transverse electromagnetic (quasi-TEM) or full wave assumptions. Quasi-TEM assumptions remain the dominant trend for analyzing IC interconnects, since the approximation is valid for most practical structures and offers relative ease and low computation cost compared to full wave approaches [2]-[3].

In TEM mode of propagation, the electric and magnetic fields surrounding the space around the line conductors are transverse or perpendicular to the line axis [1]. TEM mode exists for transmission lines with homogenous medium and perfect conductors. In inhomogeneous mediums, electromagnetic waves are generated with different velocities. Moreover, interconnect networks with imperfect conductors produce electric fields along the surface

conductor. Such interconnect structures violate the TEM wave characteristics, since TEM waves propagate with only one velocity and have no electric field along the surface conductor. However, for many structures if the cross section is electrically small and the conductor have low losses, the results are almost similar to TEM structures and thus they can be approximated as TEM mode, referred as quasi-TEM assumptions.

One of the important characteristics of TEM mode of propagation (which is approximated for non-perfect conductors in quasi-TEM modes) is the ability of expressing the voltage and current values of each point of the conductor line. The voltages and currents for the quasi-TEM distributed models are described by partial differential equations (PDEs) known as the Telegrapher's equations

$$\frac{\partial}{\partial z}\boldsymbol{v}(t,z) = -\boldsymbol{R}\boldsymbol{i}(\mathrm{t},z) - \boldsymbol{L}\frac{\partial}{\partial t}\mathrm{i}(t,z)$$

$$\frac{\partial}{\partial z}\boldsymbol{i}(t,z) = -\boldsymbol{G}\boldsymbol{v}(\mathrm{t},z) - \boldsymbol{C}\frac{\partial}{\partial t}\boldsymbol{v}(t,z) \qquad (2.1)$$

where t and z are the time and position variable; $\boldsymbol{v}(t,z)$ and $\boldsymbol{i}(t,z)$ represent the voltage and current vectors of the transmission line, respectively; $\boldsymbol{R}$, $\boldsymbol{L}$, $\boldsymbol{G}$ and $\boldsymbol{C}$ are the per unit length (p.u.l.) resistance, inductance, conductance and capacitance matrices, respectively. The p.u.l parameters are used to determine the transmission line voltages and currents and can be obtained from the cross-sectional dimensions and physical characteristics of the transmission line [1].

One of the simplest forms of the distributed models is the delay-line or lossless line where $\boldsymbol{R}=\boldsymbol{G}=\boldsymbol{0}$. More complicated models include per-unit-length losses of the conductor and the

dielectric substrate, as well as coupling between adjacent lines. At higher frequencies, edge, proximity, and skin effects become prominent and distributed models with frequency-dependent parameters are required.

The difficulty with quasi-TEM distributed models is that they cannot be directly linked to circuit simulators such as SPICE. Circuit simulators solve nonlinear ordinary differential equations (ODEs) and while Telegrapher's equations are expressed as PDEs. To overcome this difficulty, numerical techniques are used to convert distributed models into ODEs.

One of the basic solutions for linking distributed transmission lines to circuit simulators is using the conventional lumped segmentation model [1]. The number of segments required depends on the electrical length of the transmission line. For transmission lines that are electrically long (i.e. the length of the line is much greater than the wavelength) many segments are required. In addition to the lumped segmentation model, other more sophisticated algorithms exist such as exponential matrix rational approximation (MRA) [9]-[10], method of characteristics [14]-[15],[33]-[37], delay extraction based macromodeling algorithm (DEPACT) [16], which are described briefly in the next sections.

2.3 Simulating Interconnects in SPICE

For the case when the physical characteristics of the interconnect structure is known and quasi-TEM is assumed, the electrical performance of interconnects can be expressed using the Telegrapher's partial differential equations (PDE). Commercial circuit simulators like SPICE being unable to solve the PDE's in the time domain, macromodeling algorithms are

required to convert the PDE to ordinary differential equations (ODE) which can be solved by numerical integration. Moreover, macromodeling algorithms can also be extended to perform sensitivity analysis and model incident field coupling to lossy transmission lines. This sections describes some of the existing macromodeling techniques based on quasi-TEM mode of propagation, followed by a review of sensitivity and incident field analysis.

2.3.1 Lumped Segmentation

Lumped segmentation technique uses lumped equivalent circuits of the transmission lines to approximate Telegrapher's equations. Applying Euler's method [1] to (2.1) yields

$$\mathbf{v}_{z+1}(t) - \mathbf{v}_z(t) = -\Delta z \mathbf{R}\mathbf{i}_z(t) - \Delta z \mathbf{L}\frac{\partial}{\partial t}\mathbf{i}_z(t)$$

$$\mathbf{i}_{z+1}(t) - \mathbf{i}_z(t) = -\Delta z \mathbf{G}\mathbf{v}_z(t) - \Delta x \mathbf{C}\frac{\partial}{\partial t}\mathbf{v}_z(t) \qquad (2.2)$$

where z=[1,2,...,η], $\Delta z = l/\eta$, η is the number of sections and l is the length of interconnect. Equation (2.2) can be implemented by lumped equivalent circuit composed of resistors, inductors and capacitors. Figure 2-2 shows the general lumped component for a two conductor transmission line.

The commercial circuit simulators like HSPICE [38] use the following equation in order to estimate the number of sections for time domain analysis of digital systems

$$N = 20\frac{l \cdot \sqrt{LC}}{t_r} \qquad (2.3)$$

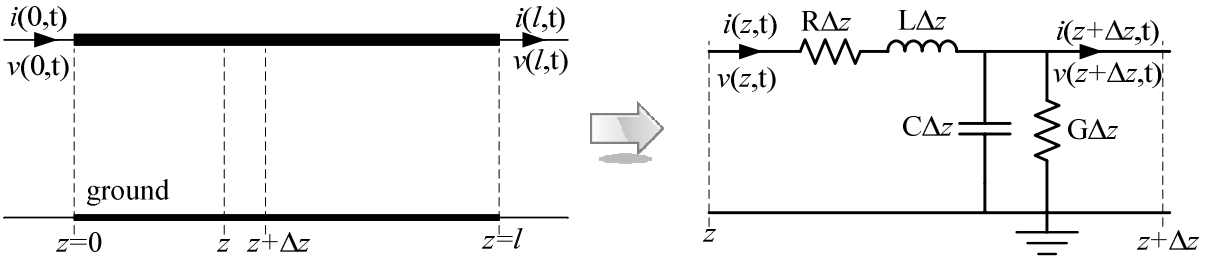

Figure 2-2: Lumped transmission line model for single transmission line.

where t_r is the rise/fall time. The lumped segmentation model is passive and provides a direct method to discretize interconnects. However the approximation is only valid if Δz is chosen to be a small fraction of the wave length. If the rise/fall time is fast or if the interconnect is electrically long, many lumped elements are required for an accurate model. This leads to large circuit matrices, increasing the simulation time.

2.3.2 Matrix Rational Approximation

Matrix rational approximation (MRA) macromodel directly converts the Telegrapher's equations into time domain macromodels based on rational approximations of exponential matrices. An important feature of this macromodel is that it guarantees the passivity of the resulting interconnect macromodel by construction. This section briefly describes the matrix rational approximation; a more detailed explanation can be found in [9]-[10].

The Telegrapher's equation can be written in the Laplace-domain as an exponential matrix function as

$$\begin{bmatrix} \boldsymbol{V}(l,s) \\ \boldsymbol{I}(l,s) \end{bmatrix} = e^{\boldsymbol{Z}} \begin{bmatrix} \boldsymbol{V}(0,s) \\ \boldsymbol{I}(0,s) \end{bmatrix}$$

$$\boldsymbol{Z} = \begin{bmatrix} \boldsymbol{0} & -\left(\boldsymbol{R}(s) + \mathrm{s}\boldsymbol{L}(s)\right) \\ -\left(\boldsymbol{G}(s) + \mathrm{s}\boldsymbol{C}(s)\right) & \boldsymbol{0} \end{bmatrix} \cdot l \tag{2.4}$$

where $[\boldsymbol{V}(0,s)\,, \boldsymbol{I}(0,s)\,]$, $[\boldsymbol{V}(l,s)\,, \boldsymbol{I}(l,s)\,]$ are the terminal voltage and current vectors of the transmission line and l is the length of the transmission line. The exponential matrix $e^{\boldsymbol{Z}}$ in (2.4) can be expressed with a matrix rational approximation as

$$\boldsymbol{P}_M(\boldsymbol{Z}) e^{\boldsymbol{Z}} = \boldsymbol{Q}_N(\boldsymbol{Z}) \tag{2.5}$$

where $\boldsymbol{P}_M(\boldsymbol{Z})$, and $\boldsymbol{Q}_N(\boldsymbol{Z})$ are polynomial matrices

$$\boldsymbol{P}_M(\boldsymbol{Z}) = \sum_{i=0}^{M} p_i \boldsymbol{Z}^i = \sum_{i=0}^{M} \frac{(2M-i)!M!}{(2M)!i!(M-i)!} \boldsymbol{Z}^i$$

$$\boldsymbol{Q}_N(\boldsymbol{Z}) = \sum_{i=0}^{N} q_i \boldsymbol{Z}^i = \sum_{i=0}^{N} \frac{(2N-i)!N!}{(2N)!i!(N-i)!} \boldsymbol{Z}^i \tag{2.6}$$

After some mathematical manipulations, (2.5) can be expressed as a macromodel represented by a set of ordinary differential equations, in a closed form. Since the MRA macromodel is described in terms of predetermined coefficients p_i and q_i, and the p.u.l parameter, the macromodel can be constructed very quickly. However, MRA is not very computationally efficient for electrically long lines since the delay of the transmission line is not extracted and hence, a higher order of approximations is required to express $e^{\boldsymbol{Z}}$ as a matrix rational

approximation. In sections 2.3.3 and 2.3.4 two common delay extraction macromodels are reviewed.

2.3.3 Method of Characteristics

Among the most commonly used algorithms are those based on the generalized method of characteristics (MoC) [14]-[15],[33]-[37]. The MoC is based on extracting the line-propagation delay and produce exact models when applied to lossless transmission lines [15]. Over the years, these algorithms have been extended to model lossy MTLs [14],[33]-[37]. The efficiency of MoC is derived by extracting the propagation delay which allows the attenuation function to be approximated with a low-order rational function. This significantly reduces the computational complexity of the transfer function; especially for long lines with low losses.

The original method of characteristics [15] is able to represent interconnects as ODEs containing time delays. Although the original method of characteristics was developed in the time-domain using what is referred as characteristic curves (hence the name), a simpler alternative derivation in the frequency-domain is presented. The frequency domain solution of (2.1) for a two-conductor transmission line [39] is

$$\begin{bmatrix} I_1 \\ I_2 \end{bmatrix} = \frac{1}{Z_0(1-e^{-2\gamma l})} \begin{bmatrix} 1+e^{-2\gamma l} & -2e^{-\gamma l} \\ -2e^{-\gamma l} & 1+e^{-2\gamma l} \end{bmatrix} \cdot \begin{bmatrix} V_1 \\ V_2 \end{bmatrix}$$

$$\gamma = \sqrt{(G+sC)(R+sL)}$$

$$Z_0 = \sqrt{(R+sL)/(G+sC)} \tag{2.7}$$

where γ is the propagation constant and Z_0 is the characteristic impedance. After some mathematical manipulations, the terms in (2.7) can be expressed as

$$V_1 = Z_0 I_1 + W_1$$
$$V_2 = Z_0 I_2 + W_2 \tag{2.8}$$

where W_1 and W_2 are defined as recursive relations

$$W_1 = e^{-\gamma l}[2V_2 - W_2]$$
$$W_2 = e^{-\gamma l}[2V_1 - W_1]. \tag{2.9}$$

For lossless transmission lines, γ and Z_0 can be reduced to

$$\gamma = s\sqrt{LC}; \quad Z_0 = \sqrt{L/C} \tag{2.10}$$

which makes γ a purely imaginary number and Z_0 a real constant. The time domain solution of MoC can be obtained by taking the inverse Laplace transform of (2.8) and (2.9) as

$$v_1(t) = Z_0 i_1(t) + w_1(t)$$
$$v_2(t) = Z_0 i_2(t) + w_2(t)$$
$$w_1(t+\tau) = 2v_2(t) - w_2(t)$$
$$w_2(t+\tau) = 2v_1(t) - w_1(t) \tag{2.11}$$

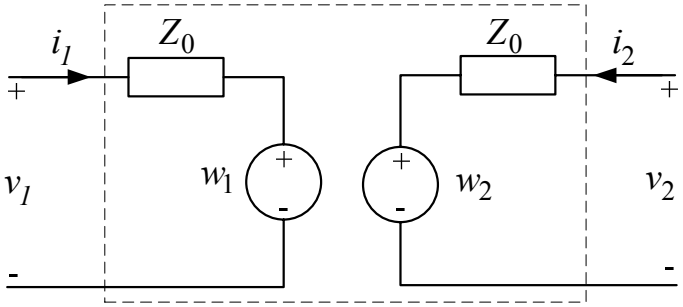

Figure 2-3: Circuit realization of MoC for a two-conductor transmission line.

where $\tau = \gamma l$ is represented as a delay term. An equivalent circuit realization of time domain macromodel of a lossless transmission line is demonstrated in Figure 2-3.

For the case of lossy transmission lines, γ is not purely imaginary and Z_0 is not a real constant and therefore, the direct time domain representation is not possible. In this case, numerical techniques have been proposed to incorporate lossy transmission line models [14],[33]-[37] using rational approximation of Z_0 and $e^{-\gamma l}$, however, these methods may have numerical passivity issues due to numerical errors of the rational approximation techniques.

Methodologies are proposed to restore the passivity of MoC [19] which are based on perturbation of rational approximation in order to make the admittance matrix positive real. In Chapter 3, a macromodel based on MoC is described where the curve fitting to realize the MoC depends only on the per-unit-length parameters and not on the discretization of the macromodel. Thus, with the knowledge of the rational functions derived by the per unit length parameters, the MoC is formulated in a closed form manner for any line length while ensuring passivity.

2.3.4 Delay Extraction-Based Passive Compact Transmission-Line Macromodeling Algorithm (DEPACT)

Consider the solution of Telegraphers equations for a general multiconductor as expressed in (2.4), where $\boldsymbol{Z}$ matrix can be written as

$$\boldsymbol{Z} = \boldsymbol{A} + \mathrm{s}\boldsymbol{B} \tag{2.12}$$

where

$$\boldsymbol{A} = \begin{bmatrix} 0 & -\boldsymbol{R}(\mathrm{s}) - \mathrm{s}(\boldsymbol{L}(\mathrm{s}) - \boldsymbol{L}_\infty) \\ -\boldsymbol{G}(\mathrm{s}) - \mathrm{s}(\boldsymbol{C}(\mathrm{s}) - \boldsymbol{C}_\infty) & 0 \end{bmatrix} \cdot l\,; \quad \boldsymbol{B} = \begin{bmatrix} 0 & -\boldsymbol{L}_\infty \\ -\boldsymbol{C}_\infty & 0 \end{bmatrix} \cdot l \tag{2.13}$$

and $\boldsymbol{L}_\infty = \boldsymbol{L}(\infty)$ and $\boldsymbol{C}_\infty = \boldsymbol{C}(\infty)$ are the extracted p.u.l inductance and capacitance of the line and l represents the line length.

The basic idea of the delay extraction-based passive compact transmission-line (DEPACT) macromodeling algorithm is to separate the extracted delay terms ($e^{s\mathbf{B}}$) from $e^{(\mathbf{A}+s\mathbf{B})}$ thereby enabling $e^{\mathbf{A}}$ to be modeled using a low order rational function. However, this is not a trivial task since the matrices $\boldsymbol{A}$ and s$\boldsymbol{B}$ do not commute, (i.e. $e^{(\mathbf{A}+s\mathbf{B})} \neq e^{\mathbf{A}} e^{s\mathbf{B}}$).

To approximate $e^{(\mathbf{A}+s\mathbf{B})}$ in terms of a product of exponentials, a modified Lie product [16] is used as

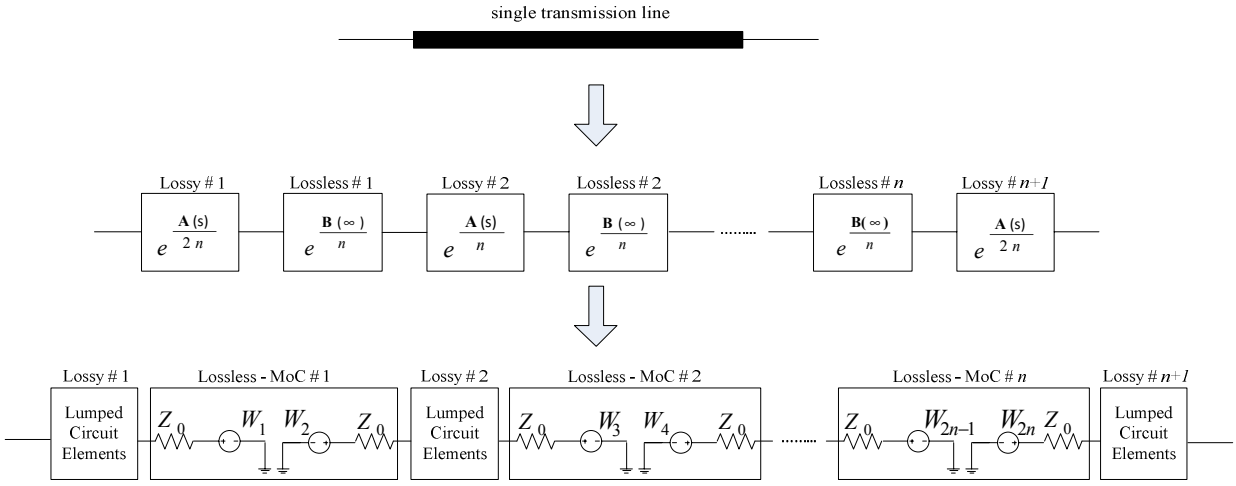

Figure 2-4: Circuit realization of DEPACT macromodel.

$$e^{\mathbf{A}+s\mathbf{B}} \approx \prod_{i=1}^{n} \boldsymbol{\Psi}_i + \boldsymbol{\varepsilon}_n \tag{2.14a}$$

$$\boldsymbol{\Psi}_i = e^{\frac{\mathbf{A}}{2n}} e^{\frac{s\mathbf{B}}{n}} e^{\frac{\mathbf{A}}{2n}} \tag{2.14b}$$

where n is the number of sections. The associated error of the approximation scale to the second power of number of sections n, as $\|\boldsymbol{\varepsilon}_n\| \cong O(1/n^2)$ [16] (i.e. (2.14) quickly converges to the exponential matrix of (2.13) with increase of number of sections, n). Equation (2.14) shows that the exponential function of (2.13) can be divided into subsections of $e^{\mathbf{A}/2n}$ and $e^{s\mathbf{B}/n}$. The matrix $e^{\mathbf{A}/2n}$ represents a lossy line segment and $e^{s\mathbf{B}/n}$ represents a lossless line segment. The products can be viewed as a cascade of transmission line subnetworks. For a two-conductor transmission line example, each $\boldsymbol{\Psi}_i$ in (2.14b) can be realized as shown in Figure 2-4. Here, the lossy terms can be macromodeled using the MRA algorithm (section 2.3.2) and the lossless sections can be modeled using the MoC approach (section 2.3.3). The

resulting macromodels are of significant lower orders since for electrically long lines a significant portion of the delay is already extracted using MoC [16].

2.3.5 Sensitivity Analysis

The design process of large distributed networks usually involves the balancing of mostly conflicting requirements to obtain the best possible performance. For example, decreasing the line width of the conductor decreases the parasitic capacitance of the line if the substrate thickness is not varied. However, this leads to greater signal attenuation as a result of the conductor losses. Hence, efficient and accurate sensitivity information with respect to interconnect parameters is important, since it provides circuit designers with valuable information in terms of identifying critical components in the design and provides gradient information needed for optimization.

A simple way to calculate the sensitivities of a transmission line network with respect to interconnect parameter is the perturbation technique. However, there are many issues regarding the speed and accuracy of these methods [40]. Perturbation based techniques can lead to inaccurate results depending on the magnitude of the perturbation [41]. In addition, the perturbed network must be solved separately for every parameter of interest.

Macromodeling algorithms have also been extended to perform sensitivity analysis [41]-[45]. To calculate the sensitivity of the network with respect to a transmission line electrical or physical parameter, the calculation of the derivatives of the modified nodal admittance

(MNA) matrices are required which depends on the transmission line model being used. In [41], a sensitivity analysis based on MoC is proposed which directly differentiates Telegrapher's equations to derive the sensitivity network. In [40], a sensitivity analysis has been proposed based on numerical inversion of Laplace transform. The method is then improved in combination with a piecewise decomposition technique [42]. Later, the algorithm has been applied in an optimization process of high speed circuits [43]. In [44] and [45], the sensitivity information has been derived using MRA and DEPACT macromodels respectively.

2.3.6 Transmission Line Macromodels with Incident Fields

Susceptibility of high-speed circuits to external electromagnetic fields is another important issue in the modeling of high-speed circuits. Electromagnetic fields can induce currents in circuits that may influence the signal integrity of networks.

The analysis of transmission lines excited by an external electromagnetic wave has been an active area of research [4]-[7],[46]-[55]. Majority of the works are based on the formulation given by Taylor in [4] which is applicable for two-conductor transmission lines. The technique is also expanded for frequency domain solution of excited MTLs in [5] and later for the time domain solutions in [6]-[7]. In these formulations, the excited transmission line model is composed of two parts: i. an unexcited transmission line and ii. forcing functions at the terminals of the transmission lines modeling the effects of the incident field. These techniques are based on the quasi-TEM mode of propagation along the transmission line. In

[52], a similar technique is proposed for the simulation of the traces in a multi-layered inhomogeneous medium. The fields in the layered medium were calculated using the physical optics technique without relying on the full wave analysis.

In [53] and [54], the analysis of MTLs in the presence of an incident field has been evaluated using MRA and DEPACT macromodels respectively. Numerical rational approximation techniques are also required to model the effect forcing functions in nonlinear circuit simulators. More recently, a simplified version of DEPACT approach has been presented in [55] where the incident field coupling is modeled by embedding additional delay sources in each DEPACT cell.

2.4 Macromodeling Based on Measured Data

Another useful approach for macromodeling of transmission lines is based on rational approximation of frequency-domain sampled data in the forms of admittance, impedance, hybrid or scattering parameters. In this section two schemes of interpolation-based complex rational approximation [56] and vector fitting (VF) [20] are reviewed.

2.4.1 Interpolation-Based Complex Rational Approximation

A network function $Y(s)$ of a linear system can be approximated by a rational function that interpolates the given function at given points. The rational function can be in a pole-residue,

pole-zero form or as a ratio of polynomials. Suppose the network function, $Y(s_i)$ at given points s_i is approximated by a rational function of degree (m,n) as

$$Y(s) \approx \frac{P_m(s)}{Q_n(s)} = \frac{p_0 + \sum_{i=1}^{m} p_i s^i}{1 + \sum_{i=1}^{n} q_i s^i} \tag{2.15}$$

with q_0 normalized to unity. Equation (2.15) has $N = m + n + 1$ independent unknown. The coefficients are determined so that the approximating function evaluated at each frequency point, gives close approximation to the function $Y(s)$

$$\frac{P_m(s_i)}{Q_n(s_i)} - Y(s_i) = 0 \tag{2.16}$$

By canceling the denominators in (2.16) and choosing N_s frequency points over the frequency range of interest to, the linear homogenous system of N_s equations and N unknowns is determined as

$$P_m(s_i) - Y(s_i) Q_n(s_i) = 0 \tag{2.17}$$

which can be written in the form an overdetermined linear system of equation

$$\mathbf{AX} = \boldsymbol{B} \tag{2.18}$$

where

$$\mathbf{A}=\begin{bmatrix} 1 & s_1 & s_1^2 & \cdots & s_1^m & -s_1Y(s_1) & -s_1^2Y(s_1) & \cdots & -s_1^nY(s_1) \\ 1 & s_2 & s_2^2 & \cdots & s_2^m & -s_2Y(s_2) & -s_2^2Y(s_2) & \cdots & -s_2^nY(s_2^2) \\ & \vdots & & & & & & & \\ 1 & s_{Ns} & s_{Ns}^2 & \cdots & s_{Ns}^m & -s_{Ns}Y(s_{Ns}) & -s_{Ns}^2Y(s_{Ns}) & \cdots & -s_{Ns}^nY(s_{Ns}) \end{bmatrix} \tag{2.19}$$

$$\mathbf{X}=\begin{bmatrix} p_0 & p_1 & p_2 & \cdots & p_m & q_1 & q_2 & \cdots & q_n \end{bmatrix}^{\mathrm{T}} \tag{2.20}$$

$$\mathbf{B}=\begin{bmatrix} Y(s_1) & Y(s_2) & \cdots & Y(s_{Ns}) \end{bmatrix}^{\mathrm{T}} \tag{2.21}$$

As the order m, n increase, the system in (2.18) becomes highly ill-conditioned and nearly singular and even with proper frequency normalization, the computational procedures are limited by the machine precision.

The least squares solution of (2.18)-(2.21) results in complex coefficients p_k and q_k which is not a physically realizable rational approximation. The approximation can be made realistic by utilizing the special properties of network functions. For instance, constraints necessary to insure a physically realizable passive network require that the coefficients of the polynomial rational function be real, and all the poles must have negative or zero real parts.

In a addition, the response of a passive network can only decay in time from any transient initial state. As a result, only the real part, imaginary part, angle, or magnitude of the network function has to be approximated and the network function itself can be found from the resulting approximation.

Next, a procedure for determining a rational function to approximate $Y(s)$ is described using the real parts of the function. The real part of a network function (2.15) can be obtained by

$real\ (Y(s)) = \frac{1}{2}(Y(s) + Y(-s))$. Taking the common denominator of $real\ (Y(s))$, the rational approximation is expressed as

$$real\ (Y(s)) \approx \frac{c_0 + \sum_{i=1}^{m} c_i s^{2i}}{1 + \sum_{i=1}^{n} q_i s^{2i}} \tag{2.22}$$

Note the poles of $real\ (Y(s))$ belong to $Y(s)$ and $Y(-s)$, (i.e. the poles on the left plane belong to $Y(s)$ and the poles on the right side belong to $Y(-s)$). Thus, the denominator coefficients of in (2.22) can be obtained from (2.15). The following system of equations results from matching the real parts of the original function with (2.22) at the set of frequencies where the superscript *r* indicates the real part of a complex value as

$$\begin{bmatrix} 1 & \omega_1^2 & \omega_1^4 & \cdots & \omega_1^{2m} & -\omega_1^2 Y^r(s_1) & -\omega_1^4 Y^r(s_1) & \cdots & -\omega_1^{2n} Y^r(s_1) \\ 1 & \omega_2^2 & \omega_2^4 & \cdots & \omega_2^{2m} & -\omega_2^2 Y^r(s_2) & -\omega_2^4 Y^r(s_2) & \cdots & -\omega_2^{2n} Y^r(s_2^2) \\ & \vdots & & & & & & & \\ 1 & \omega_{Ns}^2 & \omega_{Ns}^4 & \cdots & \omega_{Ns}^{2m} & -\omega_{Ns}^2 Y^r(s_{Ns}) & -\omega_{Ns}^4 Y^r(s_{Ns}) & \cdots & -\omega_{Ns}^{2n} Y^r(s_{Ns}) \end{bmatrix} \begin{bmatrix} c_0 \\ c_1 \\ c_2 \\ \vdots \\ c_m \\ q_1 \\ q_1 \\ \vdots \\ q_n \end{bmatrix} = \begin{bmatrix} Y^r(s_1) \\ Y^r(s_2) \\ \vdots \\ Y^r(s_{Ns}) \end{bmatrix} \tag{2.23}$$

It is to be noted that the equation (2.23) is notoriously ill-conditioned. The ill-conditioning can be improved by mapping the frequency domain $[\omega_{\min}, \omega_{\max}]$ into normalized domain of [-1,1]. The order of approximating function must be greater than or equal to the actual order

sought. Once the poles of the systems are determined from (2.23), the unstable poles are removed and the remaining poles with negative real parts are used to formulate the stable partial fraction expansion of $Y(s)$ as

$$Y(s) = \sum_{i=1}^{n} \frac{r_i}{s - a_i} + r_\infty \tag{2.24}$$

and the residues are obtained from another overdetermined equation of

$$\begin{bmatrix} 1 & \frac{-a_1}{\omega_1^2 + a_1^2} & \cdots & \frac{-a_n}{\omega_1^2 + a_n^2} \\ 1 & \frac{-a_1}{\omega_2^2 + a_1^2} & \cdots & \frac{-a_n}{\omega_2^2 + a_n^2} \\ \vdots & & & \\ 1 & \frac{-a_1}{\omega_{Ns}^2 + a_1^2} & \cdots & \frac{-a_n}{\omega_{Ns}^2 + a_n^2} \\ 0 & \frac{-\omega_1}{\omega_1^2 + a_1^2} & \cdots & \frac{-\omega_1}{\omega_1^2 + a_n^2} \\ \vdots & & & \\ 0 & \frac{-\omega_{Ns}}{\omega_{Ns}^2 + a_1^2} & \cdots & \frac{-\omega_{Ns}}{\omega_{Ns}^2 + a_n^2} \end{bmatrix} \begin{bmatrix} r_\infty \\ r_1 \\ \vdots \\ r_n \end{bmatrix} = \begin{bmatrix} Y^r(s_1) \\ Y^r(s_2) \\ \vdots \\ Y^r(s_{Ns}) \\ Y^i(s_1) \\ \vdots \\ Y^i(s_{Ns}) \end{bmatrix} \tag{2.25}$$

where superscripts i and r indicate the imaginary and real parts of a complex value. This procedure results in a stable rational approximation with real coefficients p_k and q_k [56].

2.4.2 Vector Fitting

The vector fitting (VF) algorithm [20] uses an iterative approach to provide a rational function of the measured or simulated tabulated. The algorithm was originally introduced for

the analysis of power systems and transmission line modeling, and later extended to the field of signal integrity of high speed circuits [57]-[59].

The objective of the vector fitting algorithm is to determine a rational approximation for the transfer function, as

$$\boldsymbol{Y}(s)=[Y_{ij}(s)]; \qquad (i,j\in 1,..,P) \tag{2.26a}$$

$$Y_{ij}(s)=\sum_{k=1}\frac{r_{ij}^{k}}{s-p_k}+d_{ij}+se_{ij} \tag{2.26b}$$

where p_k and r_{ij}^{k} correspond to real or complex conjugate poles and residues respectively; d_{ij} and e_{ij} are optional quotient variables; s is the Laplace variable and P is the number of ports.

To review the vector fitting algorithm, consider $Y(s)$ as a one-port structure. The transfer function of $Y(s)$ is identified by specifying a set of starting poles q_k for a weight function defined as

$$\sigma(s)=\sum_{k=1}^{N}\frac{\tilde{c}_k}{s-q_k}+1 \tag{2.27}$$

In addition, the rational approximation for $\sigma(s)Y(s)$ is also described as

$$\sigma(s)Y(s)=\sum_{k=1}^{N}\frac{c_k}{s-q_k}+d+se \tag{2.28}$$

Multiplying (2.27) with the data values of $Y(s)$ and equating with (2.28), yields the following system of equations

$$\sum_{k=1}^{N}\frac{c_k}{s-q_k}+d+se=\left(\sum_{k=1}^{N}\frac{\widetilde{c}_k}{s-q_k}+1\right)Y(s) \tag{2.29}$$

The coefficients of (2.29) are determined by choosing N_s frequency points over the frequency range of interest to obtain an overdetermined linear system. To ensure the least square approximation provides real or complex conjugate poles and residues, at each frequency point s_i the system of (6.4) is expressed as

$$\mathbf{A}_i\mathbf{X}=\mathbf{B}_i \tag{2.30}$$

where

$$\mathbf{A}_i=\begin{bmatrix}\mathrm{Re}(a_1^i)\ldots\mathrm{Re}(a_N^i) & 1 & 0 & \mathrm{Re}(\widetilde{a}_1^i)\ldots\mathrm{Re}(\widetilde{a}_N^i)\\ \mathrm{Im}(a_1^i)\ldots\mathrm{Im}(a_N^i) & 0 & \mathrm{Im}(s_i) & \mathrm{Im}(\widetilde{a}_1^i)\ldots\mathrm{Im}(\widetilde{a}_N^i)\end{bmatrix}$$

$$\mathbf{X}=\begin{bmatrix}r_1 & \cdots & r_n & d & e & \widetilde{r}_1 & \cdots & \widetilde{r}_n\end{bmatrix}^{\mathrm{T}}$$

$$\mathbf{B}_i=\begin{bmatrix}\mathrm{Re}(Y(s_i))\\ \mathrm{Im}(Y(s_i))\end{bmatrix} \tag{2.31}$$

Re(.) and Im(.) denote the real and imaginary parts of the function, respectively. For real poles and residues, the coefficients of (2.31) are

$$a_k^i=\frac{1}{s_i-q_k}$$

$$\tilde{a}_k^i = \frac{-Y(s_i)}{s_i - q_k}$$

$$r_k = c_k\,; \quad \tilde{r}_k = \tilde{c}_k \tag{2.32}$$

For complex conjugate pole and residue pairs (i.e. $q_{k,k+1} = q_{re} \pm j q_{im}$, $c_{k,k+1} = c_{re} \pm j c_{im}$, $\tilde{c}_{k,k+1} = \tilde{c}_{re} \pm j\tilde{c}_{im}$) the coefficients of (2.31) are

$$a_k^i = \frac{1}{s_i - q_k} + \frac{1}{s_i - q_{k+1}}$$

$$a_{k+1}^i = \frac{j}{s_i - q_k} - \frac{j}{s_i - q_{k+1}}$$

$$\tilde{a}_k^i = \frac{-Y(s_i)}{s_i - q_k} + \frac{-Y(s_i)}{s_i - q_{k+1}}$$

$$\tilde{a}_{k+1}^i = \frac{-j \cdot Y(s_i)}{s_i - q_k} + \frac{j \cdot Y(s_i)}{s_i - q_{k+1}}$$

$$r_k = c_{re}, \quad r_{k+1} = c_{im}$$

$$\tilde{r}_k = \tilde{c}_{re}; \quad \tilde{r}_{k+1} = \tilde{c}_{im} \tag{2.33}$$

The equations of (2.31) at N_s different frequency points are assembled to obtain an over determined linear system of equations

$$\mathbf{AX} = \mathbf{B} \tag{2.34}$$

The least square solution of (2.34) provides the rational approximations for $\sigma(s)$ and $\sigma(s)Y(s)$ which can be expressed in terms of poles and zeros as

$$\sigma(s) = \frac{\prod_{k=1}^{N}(s - \tilde{z}_k)}{\prod_{k=1}^{N}(s - q_k)}; \qquad \sigma(s)Y(s) = e\frac{\prod_{k=1}^{N+1}(s - z_k)}{\prod_{k=1}^{N}(s - q_k)} \tag{2.35}$$

Note that the poles of (2.35) cancel each other out to obtain a rational approximation estimate for $Y(s)$ as

$$Y(s) = \frac{\sigma(s)Y(s)}{\sigma(s)} = d\frac{\prod_{k=1}^{N+1}(s - z_k)}{\prod_{k=1}^{N}(s - \tilde{z}_k)} \tag{2.36}$$

where the zeros of $\sigma(s)$ become the poles of $Y(s)$. This new set of poles $\{\tilde{z}_k\}$ are used as the starting poles for the next iterations to replace $\{q_k\}$. The above procedure is repeated until the poles converge. Once the poles $\{q_k\}$ are determined, an additional least square solution is performed on (2.26) to directly determine residue and quotient values of $Y(s)$.

Due to the fact that the VF procedure of [20] allows multiple iterations to improve the pole location from an initial guess till the response of the obtained model is similar to the actual response within an error tolerance, it is more accurate than the interpolation based method described in the previous section. It is noted, however, that while both the work of [56] and VF can provide stable transfer functions, neither are by construction passive. Passivity is an important criterion to be satisfied for typical interconnect structures and EM devices since stable but non passive models can lead to unstable time domain solutions when linked with nonlinear drivers/loads. Once the transfer function is obtained using VF, passivity

enforcement techniques like those reported in [61]-[63] can be used to realize passive macromodels which can now be seamlessly integrated with commercial circuit simulators like SPICE [64].

2.5 Vector Fitting in the Presence of Noise

Although VF can be converged in a few iterations, the convergence behavior may deteriorate when the frequency data samples contain a nonrational element such as noise [65]-[69]. In the next sections, a few techniques for improving the convergence of VF are reviewed.

2.5.1 Modified Vector fitting

In [67], the vector fitting algorithm is slightly modified by changing the weight function to

$$\sigma(s) = \sum_{k=1}^{N} \frac{\tilde{c}_k}{s - q_k} + \tilde{c}_0 \tag{2.37}$$

Multiplying (2.22) with the data values of $Y(s)$ and equating with (2.28), yields the following system of equations

$$\sum_{k=1}^{N} \frac{c_k}{s - q_k} + d + se = \left(\sum_{k=1}^{N} \frac{\tilde{c}_k}{s - q_k} + \tilde{c}_0 \right) Y(s) \tag{2.38}$$

At each frequency point s_i, (6.38) is expressed in the form of (2.30) where

$$\boldsymbol{A}_i = \begin{bmatrix} \mathrm{Re}(a_1^i) \ldots \mathrm{Re}(a_N^i) & 1 & 0 & \mathrm{Re}(\tilde{a}_0^i) \ldots \mathrm{Re}(\tilde{a}_N^i) \\ \mathrm{Im}(a_1^i) \ldots \mathrm{Im}(a_N^i) & 0 & \mathrm{Im}(s_i) & \mathrm{Im}(\tilde{a}_0^i) \ldots \mathrm{Im}(\tilde{a}_N^i) \end{bmatrix}$$

$$\mathbf{X} = \begin{bmatrix} r_1 & \cdots & r_n & d & e & \tilde{c}_0 & \tilde{r}_1 & \cdots & \tilde{r}_n \end{bmatrix}^{\mathrm{T}}$$

$$\boldsymbol{B}_i = \begin{bmatrix} 0 \\ 0 \end{bmatrix} \tag{2.39}$$

For $k \geq 1$, the coefficient a_k^i, $\tilde{a}_k^i$, r_k and $\tilde{r}_k$ are defined by (2.32) and (2.33) for real and complex conjugate poles, respectively and $\tilde{a}_0^i = Y(s_i)$. Since the values of $\boldsymbol{B}_i$ are zero, to avoid the null solution an additional equation is added to the least square problem

$$\mathrm{Re}\left\{ \sum_{i=1}^{N_s} \left(\sum_{k=1}^{N} \frac{\tilde{c}_k}{s_i - q_k} + \tilde{c}_0 \right) \right\} = N_s \tag{2.40}$$

The equations of (2.39) at N_s different frequency points are assembled with (2.40) to obtain an over determined linear system of equations similar to (2.34). Equation (2.40) imposes a relaxed constraint on the weight function of (2.37). Both weight functions (2.27) and (2.37) approach unity for all frequencies (i.e. $\tilde{c}_0 \approx 1$, $\{\tilde{c}_k\} \approx 0$) as the vector fitting algorithm converges [67].

Equation (2.40) should be weighted in relative to the size of $Y(s)$ in the least squares problem

$$weight = \frac{\left\| w(s) \cdot Y(s) \right\|_2}{Ns} \tag{2.41}$$

where $w(s)$ is the specified weight for the fitting of $Y(s)$. The above formulation is referred to as the relaxed vector fitting in the literature [67]-[68] and may enhance the reallocation of the poles to improve convergence.

2.5.2 Vector Fitting with Adding and Skimming

A different modification of standard VF, referred as vector fitting with adding and skimming (VF-AS), is proposed in [65], which addresses the convergence issues of VF when the frequency data samples are contaminated with noise. This paper illustrates the associated convergence issues are due to the spurious poles that appear during the iterations. To overcome this problem, an idea is suggested which is based on the identification and removal of spurious poles and on an incremental pole addition and relocation process in order to provide automatic order estimation even in the presence of significant noise.

The spurious poles are responsible for destroying the convergence in VF since they are stuck in their location trying to fit the noise instead of the true data. Equation (2.23), which is the only constraint for relocation of poles in the VF algorithm, is not strong enough to force the spurious poles to converge to their expected location. Hence, a “hard” relocation of the poles is proposed to enhance the convergence of VF. This process is able to automatically detect the spurious poles and to place them in a location of the complex plane that is closer to the true poles. Since VF is sensitive to the initial guess of the solution, it is expected that a better guess for the poles will also improve the behavior of VF in the presence of noise.

Based on the above discussion, VF-AS involves two automatic steps of i. detection of spurious poles and ii. selection of the best location in the complex plane. In order to detect the spurious poles the following band limited norm is defined for each pole

$$\mu_n^{(p)} = \left(\int_{\Omega_n} \left| Y_n(j\omega) \right|^p d\omega \right)^{1/p} \tag{2.41}$$

where p is usually set to 2. The integral is over a bandwidth Ω_n defined by the −10 dB level of the resonance curve. The values of this norm for spurious poles are significantly smaller than the values of actual poles.

After detecting the spurious poles, it is required to determine a valid guess for the placement of poles. In order to achieve this target, the local frequency points are calculated at where the deviations between the fitted and measured data are maximum. The number of maxima to be computed equals the number of detected spurious poles. Then, the spurious poles are relocated to the complex conjugate poles corresponding to the maxima. The real part of the new staring poles is chosen to be considerably smaller than the imaginary part so that each new pole is highly resonant (this is a typical choice in VF). The adding and skimming of the poles continues iteratively until sufficient accuracy is obtained [65].

2.5.3 Variance Weighted Vector Fitting

Variance weighted vector fitting (WVVF) algorithm [66] is a modification of the VF algorithm to estimate rational models of frequency responses affected by noise. The

technique is based on the use of a least-squares weighting function that contains information about the variance of the data samples used in macromodeling techniques. The measurement of the transfer function is assumed to be perturbed by a colored additive noise with a zero-mean circular complex Gaussian distribution. The variance of the measured transferred function is then estimated by repeating the measurements on a point-by-point basis and is incorporated in the weighting function of VF algorithm as

$$w(s) = \frac{1}{\sigma^2(s)} \tag{2.42}$$

The proposed weighting function gives information about the quality of the data samples to the least-squares estimator, improving its capability of retrieving the behavior of the system under study, and reducing the disturbing effect of the noise contribution [66].

Chapter 3

3 Analysis of Transmission Lines Based on Passive Method of Characteristics

3.1 Introduction

This chapter presents an efficient passive method of characteristics (MoC) macromodeling algorithm for lossy MTLs based on concepts proposed in [70]-[72]. In [70]-[71], a closed form passive MoC macromodel was described for two-conductor transmission lines. In this chapter, the methodology proposed in [70]-[71] is extended to MTLs. A theorem is provided specifying sufficient conditions to construct passive MoC macromodels for MTLs. A key feature of the proposed algorithm is that the curve fitting to realize the MoC depends only on the per-unit-length parameters and not on the discretization of the macromodel. Thus, with the knowledge of the rational functions derived by the per unit length parameters, the MoC is formulated in a closed form manner for any line length while ensuring passivity. In addition, the circuit equivalent realization of the proposed macromodel in a SPICE-like circuit simulator is also described.

3.2 Review of Transmission Line Theory

Consider distributed transmission lines represented by Telegrapher equations in Laplace domain [1] as

$$\frac{\partial}{\partial x}\boldsymbol{V}(z,s) = -\left(\boldsymbol{R}(s) + \mathrm{s}\boldsymbol{L}(s)\right)\boldsymbol{I}(z,s)$$

$$\frac{\partial}{\partial x}\boldsymbol{I}(z,s) = -\left(\boldsymbol{G}(s) + \mathrm{s}\boldsymbol{C}(s)\right)\boldsymbol{V}(z,s) \tag{3.1}$$

where s is Laplace transform variable, x is the position variable; $\boldsymbol{V}(z,s)$ and $\boldsymbol{I}(z,s)$ represent the voltage and current vectors of the transmission line, respectively; $\boldsymbol{R}(s)$, $\boldsymbol{L}(s)$, $\boldsymbol{G}(s)$ and $\boldsymbol{C}(s)$ are the frequency dependent per unit length (p.u.l.) resistance, inductance, conductance and capacitance matrices, respectively.

The frequency domain solution of (3.1) can be expressed as [37]

$$\boldsymbol{I}_1(s) = \boldsymbol{Y}_0(s)\boldsymbol{V}_1(s) - \boldsymbol{J}_1(s)$$

$$\boldsymbol{I}_2(s) = \boldsymbol{Y}_0(s)\boldsymbol{V}_2(s) - \boldsymbol{J}_2(s)$$

$$\boldsymbol{J}_1(s) = \boldsymbol{H}(s)[\boldsymbol{Y}_0(s)\boldsymbol{V}_2(s) + \boldsymbol{I}_2(s)]$$

$$\boldsymbol{J}_2(s) = \boldsymbol{H}(s)[\boldsymbol{Y}_0(s)\boldsymbol{V}_1(s) + \boldsymbol{I}_1(s)] \tag{3.2}$$

where

$$\begin{bmatrix}\boldsymbol{V}_1(s)\\ \boldsymbol{V}_2(s)\end{bmatrix} = \begin{bmatrix}\boldsymbol{V}(0,s)\\ \boldsymbol{V}(l,s)\end{bmatrix}$$

$$\begin{bmatrix} \boldsymbol{I}_1(s) \\ \boldsymbol{I}_2(s) \end{bmatrix} = \begin{bmatrix} \boldsymbol{I}(0,s) \\ -\boldsymbol{I}(l,s) \end{bmatrix} \tag{3.3}$$

represent the terminal voltages and currents of the transmission line; l is the length of the transmission line; $\boldsymbol{H}(s)$ is the propagation operation, $\boldsymbol{\Gamma}(s)$ is the propagation function and $\boldsymbol{Y}_0(s)$ is the characteristic admittance, defined as

$$\boldsymbol{H}(s) = e^{-\boldsymbol{\Gamma}(s)l}$$

$$\boldsymbol{\Gamma}^2(s) = (\boldsymbol{G}(s) + s\boldsymbol{C}(s))(\boldsymbol{R}(s) + s\boldsymbol{L}(s)$$

$$\boldsymbol{Y}_0(s) = \boldsymbol{\Gamma}^{-1}(s)(\boldsymbol{G}(s) + s\boldsymbol{C}(s) \ . \tag{3.4}$$

The solution of Telegrapher's equations in (3.2) cannot be expressed in the time domain as ordinary differential equations, which makes it difficult to interface with nonlinear SPICE circuit simulators.

3.3 Passive Method of Characteristics Macromodel

The development of the PMoC begins for the two-conductor transmission line case [70] and then extends to multi-conductor transmission lines [73].

The PMoC is derived by extracting the propagation delay from $H(s)$ as

$$H(s) = e^{-sT} e^{-(l\Gamma(s) - sT)} \approx e^{-sT} Q(s) \tag{3.5}$$

where $T = l\sqrt{C_\infty L_\infty}$ is the extracted line delay and $Q(s) \approx e^{-(l\Gamma(s)-sT)}$ corresponds to the delayless propagation operator that takes into the account the effects due to line dispersion and attenuation. C_∞ and L_∞ are, respectively, the p.u.l. capacitance and inductance parameters evaluated at the maximum frequency point of interest. To make the curve fitting of the PMoC independent of the line length *l*, the rational approximation is performed on $\Gamma(s)$ instead of $Q(s)$, as

$$\Gamma(s) = \sqrt{\left(G(s) + sC(s)\right)\left(R(s) + sL(s)\right)} \approx sT + P(s) \tag{3.6}$$

where $P(s)$ is approximated as a rational function. In addition, the characteristic admittance $Y_0(s)$ is also approximated as a rational function. It should be noted that the curve fitting for both $\Gamma(s)$ and $Y_0(s)$ depend only on the p.u.l. parameters and is independent of the line length *l* and the discretization of the macromodel. To approximate $Q(s)$ using $P(s)$, a closed form Padé approximation of an exponential function is used as [70] [73],

$$Q(s) = \frac{Q_M(P(s)l)}{P_N(P(s)l)} = \frac{\sum_{i=0}^{M} \frac{(M+N-i)!M!}{(M+N)!i!(M-i)!}(-P(s)l)^i}{\sum_{i=0}^{N} \frac{(M+N-i)!N!}{(M+N)!i!(N-i)!}(P(s)l)^i} \tag{3.7}$$

Thus to analyze transmission lines at different line lengths, the rational function $P(s)$ is multiplied by the line length *l* and the appropriate order *M* and *N* is selected to obtain the desired frequency domain accuracy for $Q(s)$.

For the case of multi-conductor transmission lines, rational curve fitting is also performed on $\boldsymbol{\Gamma}(s)$ and $\boldsymbol{Y}_0(s)$ as

$$\boldsymbol{\Gamma}(s) \approx s(\boldsymbol{C}_\infty \boldsymbol{L}_\infty)^{1/2} + \boldsymbol{P}(s) \approx \boldsymbol{E}_I \hat{\boldsymbol{\Gamma}}(s) \boldsymbol{E}_I^{-1} = \boldsymbol{E}_I \left(s(\hat{\boldsymbol{C}}_\infty \hat{\boldsymbol{L}}_\infty)^{1/2} + \hat{\boldsymbol{P}}(s) \right) \boldsymbol{E}_I^{-1}$$

$$\boldsymbol{Y}_0(s) \approx \boldsymbol{E}_I \hat{\boldsymbol{Y}}_0(s) \boldsymbol{E}_V^{-1} \tag{3.8}$$

$\boldsymbol{E}_V$ and $\boldsymbol{E}_I$ are constant matrices and are selected such that they simultaneously diagonalize both $\boldsymbol{L}_\infty$ and $\boldsymbol{C}_\infty$ and have the following properties [1]

$$\hat{\boldsymbol{L}}_\infty = \boldsymbol{E}_V^{-1} \boldsymbol{L}_\infty \boldsymbol{E}_I \,; \quad \hat{\boldsymbol{C}}_\infty = \boldsymbol{E}_I^{-1} \boldsymbol{C}_\infty \boldsymbol{E}_V \,; \quad \boldsymbol{E}_V^t = \boldsymbol{E}_1^{-1} \tag{3.9}$$

where $\hat{\boldsymbol{L}}_\infty$ and $\hat{\boldsymbol{C}}_\infty$ are diagonal matrices of the form $\hat{\boldsymbol{L}}_\infty = diag\{l_1, l_2, ..., l_n\}$, $\hat{\boldsymbol{C}}_\infty = diag\{c_1, c_2, ..., c_n\}$; the superscript t denotes the transpose of the matrix and the matrices $\hat{\boldsymbol{P}}(s)$ and $\hat{\boldsymbol{Y}}_0(s)$ are approximated as rational functions. Note that the matrices $\boldsymbol{E}_V$ and $\boldsymbol{E}_I$, as well as the curve fitting of $\hat{\boldsymbol{\Gamma}}(s)$ and $\hat{\boldsymbol{Y}}_0(s)$ depend only on the p.u.l. parameters and not on the discretization of the macromodel or the line length. Next, it is required to extract the delay from $\boldsymbol{H}(s)$, however $\boldsymbol{H}(s)$ cannot be expressed as

$$\boldsymbol{H}(s) = \boldsymbol{E}_I e^{-l\hat{\boldsymbol{\Gamma}}(s)} \boldsymbol{E}_I^{-1} \neq \boldsymbol{E}_I e^{-sl(\hat{\boldsymbol{C}}_\infty \hat{\boldsymbol{L}}_\infty)^{1/2}} e^{-l\hat{\boldsymbol{P}}(s)} \boldsymbol{E}_I^{-1} \tag{3.10}$$

since the matrices $(\hat{\boldsymbol{C}}_\infty \hat{\boldsymbol{L}}_\infty)^{1/2}$ and $\hat{\boldsymbol{P}}(s)$ do not commute (i.e. $(\hat{\boldsymbol{C}}_\infty \hat{\boldsymbol{L}}_\infty)^{1/2} \cdot \hat{\boldsymbol{P}}(s) \neq \hat{\boldsymbol{P}}(s) \cdot (\hat{\boldsymbol{C}}_\infty \hat{\boldsymbol{L}}_\infty)^{1/2}$). To approximate $\boldsymbol{H}(s)$ in a closed form manner, the matrix $l(\hat{\boldsymbol{C}}_\infty \hat{\boldsymbol{L}}_\infty)^{1/2}$ is expressed as

$$l(\hat{\boldsymbol{C}}_{\infty}\hat{\boldsymbol{L}}_{\infty})^{1/2} = \hat{\boldsymbol{T}}_{\min} + l\hat{\boldsymbol{P}}_{CL} \tag{3.11}$$

where

$$\hat{\boldsymbol{P}}_{CL} = diag(\sqrt{c_1 l_1} - \lambda_{\min}, \sqrt{c_2 l_2} - \lambda_{\min}, ..., \sqrt{c_n l_n} - \lambda_{\min}) \tag{3.12}$$

$$\hat{\boldsymbol{T}}_{\min} = l\lambda_{\min}\boldsymbol{I} \tag{3.13}$$

$\lambda_{\min} = \min(\sqrt{c_i l_i})$ is the minimum eigenvalue of $(\hat{\boldsymbol{C}}_{\infty}\hat{\boldsymbol{L}}_{\infty})^{1/2}$ and $\boldsymbol{I}$ is the identity matrix. Since the matrices $\hat{\boldsymbol{T}}_{\min}$ and $sl\hat{\boldsymbol{P}}_{CL} + l\hat{\boldsymbol{P}}(s)$ commute, $\boldsymbol{H}(s)$ can be expressed as

$$\boldsymbol{H}(s) = \boldsymbol{E}_I \hat{\boldsymbol{H}}(s)\boldsymbol{E}_I^{-l} = \boldsymbol{E}_I e^{-s\hat{\boldsymbol{T}}_{min}} \boldsymbol{Q}(s)\boldsymbol{E}_I^{-l} \tag{3.14}$$

where $\boldsymbol{Q}(s) = e^{-\boldsymbol{\Phi}}$ and $\boldsymbol{\Phi} = sl\hat{\boldsymbol{P}}_{CL} + l\hat{\boldsymbol{P}}(s)$. The matrix $\boldsymbol{Q}(s)$ can now be approximated using the Padé approximation of an exponential function as

$$\boldsymbol{Q}(s) = \left[P_N(\boldsymbol{\Phi})\right]^{-1} Q_M(\boldsymbol{\Phi}) \tag{3.15}$$

where

$$Q_M(\boldsymbol{\Phi}) = \sum_{i=0}^{M} \frac{(M+N-i)!M!}{(M+N)!i!(M-i)!}(\boldsymbol{\Phi})^i$$

$$P_N(\boldsymbol{\Phi}) = \sum_{i=0}^{N} \frac{(M+N-i)!N!}{(M+N)!i!(N-i)!}(-\boldsymbol{\Phi})^i \tag{3.16}$$

The above formulation uses the minimum eigenvalue of $(\hat{\boldsymbol{C}}_{\infty}\hat{\boldsymbol{L}}_{\infty})^{1/2}$ to extract the same delay for each line. As a result, the rational approximation for $\boldsymbol{Q}(s)$ using (3.15) may

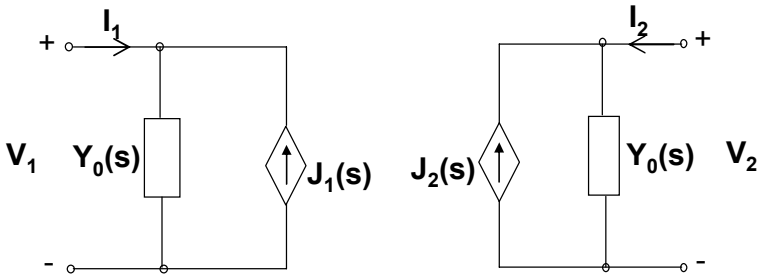

Figure 3-1: Basic equivalent circuit for the method of characteristics model.

require a higher order approximation when compared to other MoC macromodels which use the eigenvalue of each line to extract the line delay [73]. However, the advantages of this approach are that the curve fitting depends only on the p.u.l. parameters and is independent of the discretization of the MoC. Thus with the knowledge of $\boldsymbol{E}_V$, $\boldsymbol{E}_I$, $\hat{\boldsymbol{\Gamma}}(s)$ and $\hat{\boldsymbol{Y}}_0(s)$, the proposed MoC can be formulated in a closed form manner for any line length. This avoids computationally expensive and sometimes unreliable numerical fitting techniques that are on occasion associated with the MoC-based algorithms since $\boldsymbol{E}_V$, $\boldsymbol{E}_I$, $\hat{\boldsymbol{\Gamma}}(s)$ and $\hat{\boldsymbol{Y}}_0(s)$ are determined offline and the accuracy of these values can be verified. In addition, the passivity of the PMoC is assured by construction for any line length, provided that the rational approximations of $\hat{\boldsymbol{\Gamma}}(s)$ and $\hat{\boldsymbol{Y}}_0(s)$ satisfy the conditions of the passivity theorem in section 3.4.

The PMoC macromodel can be realized in term of equivalent circuits as shown in Figure 3-1 for a 2 conductor transmission line and Figure 3-2 for a 3-conductor transmission line (2 signal conductor and 1 reference line). Figure 3-2a realizes the transformation of the modal voltages and currents at the near and far end and Figure 3-2b realizes the partially decoupled transmission line.

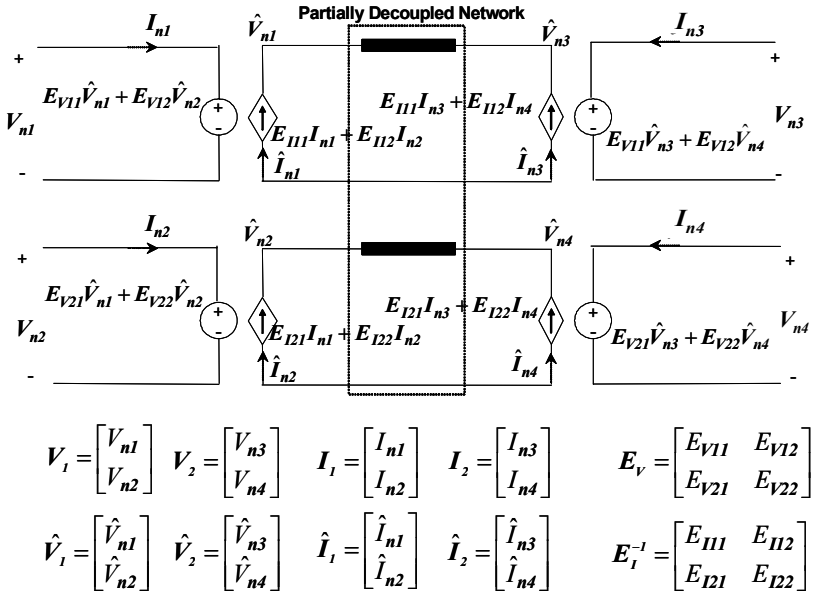

(a)

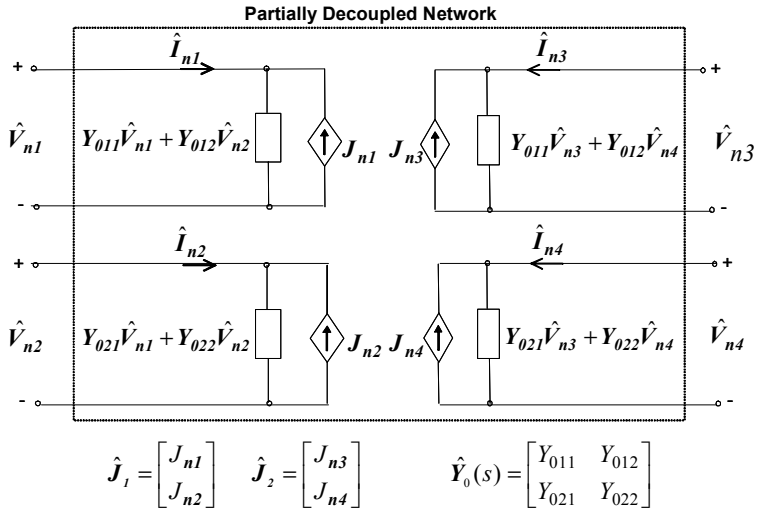

(b)

Figure 3-2: Basic equivalent circuit of MoC model (a) Transformation of modal voltages and currents (b) Realization of partially decoupled network.

3.4 Passivity Theorem

A linear network with admittance matrix $\boldsymbol{Y}(s)$ is said to be passive if it satisfies the following conditions [74]-[75]

1) $\boldsymbol{Y}(s^*) = \boldsymbol{Y}^*(s)$ for all s, where "*" is the complex conjugate operator.

2) $\boldsymbol{Y}(s)$ is analytic for all complex values of $s = \sigma + j\omega$ satisfying $\sigma > 0$.

3) $\boldsymbol{Y}(s)$ is a positive-real matrix. That is the product $\boldsymbol{z}^{*t}(\boldsymbol{Y}^t(s^*) + \boldsymbol{Y}(s))\boldsymbol{z} \geq 0$ for all complex values of $s = \sigma + j\omega$ satisfying $\sigma > 0$ and arbitrary vector $\boldsymbol{z}$.

To obtain passive macromodels, a theorem that specifies sufficient conditions to guarantee the passivity of the MoC by construction is described. This theorem is similar to the one present in [70] for two-conductor transmission lines and it is extended to MTLs in [73].

Theorem 1: Let the MoC satisfy the following conditions:

1) The rational approximations of $\hat{\boldsymbol{Y}}_{\boldsymbol{0}}(s)$, $\hat{\boldsymbol{\Gamma}}(s)$ and $s\hat{\boldsymbol{P}}_{CL} + \hat{\boldsymbol{P}}(s)$ are positive real and the imaginary part of $s\hat{\boldsymbol{P}}_{CL} + \hat{\boldsymbol{P}}(s)$ satisfies $\boldsymbol{z}^{*t}\,\mathrm{Im}(s\hat{\boldsymbol{P}}_{CL} + \hat{\boldsymbol{P}}(s))\boldsymbol{z} > 0$ for $\omega > 0$ and $\boldsymbol{z}^{*t}\,\mathrm{Im}(s\hat{\boldsymbol{P}}_{CL} + \hat{\boldsymbol{P}}(s))\boldsymbol{z} < 0$ for $\omega < 0$ where $\boldsymbol{z}$ is any arbitrary complex vector and Im() denotes the imaginary part of the matrix function.

2) The products formed by the rational functions of $\hat{\boldsymbol{\Gamma}}(s)\hat{\boldsymbol{Y}}_{\boldsymbol{0}}(s)$ and $\hat{\boldsymbol{Y}}_{\boldsymbol{0}}(s)^{-1}\hat{\boldsymbol{\Gamma}}(s)$ are positive real.

3) The scalar rational approximation of e^{-s} can be expressed as

$$e^{-s} = e^{-\sigma}(\cos\omega - j\sin\omega) \approx \frac{\hat{Q}_M(s)}{\hat{P}_N(s)} = A - jB \tag{3.17}$$

where $A \approx e^{-\sigma}\cos\omega$ and $B \approx e^{-\sigma}\sin\omega$ are the real and imaginary parts of $\hat{Q}_M(s)/\hat{P}_N(s)$, respectively, and (3.17) satisfies the following inequalities

$$\left|\frac{2e^{-\sigma}\cos\omega}{1-e^{-2\sigma}}\right| \approx \left|\frac{2A}{1-A^2-B^2}\right| \le \left|\frac{1}{\sigma}\right| \tag{3.18}$$

$$\left|\frac{2e^{-\sigma}\sin\omega}{1-e^{-2\sigma}}\right| \approx \left|\frac{2B}{1-A^2-B^2}\right| \le \left|\frac{\omega}{\sigma}\right| \tag{3.19}$$

$$\left(e^{-\sigma}\cos\omega\right)^2 + \left(e^{-\sigma}\sin\omega\right)^2 \approx A^2 + B^2 \le 1 \tag{3.20}$$

for $\mathrm{Re}(s) = \sigma \ge 0$. If all the above three conditions are satisfied and $\boldsymbol{Q}(s) = e^{-(sd\hat{\boldsymbol{P}}_{CL} + d\hat{\boldsymbol{P}}(s))}$ is approximated by replacing the scalar s in (3.17) by the rational approximation of $s\hat{\boldsymbol{P}}_{CL} + \hat{\boldsymbol{P}}(s)$ multiplied by the line length l as in (3.15), then the resulting MoC macromodel given by (3.2)-(3.4) is passive.

It should be noted that conditions 1 and 2 of theorem 1 are due to the physical properties of transmission lines, while the third condition results from the mathematical properties of the exponential function. As a result, these conditions are not restrictive in realizing transmission lines governed by (3.1) and only serve to ensure the passivity of the MoC macromodel. Since the p.u.l. parameters are nonnegative definite at each frequency point, the characteristic impedance $\boldsymbol{Y}_0(s)$, the propagation function $\boldsymbol{\Gamma}(s)$, and the products $\boldsymbol{\Gamma}(s)\boldsymbol{Y}_0(s) = \boldsymbol{G}(s) + s\boldsymbol{C}(s)$, $\boldsymbol{Y}_0^{-1}(s)\boldsymbol{\Gamma}(s) = \boldsymbol{R}(s) + s\boldsymbol{L}(s)$ are all positive real functions [1].

Thus the rational approximations of the modal characteristic admittance $\hat{\boldsymbol{Y}}_{\boldsymbol{0}}(s)$ and modal propagation constant $\hat{\boldsymbol{\Gamma}}(s)$ should also satisfy the aforementioned physical properties of transmission lines as given by conditions 1 and 2 of theorem 1. The modal propagation constant $\hat{\boldsymbol{\Gamma}}(s)$ is positive real since the matrices $\boldsymbol{\Gamma}(s)$ and $\hat{\boldsymbol{\Gamma}}(s) = \boldsymbol{E}_I^{-1}\boldsymbol{\Gamma}(s)\boldsymbol{E}_I$ are similar matrices and both have the same eigenvalues [1] [76]. Furthermore, using (3.8) and (3.9), $\hat{\boldsymbol{Y}}_{\boldsymbol{0}}(s)$, $\hat{\boldsymbol{\Gamma}}(s)\hat{\boldsymbol{Y}}_0(s)$ and $\hat{\boldsymbol{Y}}_0^{-1}(s)\hat{\boldsymbol{\Gamma}}(s)$ are also positive real since they are expressed in terms of a congruent transform of positive real functions [8] [76],

$$\begin{aligned}
\hat{\boldsymbol{Y}}_0(s) &= \boldsymbol{E}_V^t\boldsymbol{Y}_0(s)\boldsymbol{E}_V \\
\hat{\boldsymbol{\Gamma}}(s)\hat{\boldsymbol{Y}}_0(s) &= \boldsymbol{E}_V^t\boldsymbol{\Gamma}(s)\boldsymbol{Y}_0(s)\boldsymbol{E}_V \\
\hat{\boldsymbol{Y}}_0^{-1}(s)\hat{\boldsymbol{\Gamma}}(s) &= \boldsymbol{E}_I^t\boldsymbol{Y}_0^{-1}(s)\boldsymbol{\Gamma}(s)\boldsymbol{E}_I
\end{aligned} \tag{3.21}$$

Also, the nonnegative p.u.l. parameters make the imaginary part of $\boldsymbol{\Gamma}(s)$ satisfy $\boldsymbol{z}^{*t}\,\mathrm{Im}(\boldsymbol{\Gamma}(s))\boldsymbol{z} > 0$ for $\omega > 0$ and $\boldsymbol{z}^{*t}\,\mathrm{Im}(\boldsymbol{\Gamma}(s))\boldsymbol{z} < 0$ for $\omega < 0$. To ensure that $s\hat{\boldsymbol{P}}_{CL} + \hat{\boldsymbol{P}}(s)$ satisfies the same conditions as $\boldsymbol{\Gamma}(s)$, the extracted delay $\hat{\boldsymbol{T}}_{\min}$ is selected such that $l(s\hat{\boldsymbol{P}}_{CL} + \hat{\boldsymbol{P}}(s)) = d\hat{\boldsymbol{\Gamma}}(s) - \hat{\boldsymbol{T}}_{\min}$ satisfies the first condition of theorem 1.

The third condition of the theorem is due to the mathematical properties of the exponential function. As a result, these conditions are not restrictive in realizing transmission lines governed by (1) and only serve to ensure the passivity of the MoC macromodel. Furthermore, it can be shown that the exponential function of

$e^{-s} = e^{-\sigma}(\cos\omega - j\sin\omega)$ satisfies the inequalities of (3.18)-(3.20) by using the following facts $|\cos\omega| \le 1$, $|\sin\omega| \le \omega$, $\left|(e^{\sigma} - e^{-\sigma})/2\right| \ge |\sigma|$ and $\cos^2\omega + \sin^2\omega = 1$, as

$$\left|\frac{2e^{-\sigma}\cos\omega}{1-e^{-2\sigma}}\right| = \left|\frac{\cos\omega}{(e^{\sigma}-e^{-\sigma})/2}\right| \le \left|\frac{1}{(e^{\sigma}-e^{-\sigma})/2}\right| \le \left|\frac{1}{\sigma}\right| \tag{3.22}$$

$$\left|\frac{2e^{-\sigma}\sin\omega}{1-e^{-2\sigma}}\right| = \left|\frac{\sin\omega}{(e^{\sigma}-e^{-\sigma})/2}\right| \le \left|\frac{\omega}{\sigma}\right| \tag{3.23}$$

$$\left(e^{-\sigma}\cos\omega\right)^2 + \left(e^{-\sigma}\sin\omega\right)^2 = e^{-2\sigma} \le 1 \tag{3.24}$$

Thus the rational function used to approximate $e^{-s} = e^{-\sigma}(\cos\omega - j\sin\omega)$ given by (3.7) should also satisfy the inequalities of (3.18)-(3.20) as described by condition 3 of theorem 1. The proof of the theorem is given in [73].

3.5 Numerical Examples

Two examples are presented in this section to demonstrate the validity and efficiency of the proposed MoC macromodel. The transient responses were obtained using HSPICE [38] and the comparison of CPU time was done using the Sun Blade 1500 workstation.

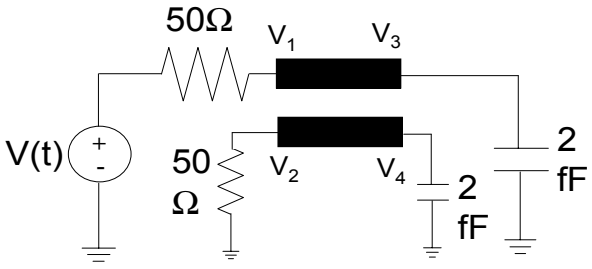

Figure 3-3: On-chip coupled transmission line network with frequency dependent p.u.l (example1).

Example 1) An on-chip coupled interconnect network with frequency dependent per-unit-length parameters proposed in [37] is shown in Figure 3-3. The frequency dependent p.u.l. parameters are listed in [37]. In this example, $\boldsymbol{L}_\infty$ and $\boldsymbol{C}_\infty$ are set to the p.u.l. inductance and capacitance values at the highest frequency point of interest chosen to be 10GHz. The linear transformation matrices $\boldsymbol{E}_V$ and $\boldsymbol{E}_I$ are selected such that they simultaneously diagonalize both $\boldsymbol{L}_\infty$ and $\boldsymbol{C}_\infty$. The diagonal eigenvalues for $(\hat{\boldsymbol{C}}_\infty \hat{\boldsymbol{L}}_\infty)^{1/2}$ are *7.5295e-9 s/m* and *13.205e-9 s/m* and the eigenvalue extracted is $\lambda_{\min}$ *=7.5295e-9 s/m*. For this example 73% of the delay is extracted from (3.14). The data of the per-unit-length parameters are fitted to rational functions to approximate $\hat{\boldsymbol{Y}}_0(s)$ and $\hat{\boldsymbol{\Gamma}}(s)$ using the procedure outlined in [73] to ensure the condition of theorem 1 are satisfied. The maximum error tolerances are selected to be 0.5% with respect to the tabulated data. The interconnect network of Figure 3-3 was analyzed at 0.2cm, 0.5cm and 1cm. For the 0.2cm line, a Padé approximation of M = 0 and N = 2 was used to match $\boldsymbol{Q}(s)$ up to 10GHz, while for the 0.5cm and 1cm the order was set to M = 1 and N = 3. Figure 3-4 shows the rational approximation of $Q_{12}(s)$ for the 0.2cm and 1cm line.

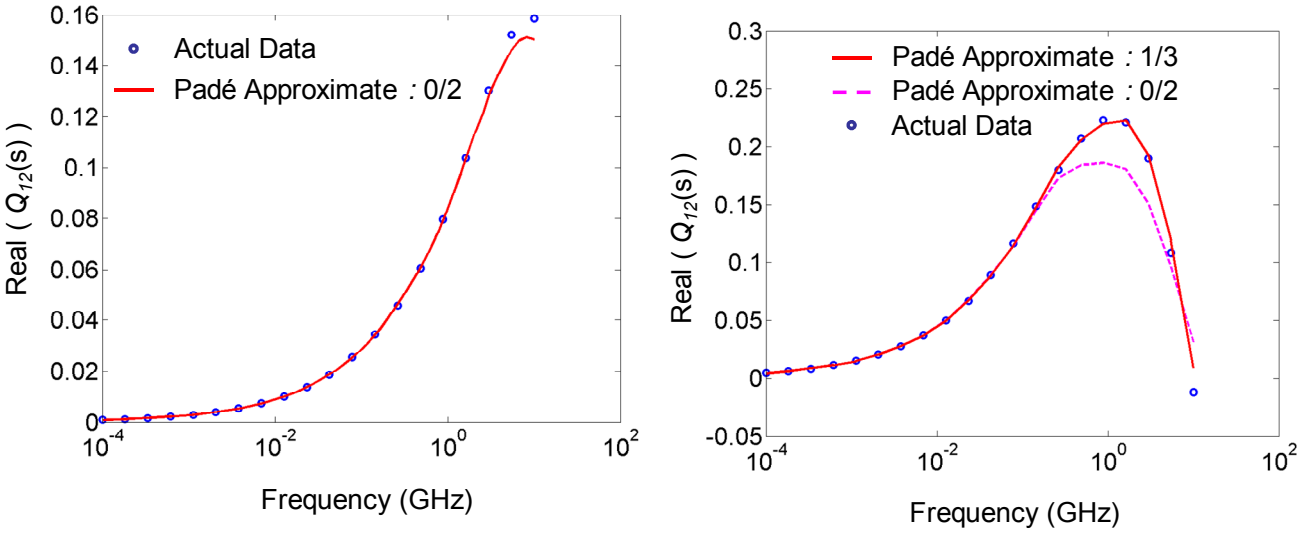

(a) (b)

Figure 3-4: Padé approximation: Real part of Q12(s) (Example 1) (a) d = 0.2cm (b) d = 1cm.

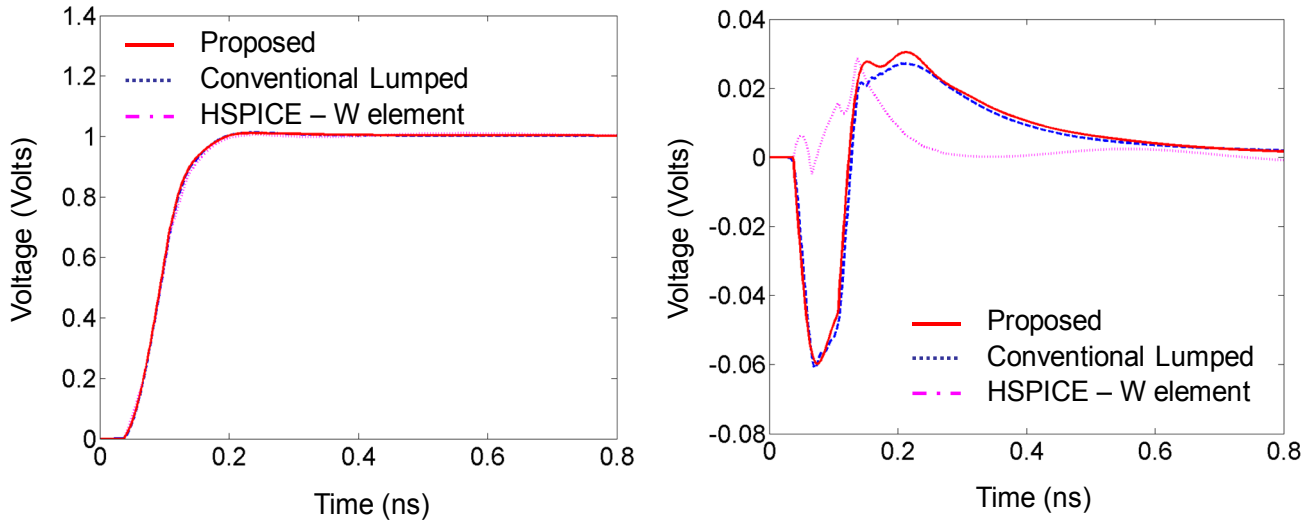

(a) (b)

Figure 3-5: On-chip line (0.5cm) Transient response (Example 1) (a) Active line (node V3) (b) Victim line (node V4)

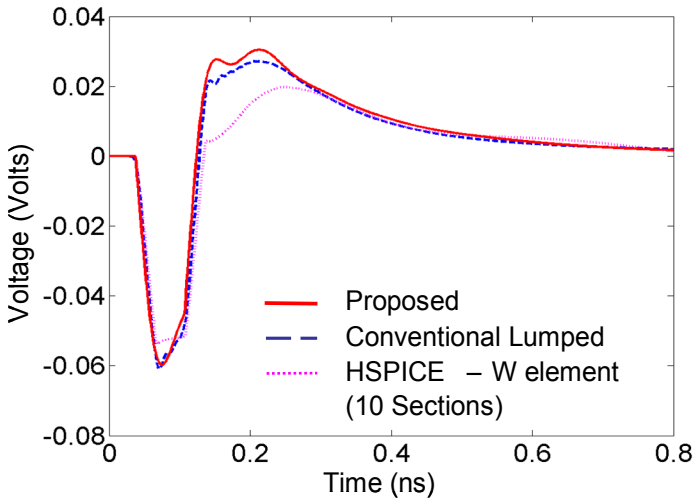

Figure 3-6: On-chip line (0.5cm) transient response at node V4 (10 sections W-element) (Example 1)

The transient response of the transmission line of length 0.5cm corresponding to a unit step input voltage with a rise time of 0.07ns is provided in Figure 3-5. For their respective orders, both the proposed macromodel and the conventional lumped model [1] produce similar responses, while the W-element [38] gives a different response for the victim line as shown in Fig 3-5b. The responses produced by the proposed and conventional lumped model also match the results published in [37].

Both the proposed algorithm and W-element use delay extraction to model the transmission line. For this example, the curve fitting to realize both macromodels is very challenging since this transmission line is very lossy and the coupling between the two lines is week. However unlike the W-element, the realization of the proposed algorithm is independent of the discretization of the macromodel. Both the eigen-mode decomposition of $\boldsymbol{E}_V$, $\boldsymbol{E}_I$ and the rational approximations of $\hat{\boldsymbol{Y}}_0(s)$ and $\hat{\boldsymbol{\Gamma}}(s)$ can be determined offline while ensuring conditions 1 and 2 of the theorem and the accuracy of these values

Table 3-1: CPU time comparision (Example 1) (sun blade 1500 workstation)

Simulations	Proposed MoC (sec)	Lumped (sec)	W-element (1 section) (sec)	W-element (10 section) (sec)
d=0.2cm	0.15	0.28	0.13	0.72
d = 0.5cm	0.16	0.62	0.13	0.72
d = 1cm	0.16	1.21	0.13	0.72

can be verified. On the other hand, the numerical realization of the W-element depends on the discretization of the macromodel. As a result the accuracy of the W-element cannot be assured. One way to decrease the transfer function complexity of the W-element is to decrease the length of the line. Fig 3-6 shows the transient response of the victim line by segmenting the W-element into 10 sections. The transient responses shows better agreement with the proposed model as the number of W-element segments increase.

Table 3-1 gives a comparison of the CPU expense. It should be pointed out that the proposed method and conventional lumped model are implemented using external circuit elements while the W-element is an internal model provided by HSPICE. It was demonstrated in [37], that implementing macromodels internally can significantly improve the simulation times when compared to external circuit representations. As seen

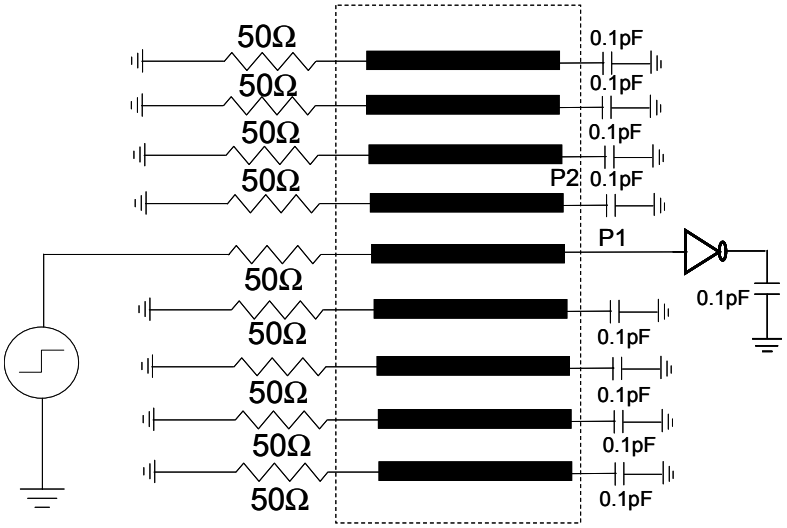

Figure 3-7: Nine-coupled transmission line network with nonlinear CMOS inverters (Example2).

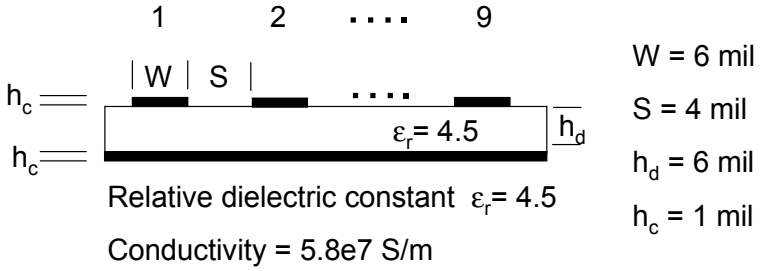

Figure 3-8: Cross-section of 9-coupled transmission line (Example 2).

from the table, the proposed method is about 2-to-7 times faster compared to the conventional lumped model, while ensuring the passivity of the macromodel.

Example 2) In this example, a 9-coupled interconnect network (Figure 3-7) with nonlinear CMOS inverter is considered. Figure 3-8 shows the cross-section of the 9-coupled transmission line. The p.u.l. parameters of the interconnect structure are

Table 3-2: Minimum and maximum eigenvalues of $(\hat{\boldsymbol{C}}_{\infty}\hat{\boldsymbol{L}}_{\infty})^{1/2}$ and the percentage of the delay extracted (Example 2)

ε_r	Minimum Eigenvalue (s/m)	Maximum Eigenvalue (s/m)	Percentage of delay extracted $100*(n\lambda_{\min}/\Sigma_{i=1}^{n}\lambda_i)$
1	3.3429e-9	3.3585e-9	99.8%
2	3.9933e-9	4.5461e-9	95.8%
4.5	5.2423e-9	6.6267e-9	92.2%
8	6.5987e-9	8.7278e-9	90.6%
16	8.9539e-9	12.234e-9	89.4%

determined by using the HSPICE field solver [38] and include skin-effect losses. The matrices $\boldsymbol{L}_{\infty}$ and $\boldsymbol{C}_{\infty}$ are set to the p.u.l. inductance and capacitance values at the highest frequency point of interest chosen to be 3.5 GHz.

Before proceeding with the solution, the relative dielectric constant is varied from ε_r=1 to ε_r=16 to examine the amount of delay that is extract from (3.10). Table 3-2 shows the minimum and maximum eigenvalues for $(\hat{\boldsymbol{C}}_{\infty}\hat{\boldsymbol{L}}_{\infty})^{1/2}$ at 3.5 GHz and the percentage of the delay that is extracted from (3.10). When ε_r=1, the velocity of the electromagnetic wave through the dielectric slab and air are the same. Furthermore at 3.5GHz, the p.u.l. inductance is mainly due to the magnetic field external to the conductors. As ε_r increases, the electromagnetic wave velocity in the dielectric slab decreases. The different wave velocities violate the TEM characteristics since pure TEM waves travel

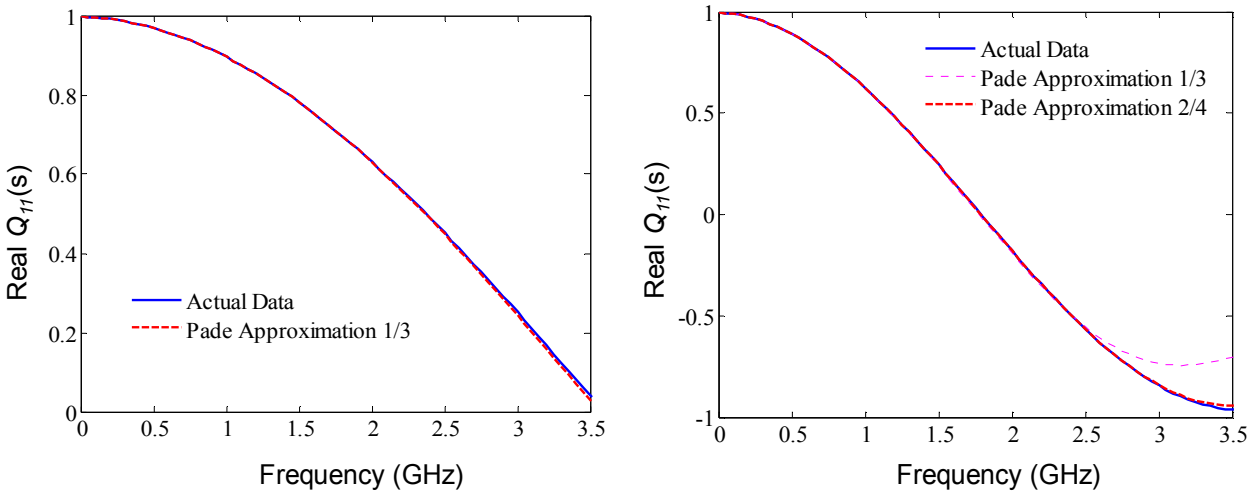

Figure 3-9: Padé approximation: Real part of Q11(s) (Example 2) (a) d = 0.5cm (b) d = 10cm.

with only one velocity. This causes the eigenvalues of $(\hat{\boldsymbol{C}}_{\infty}\hat{\boldsymbol{L}}_{\infty})^{1/2}$ to be different. Nonetheless, quasi-TEM assumes that the velocities at different mediums are not substantially different and that the resulting field structure is similar to a TEM structure. As a result, the difference between the maximum and minimum eigenvalue is not too far apart and a significant portion of the delay can be extracted. For this example, 89.4% of the delay is extracted from (3.10) when ε_r=16. In addition, the proposed MoC macromodel can be formulated in a closed form manner while guaranteeing passivity. On the other hand, traditional MoC algorithms requires approximating 45 transfer functions for $\boldsymbol{Q}(s)$ (i.e. $(n^2+n)/2$; n=9 coupled lines) for each line length and the passivity of the macromodel is not assured.

The data of the per-unit-length parameters are fitted to rational functions to approximate $\hat{\boldsymbol{Y}}_0(s)$ and $\hat{\boldsymbol{\Gamma}}(s)$ using the procedure outlined in Section 3.3. The maximum error tolerances are selected to be 0.5% with respect to the tabulated data. The interconnect

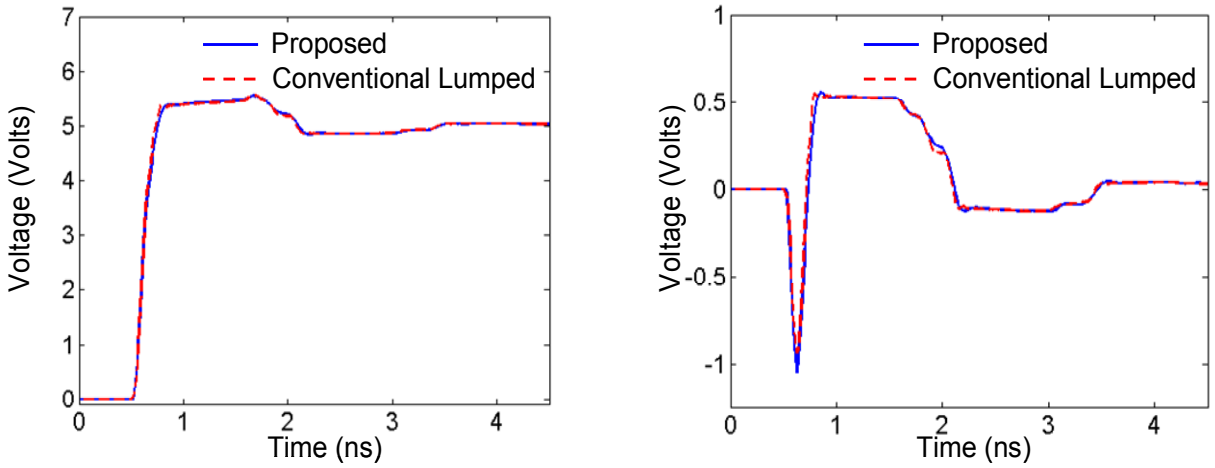

Figure 3-10: Transient response for 10cm line (a) at node P1 (b) at node P2 (Example 2).

Table 3-3: CPU time Comparison (Example 2) (Sun Blade 1500 workstation)

Simulations	Proposed MoC (sec)	Lumped (sec)
d = 5cm	5.1	114
d = 10cm	8.9	305

network of Figure 3-7 was analyzed at 5cm and 10cm. For the 5cm line, a Padé approximation of $M = 1$ and $N = 3$ was used to match $\boldsymbol{Q}(s)$ up to 3.5GHz, while for the 10cm the order was set to $M = 2$ and $N = 4$. Figure 3-9 shows the rational approximation of $Q_{11}(s)$ for the 5cm and 10cm lines. Figure 3-10 shows the time domain responses of the transmission line of length 10cm corresponding to a unit step input voltage with a rise time of 0.1ns at nodes P1 and P2.

Table 3-3 gives a comparison of the CPU expense using the proposed method and conventional lumped model [1]. For this example, the proposed method is 22 to 34 times faster compared to the conventional lumped model, while ensuring the passivity of the macromodel.

3.6 Conclusion

In this chapter, an algorithm is described to construct passive MoC macromodels for MTLs. A key feature of the proposed algorithm is that the curve fitting of the MoC depends only on the p.u.l. parameters and not on the discretization of the macromodel. Thus with the knowledge of the rational functions describing $\hat{\boldsymbol{Y}}_0(s)$ and $\hat{\boldsymbol{\Gamma}}(s)$ the proposed MoC can be formulated in a closed form manner for any line length, while guaranteeing the passivity of the macromodel. This avoids computationally expensive and sometimes unreliable numerical fitting algorithms that are on occasion associated with the MoC-based algorithms.

Chapter 4

4 Sensitivity Analysis of Multiconductor Transmission Line

4.1 Introduction

In this chapter, a new algorithm to perform sensitivity analysis of nonlinear circuits with distributed interconnects is presented based on the passive method of characteristics (PMoC). The proposed algorithm differentiates the solution of Telegrapher's equation and uses the PMoC to derive the sensitivity network with respect to any interconnect parameter. This approach differs from [41], which directly differentiates Telegrapher's equations to derive the sensitivity network. A major advantage of the proposed algorithm is that the sensitivities are calculated from the solution of the original system (which is formulated in a closed form manner) resulting in significant computational advantages. Numerical examples are presented to illustrate the validity of the proposed approach.

4.2 Sensitivity Analysis

This section extends the PMoC to efficiently calculate sensitivities of distributed transmission lines with nonlinear circuits.

4.2.1 Derivation of Sensitivity Network

To derive the sensitivity network, let the system of (3.2) be expressed as

$$\boldsymbol{AX} = \boldsymbol{Bu} \tag{4.1}$$

where

$$\boldsymbol{A} = \begin{bmatrix} \boldsymbol{Y}_0(s) & \boldsymbol{0} & -\boldsymbol{H}(s) & \boldsymbol{0} \\ \boldsymbol{0} & \boldsymbol{Y}_0(s) & \boldsymbol{0} & -\boldsymbol{H}(s) \\ -\boldsymbol{Y}_0(s) & \boldsymbol{0} & \boldsymbol{0} & \boldsymbol{I} \\ \boldsymbol{0} & -\boldsymbol{Y}_0(s) & \boldsymbol{I} & \boldsymbol{0} \end{bmatrix}; \quad \boldsymbol{X} = \begin{bmatrix} \boldsymbol{V}_1 \\ \boldsymbol{V}_2 \\ \boldsymbol{K}_1 \\ \boldsymbol{K}_2 \end{bmatrix}; \quad \boldsymbol{B} = \begin{bmatrix} \boldsymbol{I} & \boldsymbol{0} \\ \boldsymbol{0} & \boldsymbol{I} \\ \boldsymbol{I} & \boldsymbol{0} \\ \boldsymbol{0} & \boldsymbol{I} \end{bmatrix}; \quad \boldsymbol{u} = \begin{bmatrix} \boldsymbol{I}_1 \\ \boldsymbol{I}_2 \end{bmatrix} \tag{4.2}$$

Differentiating (4.1) with respect to a transmission line parameter λ yields

$$\boldsymbol{AX}^s = \boldsymbol{Bu}^s - \frac{\partial \boldsymbol{A}}{\partial \lambda}\mathbf{X} \tag{4.3}$$

where

$$\boldsymbol{X}^s = \begin{bmatrix} \boldsymbol{V}_1^s \\ \boldsymbol{V}_2^s \\ \boldsymbol{K}_1^s \\ \boldsymbol{K}_2^s \end{bmatrix} = \begin{bmatrix} \dfrac{\partial \boldsymbol{V}_1}{\partial \lambda} \\ \dfrac{\partial \boldsymbol{V}_2}{\partial \lambda} \\ \dfrac{\partial \boldsymbol{K}_1}{\partial \lambda} \\ \dfrac{\partial \boldsymbol{K}_2}{\partial \lambda} \end{bmatrix}; \qquad \boldsymbol{u}^s = \begin{bmatrix} \boldsymbol{I}_1^s \\ \boldsymbol{I}_2^s \end{bmatrix} = \begin{bmatrix} \dfrac{\partial \boldsymbol{I}_1}{\partial \lambda} \\ \dfrac{\partial \boldsymbol{I}_2}{\partial \lambda} \end{bmatrix} \tag{4.4}$$

Equation (4.3) represents the sensitivity network with respect to λ, where $\boldsymbol{V}_1^s$ and $\boldsymbol{V}_2^s$ are the sensitivities of the voltages; $\boldsymbol{I}_1^s$ and $\boldsymbol{I}_2^s$ are the sensitivities of the currents; and $\boldsymbol{K}_1^s$ and $\boldsymbol{K}_2^s$ are the sensitivities of the $\boldsymbol{K}_1$ and $\boldsymbol{K}_2$ variables, respectively.

The sensitivity network of (4.3) is similar to (4.1) and contains the following additional terms

$$\frac{\partial \boldsymbol{A}}{\partial \lambda}\boldsymbol{X} = \begin{bmatrix} \boldsymbol{\Psi}_1 \\ \boldsymbol{\Psi}_2 \\ \boldsymbol{\Psi}_3 \\ \boldsymbol{\Psi}_4 \end{bmatrix} = \begin{bmatrix} \dfrac{\partial \boldsymbol{Y_o}}{\partial \lambda}\boldsymbol{V_1} - \dfrac{\partial \boldsymbol{H}}{\partial \lambda}\boldsymbol{K}_1 \\ \dfrac{\partial \boldsymbol{Y_o}}{\partial \lambda}\boldsymbol{V_2} - \dfrac{\partial \boldsymbol{H}}{\partial \lambda}\boldsymbol{K}_2 \\ -\dfrac{\partial \boldsymbol{Y_o}}{\partial \lambda}\boldsymbol{V}_1 \\ -\dfrac{\partial \boldsymbol{Y_o}}{\partial \lambda}\boldsymbol{V}_2 \end{bmatrix} \tag{4.5}$$

From the above analysis, both the original and sensitivity networks have same $\boldsymbol{A}$ and $\boldsymbol{B}$ matrices and that $(\partial \boldsymbol{A}/\partial\lambda)\boldsymbol{X}$ can be modeled with additional voltage and current sources. As a result, the Modified Nodal Analysis (MNA) matrices of the original and sensitivity networks will be the same, however, the applied sources of the two networks will be different due to $(\partial \boldsymbol{A}/\partial\lambda)\boldsymbol{X}$. Thus the solution of the sensitivity network does not require additional Lower-Upper (LU) decompositions to invert the sensitivity matrix equations, since the LU matrices are known from the solution of the original network. This leads to significant computational savings, since the sensitivities with respect to all design parameters are obtained from the solution of the original network.

4.2.2 Calculating $\partial \boldsymbol{Y_0}(s)/\partial\lambda$ and $\partial \boldsymbol{H}(s)/\partial\lambda$

This section discusses how to derive $\partial \boldsymbol{A}/\partial\lambda$ which is obtained by differentiating (3.4) with respect to λ to calculate $\partial \boldsymbol{Y_0}(s)/\partial\lambda$ and $\partial \boldsymbol{H}(s)/\partial\lambda$. For two-conductor transmission lines, $Y_0(s)$ and $H(s)$ are scalar functions and differentiating these functions at each frequency point with respect to λ yields

$$\frac{\partial}{\partial\lambda}Y_o(s)=\frac{1}{2}\left(\frac{G(s)+sC(s)}{R(s)+sL(s)}\right)^{-\frac{1}{2}}\frac{\partial}{\partial\lambda}\left(\frac{G(s)+sC(s)}{R(s)+sL(s)}\right) \tag{4.6}$$

$$\frac{\partial}{\partial\lambda}H(s)=-\left(\frac{\partial l}{\partial\lambda}\cdot\Gamma(s)+l\cdot\frac{\partial\Gamma(s)}{\lambda}\right)\cdot H(s) \tag{4.7}$$

where

$$\frac{\partial\Gamma(s)}{\lambda}=\frac{1}{2}\left(\left(G(s)+sC(s)\right)\left(R(s)+sL(s)\right)\right)^{-\frac{1}{2}}\cdot\frac{\partial}{\partial\lambda}\left(\left(G(s)+sC(s)\right)\left(R(s)+sL(s)\right)\right) \tag{4.8}$$

The time domain realization of the sensitivity network is obtained by approximating $\partial H(s)/\partial\lambda$ as a delay rational function, where $H(s)$ is obtained using (3.4), and $\partial\Gamma(s)/\partial\lambda$ and $\Gamma(s)$ are approximated as rational functions. Similarly, $\partial Y_0(s)/\partial\lambda$ is also approximated as a rational function.

For multi-conductor transmission lines, $\boldsymbol{Y_0}(s)$ is differentiated with respect to λ

$$\frac{\partial \boldsymbol{Y}_0(s)}{\partial\lambda}=\boldsymbol{\Gamma}(s)^{-1}\left(\frac{\partial \boldsymbol{G}(s)}{\partial\lambda}+s\frac{\partial \boldsymbol{C}(s)}{\partial\lambda}-\frac{\partial \boldsymbol{\Gamma}(s)}{\partial\lambda}\cdot\boldsymbol{Y}_0(s)\right) \tag{4.9}$$

where

$$\frac{\partial \boldsymbol{\Gamma}(s)}{\partial \lambda}\cdot \boldsymbol{\Gamma}(s)+\boldsymbol{\Gamma}(s)\cdot\frac{\partial \boldsymbol{\Gamma}(s)}{\partial \lambda}=\frac{\partial}{\partial \lambda}\left((\boldsymbol{G}(s)+s\boldsymbol{C}(s))(\boldsymbol{R}(s)+s\boldsymbol{L}(s))\right) \tag{4.10}$$

Since the p.u.l. parameters are known, (4.9) and (4.10) can be used to calculate values $\partial \boldsymbol{Y_0}(s)/\partial\lambda$ at each frequency point.

The calculation of $\partial \boldsymbol{H}(s)/\partial\lambda$ is slightly more complicated, since it corresponds to an exponential matrix where the p.u.l. matrices do not compute (i.e. $\partial e^{-\boldsymbol{\Gamma} l}/\partial\lambda \neq \partial(\boldsymbol{\Gamma} l)/\partial\lambda \cdot e^{-\boldsymbol{\Gamma} l}$). Thus to calculate $\partial \boldsymbol{H}(s)/\partial\lambda$, the delay rational approximation of (3.10) is differentiated with respect to λ,

$$\frac{\boldsymbol{H}(s)}{\partial \lambda}=-s\frac{\partial \hat{\boldsymbol{T}}_{\min}}{\partial \lambda}\cdot \boldsymbol{H}(s)+e^{-s\hat{\boldsymbol{T}}_{min}}\cdot\frac{\partial e^{-\boldsymbol{\Phi}}}{\partial \lambda} \tag{4.11}$$

where the Padé approximation of (3.7) is used to calculate $\partial e^{-\boldsymbol{\Phi}}/\partial\lambda$, as

$$\frac{\partial e^{-\boldsymbol{\Phi}}}{\partial \lambda}\approx P_N(\boldsymbol{\Phi})^{-1}\left(\frac{\partial Q_M(\boldsymbol{\Phi})}{\partial \lambda}-\frac{\partial P_N(\boldsymbol{\Phi})}{\partial \lambda}\cdot e^{-\boldsymbol{\Phi}}\right) \tag{4.12}$$

The terms $\partial Q_M(\boldsymbol{\Phi})/\partial\lambda$ and $\partial P_N(\boldsymbol{\Phi})/\partial\lambda$ are obtained by differentiating (3.16),

$$\frac{\partial Q_M(\boldsymbol{\Phi})}{\partial \lambda}=q_1\frac{\partial \boldsymbol{\Phi}}{\partial \lambda}+q_2\left(\frac{\partial \boldsymbol{\Phi}}{\partial \lambda}\cdot\boldsymbol{\Phi}+\boldsymbol{\Phi}\cdot\frac{\partial \boldsymbol{\Phi}}{\partial \lambda}\right)+q_3\left(\frac{\partial \boldsymbol{\Phi}}{\partial \lambda}\cdot\boldsymbol{\Phi}^2+\boldsymbol{\Phi}\cdot\frac{\partial \boldsymbol{\Phi}}{\partial \lambda}\cdot\boldsymbol{\Phi}+\boldsymbol{\Phi}^2\cdot\frac{\partial \boldsymbol{\Phi}}{\partial \lambda}\right)+\cdots \tag{4.13}$$

$$\frac{\partial P_N(\boldsymbol{\Phi})}{\partial \lambda}=p_1\frac{\partial \boldsymbol{\Phi}}{\partial \lambda}+p_2\left(\frac{\partial \boldsymbol{\Phi}}{\partial \lambda}\cdot\boldsymbol{\Phi}+\boldsymbol{\Phi}\cdot\frac{\partial \boldsymbol{\Phi}}{\partial \lambda}\right)+p_3\left(\frac{\partial \boldsymbol{\Phi}}{\partial \lambda}\cdot\boldsymbol{\Phi}^2+\boldsymbol{\Phi}\cdot\frac{\partial \boldsymbol{\Phi}}{\partial \lambda}\cdot\boldsymbol{\Phi}+\boldsymbol{\Phi}^2\cdot\frac{\partial \boldsymbol{\Phi}}{\partial \lambda}\right)+\cdots \tag{4.14}$$

where q_i and p_i correspond to the Padé coefficients of (3.16), defined as $q_i = \big((M+N-i)!M!\big)/\big((M+N)!i!(M-i)!\big)$, $p_i = \big((M+N-i)!N!\big)/\big((M+N)!i!(N-i)!\big)$ and

$$\frac{\partial \boldsymbol{\Phi}}{\partial \lambda} = \frac{\partial l}{\partial \lambda} \cdot \boldsymbol{\Gamma}(s) + l \cdot \frac{\partial \boldsymbol{\Gamma}(s)}{\partial \lambda} - s \frac{\partial \hat{\boldsymbol{T}}_{min}}{\partial \lambda} \tag{4.15}$$

The value $\partial \hat{\boldsymbol{T}}_{min} / \partial \lambda$ corresponds to the derivative of the minimum eigenvalue of $l(\hat{\boldsymbol{C}}_{\infty} \hat{\boldsymbol{L}}_{\infty})^{1/2}$ and is obtained using the procedure of [77]. Thus by solving (4.10)-(4.15), $\partial \boldsymbol{H}(s) / \partial \lambda$ can be calculated.

In this work, the time domain representations for both the original and sensitivity networks are obtained by using the vector fitting algorithm [20] to approximate $\boldsymbol{\Gamma}(s)$ and $\boldsymbol{Y_0}(s)$ as rational functions and using the Padé approximation of (3.14)-(3.16) to approximate $\boldsymbol{H}(s)$. For the sensitivity network, $\partial \boldsymbol{Y_0}(s)/\partial \lambda$ and $\partial e^{-\boldsymbol{\Phi}} / \partial \lambda$ are also approximated as rational functions using the vector fitting algorithm [20]. With the knowledge of the rational functions $\boldsymbol{H}(s)$ and $\partial e^{-\boldsymbol{\Phi}} / \partial \lambda$, (4.11) is used to derive the rational approximation for $\partial \boldsymbol{H}(s) / \partial \lambda$. Noted that the rational approximations of $\partial \boldsymbol{Y_0}(s)/\partial \lambda$ and $\partial \boldsymbol{H}(s) / \partial \lambda$ do not significantly increase the computational complexity of the sensitivity network since they are modeled as external sources which depend on $\boldsymbol{X}$ (i.e. solution of the original network). As a result, MNA matrices for both the original and sensitivity networks are the same and the solution of the sensitivity network is obtained from the same LU matrices used to solve the original network.

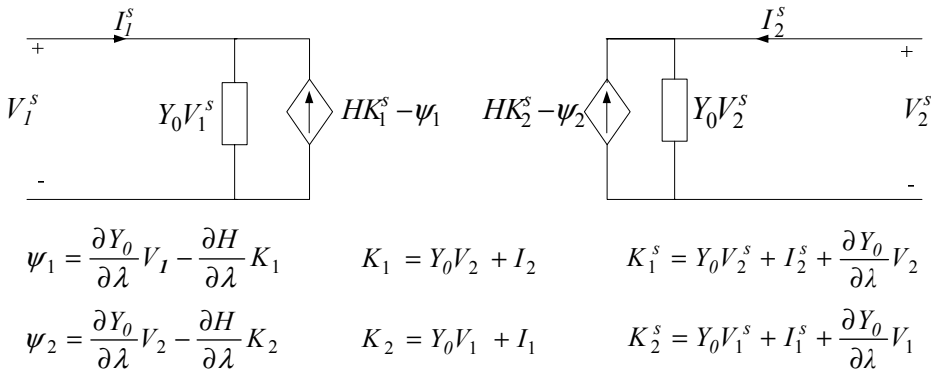

Figure 4-1: Basic sensitivity network realization of a 2-conductor transmission line based on PMoC.

4.2.3 Circuit Realization of Sensitivity Network

The circuit realization of the original network using the PMoC macromodel is described in Chapter 3 for the two-conductor and multi-conductor cases. This section describes the circuit realization of the sensitivity network of (4.3).

Figure 4-1 shows the circuit realization of the sensitivity network for a two-conductor transmission line, where $Y_0(s)$ and $\partial Y_0(s)/\partial\lambda$ are approximated as rational functions and $H(s)$ and $\partial H(s)/\partial\lambda$ are approximated as delayed rational functions as described in Section 4.2.2. As an example of a multi-conductor transmission line, Figure 4-2 shows the circuit realization of the sensitivity network of a three-conductor transmission line (two signal and one reference conductors). Figure 4-2a realizes the sensitivity variables at the near and far end due to the transformation matrices $\boldsymbol{E}_V$ and $\boldsymbol{E}_I$. Figure 4-2b realizes the partially decoupled sensitivity network described by the transformed variables of $\hat{\boldsymbol{Y}}_{\boldsymbol{0}}(s)$, $\hat{\boldsymbol{H}}(s)$, $\partial\hat{\boldsymbol{Y}}_{\boldsymbol{0}}(s)/\partial\lambda$ and $\partial\hat{\boldsymbol{H}}(s)/\partial\lambda$.

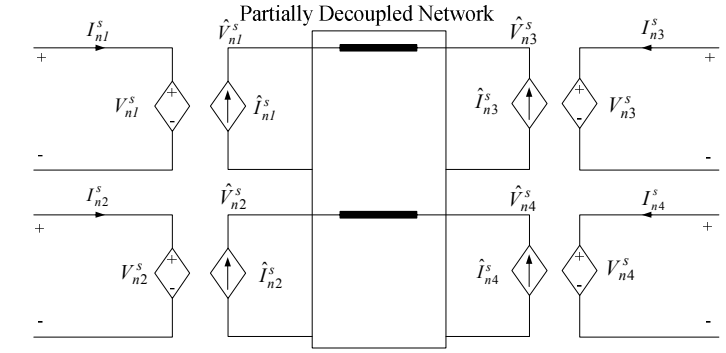

$$\boldsymbol{V}_1^s=\begin{bmatrix}V_{n1}^s\\V_{n2}^s\end{bmatrix}\quad \boldsymbol{V}_2^s=\begin{bmatrix}V_{n3}^s\\V_{n4}^s\end{bmatrix}\quad \boldsymbol{I}_1^s=\begin{bmatrix}I_{n1}^s\\I_{n2}^s\end{bmatrix}\quad \boldsymbol{I}_2^s=\begin{bmatrix}I_{n3}^s\\I_{n4}^s\end{bmatrix}\qquad \boldsymbol{E}_V^s=\begin{bmatrix}\frac{\partial E_{V11}}{\partial\lambda} & \frac{\partial E_{V12}}{\partial\lambda}\\ \frac{\partial E_{V21}}{\partial\lambda} & \frac{\partial E_{V22}}{\partial\lambda}\end{bmatrix}=\begin{bmatrix}E_{V11}^s & E_{V12}^s\\E_{V21}^s & E_{V22}^s\end{bmatrix}$$

$$\hat{\boldsymbol{V}}_1^s=\begin{bmatrix}\hat{V}_{n1}^s\\\hat{V}_{n2}^s\end{bmatrix}\quad \hat{\boldsymbol{V}}_2^s=\begin{bmatrix}\hat{V}_{n3}^s\\\hat{V}_{n4}^s\end{bmatrix}\quad \hat{\boldsymbol{I}}_1^s=\begin{bmatrix}\hat{I}_{n1}^s\\\hat{I}_{n2}^s\end{bmatrix}\quad \hat{\boldsymbol{I}}_2^s=\begin{bmatrix}\hat{I}_{n3}^s\\\hat{I}_{n4}^s\end{bmatrix}$$

$$\boldsymbol{E}_I^s=\begin{bmatrix}\frac{\partial E_{I11}}{\partial\lambda} & \frac{\partial E_{I12}}{\partial\lambda}\\ \frac{\partial E_{I21}}{\partial\lambda} & \frac{\partial E_{I22}}{\partial\lambda}\end{bmatrix}=\begin{bmatrix}E_{I11}^s & E_{I12}^s\\E_{I21}^s & E_{I22}^s\end{bmatrix}$$

$$\boldsymbol{V}_1=\begin{bmatrix}V_{n1}\\V_{n2}\end{bmatrix}\quad \boldsymbol{V}_2=\begin{bmatrix}V_{n3}\\V_{n4}\end{bmatrix}\quad \boldsymbol{I}_1=\begin{bmatrix}I_{n1}\\I_{n2}\end{bmatrix}\quad \boldsymbol{I}_2=\begin{bmatrix}I_{n3}\\I_{n4}\end{bmatrix}$$

$$\hat{\boldsymbol{V}}_1=\begin{bmatrix}\hat{V}_{n1}\\\hat{V}_{n2}\end{bmatrix}\quad \hat{\boldsymbol{V}}_2=\begin{bmatrix}\hat{V}_{n3}\\\hat{V}_{n4}\end{bmatrix}\quad \hat{\boldsymbol{I}}_1=\begin{bmatrix}\hat{I}_{n1}\\\hat{I}_{n2}\end{bmatrix}\quad \hat{\boldsymbol{I}}_2=\begin{bmatrix}\hat{I}_{n3}\\\hat{I}_{n4}\end{bmatrix}\qquad \boldsymbol{E}_V=\begin{bmatrix}E_{V11} & E_{V12}\\E_{V21} & E_{V22}\end{bmatrix}\quad \boldsymbol{E}_I^{-1}=\begin{bmatrix}E_{I11} & E_{I12}\\E_{I21} & E_{I22}\end{bmatrix}$$

$$\boldsymbol{V}_1^s=\boldsymbol{E}_V\hat{\boldsymbol{V}}_1^s+\boldsymbol{E}_V^s\hat{\boldsymbol{V}}_1\quad \boldsymbol{V}_2^s=\boldsymbol{E}_V\hat{\boldsymbol{V}}_2^s+\boldsymbol{E}_V^s\hat{\boldsymbol{V}}_2\quad \hat{\boldsymbol{I}}_1^s=\boldsymbol{E}_I^{-1}(\boldsymbol{I}_1^s-\boldsymbol{E}_I^s\hat{\boldsymbol{I}}_1)\quad \hat{\boldsymbol{I}}_2^s=\boldsymbol{E}_I^{-1}(\boldsymbol{I}_2^s-\boldsymbol{E}_I^s\hat{\boldsymbol{I}}_2)$$

(a)

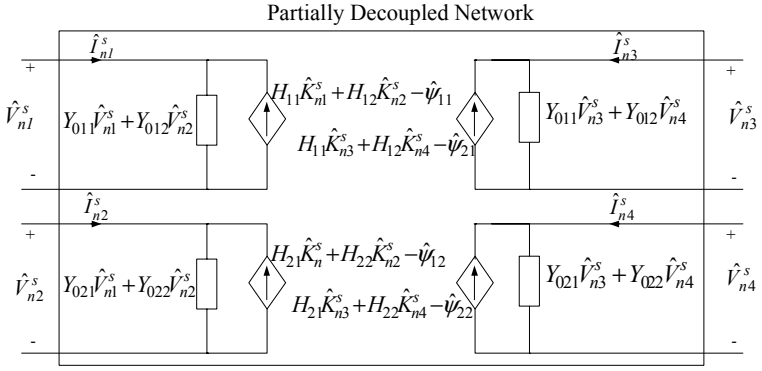

$$\hat{\boldsymbol{\psi}}_1=\begin{bmatrix}\hat{\psi}_{11}\\\hat{\psi}_{12}\end{bmatrix}=\frac{\partial\hat{\boldsymbol{Y}}_0}{\partial\lambda}\hat{\boldsymbol{V}}_1-\frac{\partial\hat{\boldsymbol{H}}}{\partial\lambda}\hat{\boldsymbol{K}}_1\quad \hat{\boldsymbol{K}}_1^s=\begin{bmatrix}\hat{K}_{n1}^s\\\hat{K}_{n2}^s\end{bmatrix}=\hat{\boldsymbol{Y}}_0\hat{\boldsymbol{V}}_2^s+\hat{\boldsymbol{I}}_2^s+\frac{\partial\hat{\boldsymbol{Y}}_0}{\partial\lambda}\hat{\boldsymbol{V}}_2\quad \hat{\boldsymbol{Y}}_0=\begin{bmatrix}Y_{011} & Y_{012}\\Y_{021} & Y_{022}\end{bmatrix}$$

$$\hat{\boldsymbol{\psi}}_2=\begin{bmatrix}\hat{\psi}_{21}\\\hat{\psi}_{22}\end{bmatrix}=\frac{\partial\hat{\boldsymbol{Y}}_0}{\partial\lambda}\hat{\boldsymbol{V}}_2-\frac{\partial\hat{\boldsymbol{H}}}{\partial\lambda}\hat{\boldsymbol{K}}_2\quad \hat{\boldsymbol{K}}_2^s=\begin{bmatrix}\hat{K}_{n3}^s\\\hat{K}_{n4}^s\end{bmatrix}=\hat{\boldsymbol{Y}}_0\hat{\boldsymbol{V}}_1^s+\hat{\boldsymbol{I}}_1^s+\frac{\partial\hat{\boldsymbol{Y}}_0}{\partial\lambda}\hat{\boldsymbol{V}}_1\quad \hat{\boldsymbol{H}}=\begin{bmatrix}H_{11} & H_{12}\\H_{21} & H_{22}\end{bmatrix}$$

$$\hat{\boldsymbol{K}}_1=\hat{\boldsymbol{Y}}_0\hat{\boldsymbol{V}}_2+\hat{\boldsymbol{I}}_2\qquad \hat{\boldsymbol{K}}_2=\hat{\boldsymbol{Y}}_0\hat{\boldsymbol{V}}_1+\hat{\boldsymbol{I}}_1$$

(b)

Figure 4-2: Basic sensitivity network realization of a 3-conductor transmission line based on PMoC (a) sensitivity of modal transformation (b) sensitivity of partially decoupled network.

4.2.4 Sensitivity Analysis with respect to Other Physical Parameters

When studying the sensitivity analysis of distributed networks, the design parameters of interconnects are usually required with respect to physical parameters (such as width and spacing of conductors). The sensitivity of electrical parameters is often intermediate steps to calculation of sensitivities of physical parameters. In the case where λ represents a physical parameter of an interconnect, the sensitivity analysis can be obtained using the chain rule as

$$\frac{\partial \boldsymbol{X}}{\partial \lambda} = \sum_{i=1} \sum_{j=1} \left(\frac{\partial \boldsymbol{X}}{\partial R_{i,j}} \frac{\partial R_{i,j}}{\partial \lambda} + \frac{\partial \boldsymbol{X}}{\partial L_{i,j}} \frac{\partial L_{i,j}}{\partial \lambda} + \frac{\partial \boldsymbol{X}}{\partial G_{i,j}} \frac{\partial G_{i,j}}{\partial \lambda} + \frac{\partial \boldsymbol{X}}{\partial C_{i,j}} \frac{\partial C_{i,j}}{\partial \lambda} \right) \tag{4.16}$$

where $R_{i,j}$, $L_{i,j}$, $G_{i,j}$, and $C_{i,j}$ are the p.u.l parameters and subscript i and j are matrix indices.

4.3 Numerical Examples

Three examples are presented in this section to demonstrate the validity and efficiency of the proposed sensitivity analysis. The transient responses were obtained using HSPICE [38], and the comparison of CPU time was done using the SUN Blade 1500 workstation.

Example 1: In this example, a seven-transmission line network with nonlinear CMOS inverters is shown in Figure 4-3. The p.u.l. parameters of each line are R=8.26Ω/m, L=361nH/m, C=140pF/m, G=0.0 and the length of each line is 10cm. The input voltage is a trapezoidal pulse of amplitude 5V with rise/fall time of 0.2ns, pulse width of 5ns and

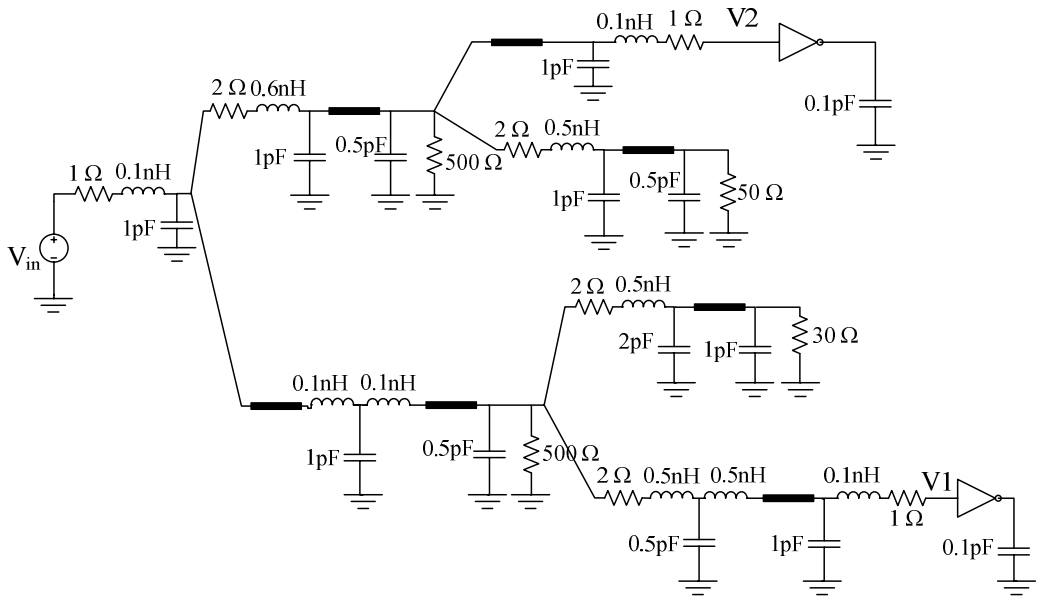

Figure 4-3: Transmission line network with nonlinear termination (Example1).

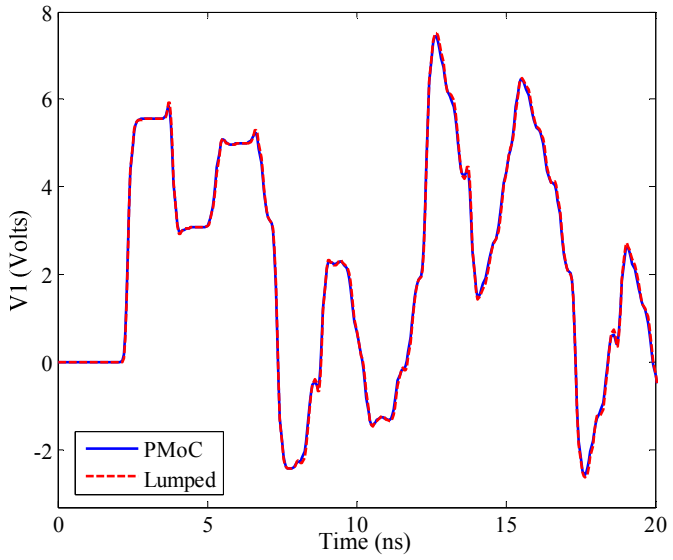

Figure 4-4: Transient response of V1 (Example1).

a period of 10ns. The transient response at node V1 using the PMoC and the conventional lumped model [1] is shown in Figure 4-4. Figure 4-5 shows the sensitivities with respect to the electrical p.u.l. parameters of the resistance, inductance, capacitance, and line

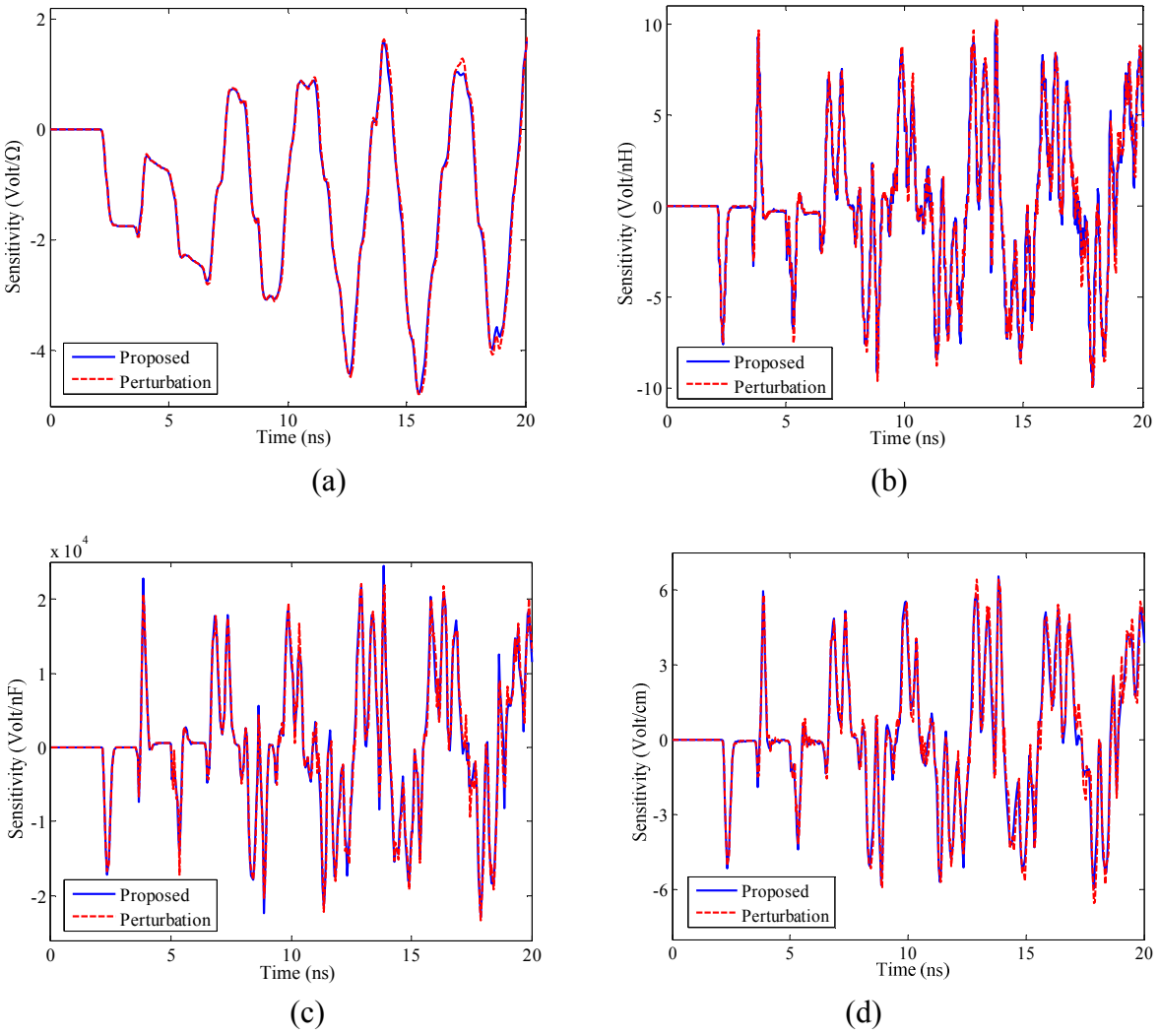

Figure 4-5: Sensitivity of V1 with respect to (a) p.u.l resistance (b) p.u.l inductance (c) p.u.l capacitance and (d) line length (Example1).

length. The results of the proposed method are compared with the perturbation of the conventional lumped segmentation model (referred to as SPICE Perturbation). Both the proposed method and the SPICE perturbation results are in good agreement.

It is to be noted that using the proposed PMoC provides the following advantages. i) Using the PMoC provides significant CPU advantage compared to lumped segmentation model. For this example the PMoC required 3.7 seconds while the conventional lumped

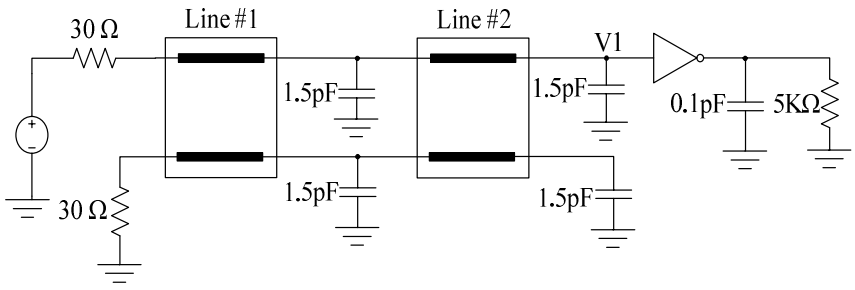

Figure 4-6: Multiconductor transmission line network with nonlinear CMOS inverter (example 2).

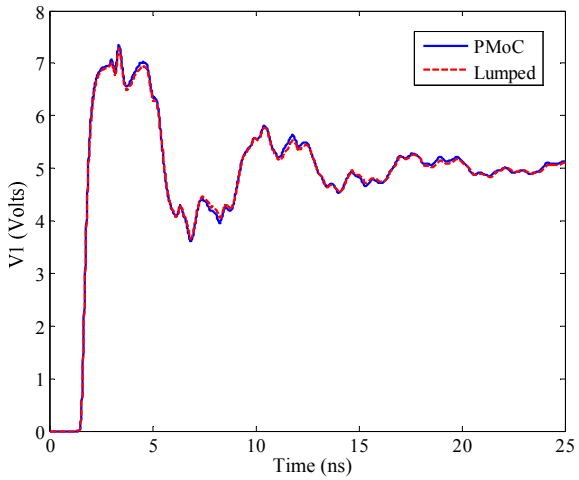

Figure 4-7: Transient response of V1 (example 2).

model required 36 seconds ii) Perturbation based techniques can lead to inaccurate results depending on the magnitude of the perturbation [41]. iii) In addition the perturbed network must be solved separately for every parameter of interest. However, in the proposed approach, the sensitivity information with respect to all the parameters can be essentially obtained from the solution of the original network, since both the original and sensitivity networks have the same MNA matrices and additional LU decompositions to invert the sensitivity network matrices are not required.

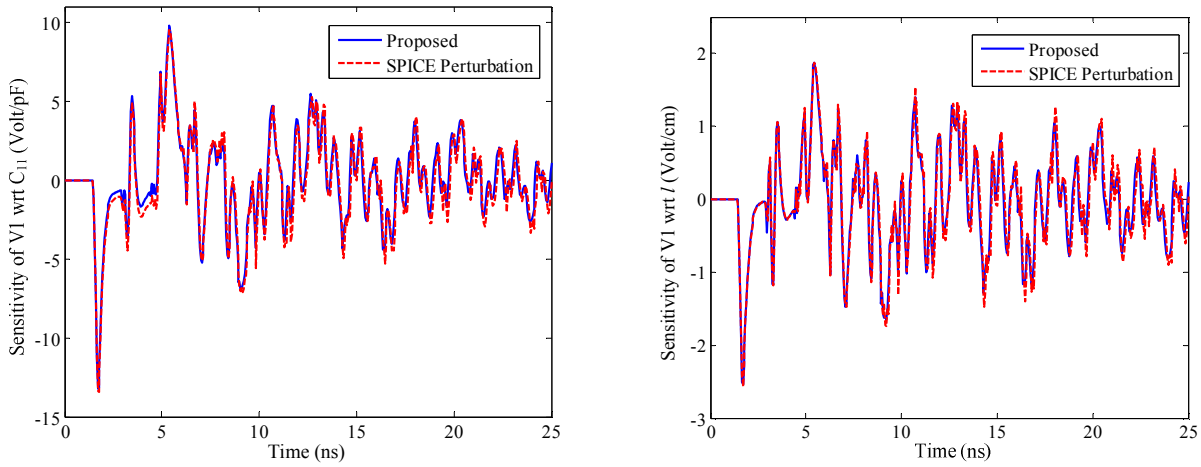

Figure 4-8: Sensitivity of V1 with respect to (a) p.u.l R11 (b) p.u.l L11 (c) p.u.l C11 and (d) line length l (Example 2).

Example 2: A coupled interconnect network terminated with nonlinear CMOS inverters is shown in Figure 4-6. The length of each line is 10 cm and the p.u.l parameters are

$$R=\begin{bmatrix}0.14 & 0\\ 0 & 0.14\end{bmatrix}\ \Omega/\text{cm};\quad L=\begin{bmatrix}6.3 & 2.9\\ 2.9 & 6.3\end{bmatrix}\ \text{nH/cm};\quad C=\begin{bmatrix}1.1 & -0.45\\ -0.45 & 1.1\end{bmatrix}\ \text{pF/cm}. \quad (4.17)$$

The input voltage is a step of amplitude 5V with rise time of 0.2ns. The transient response at node V1 using the PMoC and the conventional lumped model is shown in Figure 4-7. Figure 4-8 shows the sensitivities with respect to the electrical p.u.l. capacitance of C_{11} and line length l. The results of the proposed method are compared with the perturbation of the conventional lumped segmentation model. Both the proposed method and the SPICE perturbation results are in good agreement.

Example 3: This example illustrates the proposed sensitivity algorithm in a network optimization process. Figure 4-9 shows multi-conductor transmission lines, terminated

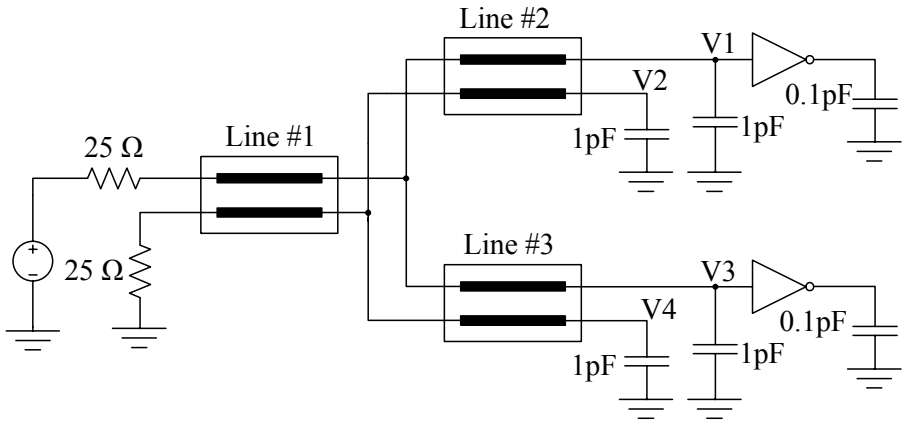

Figure 4-9: Multiconductor transmission line network with nonlinear CMOS inverter (example 3).

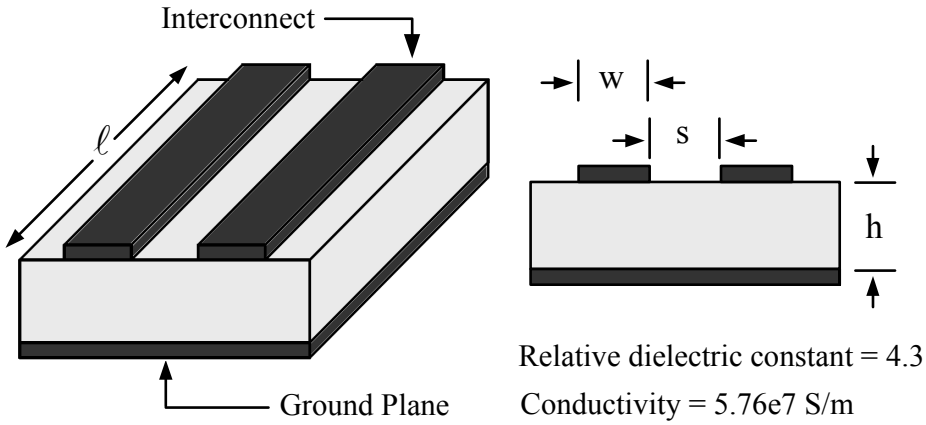

Figure 4-10: Physical/geometrical parameters for the MTL subnetwork in Figure 4-9 (Example 3).

with two nonlinear CMOS inverters. The physical description of the interconnect networks are depicted in Figure 4-10. The p.u.l parameters are computed from the physical description of Figure 4-10 using HSPICE field solver and include skin effect losses [64]. For this example, it is desired to achieve the following performance specifications:

1. The delays of V1 and V3 should not exceed 0.6 ns and 0.7 ns based on threshold voltage of 2 V.
2. The voltage V1 > 2.6 V for t > 1 ns and V3 > 2.6 for t > 1.1 ns.
3. The crosstalk of the victim line voltages (V2 and V4) should be confined between -0.5 V and 0.5V.

The above performance specifications are subject to the following constraints:

$$\ell_1 + \ell_2 + \ell_3 = 10\,\text{cm}; \qquad 2w + s = 500\ \mu\text{m}$$
$$50\ \mu\text{m} \le w \le 200\ \mu\text{m}; \qquad 300\ \mu\text{m} \le h \le 600\ \mu\text{m} \tag{4-18}$$

The initial values are taken as

$$\ell_1 = 4\,\text{cm}; \quad \ell_2 = \ell_3 = 3\,\text{cm}; \quad w = 100\ \mu\text{m}; \quad h = 400\ \mu\text{m} \tag{4-19}$$

The input voltage of the circuit is a 3 V step source with a time rise of 0.2 ns. Sample sensitivities of node voltages V1 and V2 with respect to the conductor width w and the length of the second line ℓ_2 for the initial values of (4-19) are shown in Figure 4-11, showing good agreement between the proposed algorithm and perturbation of the conventional lumped model. Figure 4-12 shows the transient response of the circuit, clearly showing the performance specifications are being violated before optimization.

Using the MATLAB optimization toolbox [78], coupled with the proposed sensitivity analysis implemented in HSPICE, the following optimized variable were obtained

$$\ell_1 = 0.500\,\text{cm}; \quad \ell_2 = 4.744\,\text{cm}; \quad \ell_3 = 4.756\,\text{cm}$$
$$w = 135.11\ \mu\text{m}; \quad h = 300.00\ \mu\text{m} \tag{4.20}$$

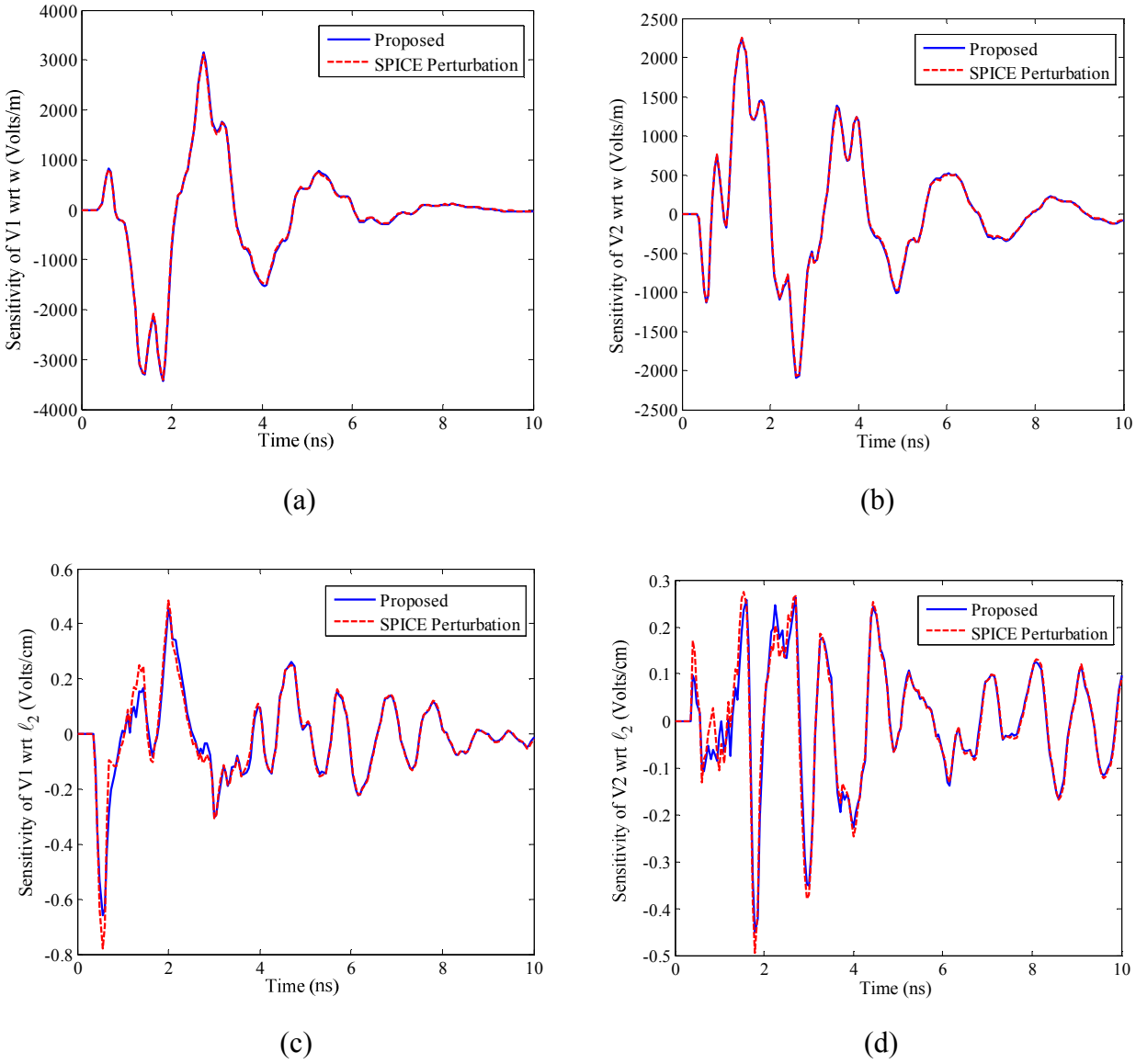

Figure 4-11: Sensitivity of V1 and V2 with respect to interconnect width and length (Example 3).

Figure 4-12 shows the comparison between the circuit responses before and after optimization. As observed from the figure, the node voltages meet all the circuit specifications without violating any design constraints.

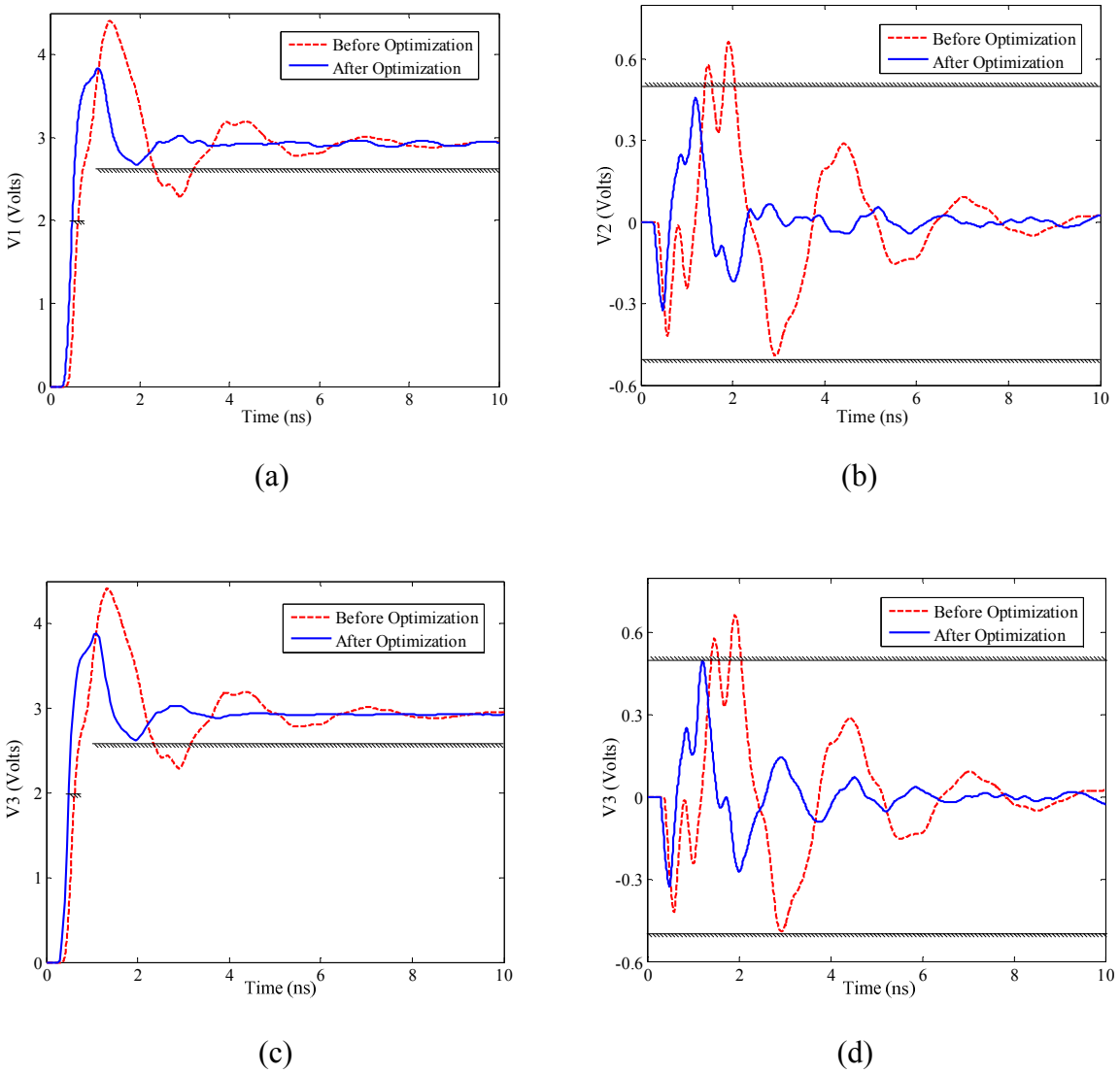

Figure 4-12: Comparison of circuit responses before and after optimization (Example 3).

4.4 Conclusion

This chapter describes an efficient approach to perform sensitivity analysis of lossy transmission lines in the presence of nonlinear terminations. The sensitivity information is derived using the developed Passive Method of Characteristics (PMoC). An important

feature of the proposed method is that the sensitivities are calculated from the solution of the original system resulting in significant computational advantages when compared to perturbation methods.

Chapter 5

5 Analysis of Excited Transmission Lines

5.1 Introduction

Electrically long interconnects exposed to electromagnetic interference may induce undesired results such as signal degradation, false switching and may even damage sensitive devices [1],[4]-[7]. As a result, circuit designers must analyze the electromagnetic interference and compatibility of high speed devices to ensure proper performance and operation.

A passive MoC algorithm was developed in Chapter 3 where the curve fitting to realize the macromodel depends only on per-unit-length parameters and not on the discretization of the macromodel [70],[73]. In this chapter the PMoC macromodel is extended to model high speed interconnects exposed to incident fields. When compared to other passive incident field coupling macromodels, the proposed algorithm is efficient in modeling

electrically long interconnects since it uses delay extraction without segmentation to capture the frequency response. This will be illustrated by numerical examples.

5.2 Formulation of Incident Field Coupling Equations

To model transmission lines with incident field coupling, the transmission line equations of (3.1) are modified to [1]

$$\frac{\partial}{\partial z}\mathbf{V}(z,s)+\left(\mathbf{R}(s)+s\mathbf{L}(s)\right)\mathbf{I}(z,s)=\mathbf{V}_{\mathrm{F}}(z,s)$$

$$\frac{\partial}{\partial z}\mathbf{I}(z,s)+\left(\mathbf{G}(s)+s\mathbf{C}(s)\right)\mathbf{V}(z,s)=\mathbf{I}_{\mathrm{F}}(z,s) \tag{5.1}$$

where s is Laplace transform variable; z is the position variable; $\mathbf{V}(z,s)$ and $\mathbf{I}(z,s)$ represent the voltages and currents of the transmission line; $\mathbf{R}(s)$, $\mathbf{L}(s)$, $\mathbf{G}(s)$ and $\mathbf{C}(s)$ are p.u.l. resistance, inductance, conductance and capacitance matrix parameters, respectively; $\mathbf{V}_{\mathrm{F}}(z,s)$ and $\mathbf{I}_{\mathrm{F}}(z,s)$ are the distributed forcing functions due to the incident field and can be expressed as

$$\mathbf{V}_{\mathrm{F}}(z,s)=-\frac{\partial}{\partial z}\mathbf{E}_{\mathrm{T}}(z,s)+\mathbf{E}_{\mathrm{L}}(z,s)$$

$$\mathbf{I}_{\mathrm{F}}(z,s)=-\left(\mathbf{G}(s)+s\mathbf{C}(s)\right)\mathbf{E}_{\mathrm{T}}(z,s) \tag{5.2}$$

where

$$\mathbf{E}_{\mathrm{L}}(z,s)=\left(\varepsilon_z(x_i,y_i,z)-\varepsilon_z(x_0,y_0,z)\right)$$

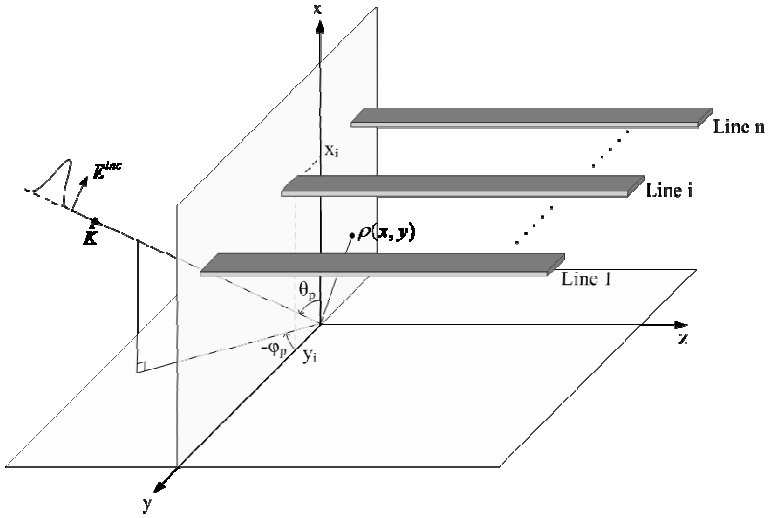

Figure 5-1: Geometry of a multiconductor transmission line exposed to an incident field.

$$\mathbf{E}_{\mathrm{T}}(z,s) = \int_{\rho(x,y)} \vec{\varepsilon}_t\,(\rho,z)\cdot d\vec{l} \tag{5.3}$$

and ε_z and ε_t are longitudinal and transverse components of the incident electric field; (x_i, y_i) and (x_0, y_0) refer to the coordinates of the signal corresponding to the i th conductor; ρ is a parameter of x and y in the transverse plane (Figure 5-1) and $d\vec{l}$ is the differential path length between the signal and reference conductor.

The frequency domain solution of (12) can be expressed as

$$\mathbf{V}(z,s) = \mathbf{Y}_0^{-1} e^{-\boldsymbol{\Gamma} z}\mathbf{I}^{+}(s) - \mathbf{Y}_0^{-1} e^{\boldsymbol{\Gamma} z}\mathbf{I}^{-}(s) + \mathbf{V}^{inc}(z,s)$$

$$\mathbf{I}(z,s) = e^{-\boldsymbol{\Gamma} z}\mathbf{I}^{+}(s) + e^{\boldsymbol{\Gamma} z}\mathbf{I}^{-}(s) + \mathbf{I}^{inc}(z,s) \tag{5.4}$$

where $\mathbf{I}^{+}$ and $\mathbf{I}^{-}$ represent the frequency-varying coefficients of the homogeneous solution; $\mathbf{V}^{\text{inc}}(z,s)$ and $\mathbf{I}^{\text{inc}}(z,s)$ describe the interaction of incident $\mathbf{V}_{\text{F}}(z,s)$ and $\mathbf{I}_{\text{F}}(z,s)$ sources on the transmission line; l is the length of the transmission line; [$\mathbf{I}_1(s)$, $\mathbf{V}_1(s)$] and [$\mathbf{I}_2(s)$, $\mathbf{V}_2(s)$] are the current-voltage pairs at the near-end and far-end ports respectively; $\mathbf{J}_1(s)$ and $\mathbf{J}_2(s)$ are controlled current sources and

$$\boldsymbol{\Gamma}^2 = (\mathbf{G}(s)+s\mathbf{C}(s))(\mathbf{R}(s)+s\mathbf{L}(s))$$

$$\mathbf{Y}_0 = \boldsymbol{\Gamma}^{-1}(\mathbf{G}(s)+s\mathbf{C}(s)) \tag{5.4}$$

are the propagation function and characteristic admittance, respectively.

Electromagnetic fields generated from a far radiating source are treated locally as uniform plane waves [7]. In this case, the electric field of the incident field can be expressed as

$$\vec{E}^{i}(x,y,z) = E(s)(A_x\vec{a}_x + A_y\vec{a}_y + A_z\vec{a}_z)e^{-s\beta_x x}e^{-s\beta_y y}e^{-s\beta_z z} \tag{5.5}$$

where $E(s)$ is the electric field amplitude, A_x, A_y, and A_z are the direction cosines of the incoming wave and $\beta = [\beta_x\ \beta_y\ \beta_z]^T$ is the propagation vector. Substituting (16) into (13) and solving (12), the particular solution of $\mathbf{V}^{\text{inc}}(z,s)$ and $\mathbf{I}^{\text{inc}}(z,s)$ can be expressed as

$$\mathbf{V}^{\text{inc}}(z,s) = E(s)\tilde{\mathbf{V}}^{\text{inc}}(s)e^{-s\beta_z z}$$

$$\mathbf{I}^{\text{inc}}(z,s) = E(s)\tilde{\mathbf{I}}^{\text{inc}}(s)e^{-s\beta_z z} \tag{5.6}$$

where

$$\tilde{\mathbf{V}}^{\text{inc}}(s) = \left(s^2\beta_z{}^2\mathbf{I}_{\text{n}} - (\mathbf{R}+s\mathbf{L})(\mathbf{G}+s\mathbf{C})\right)^{-1} \cdot \left(-s\beta_z\tilde{\mathbf{V}}_{\text{F}} - (\mathbf{R}+s\mathbf{L})\tilde{\mathbf{I}}_{\text{F}}(s)\right)$$

$$\tilde{\mathbf{I}}^{\text{inc}}(s) = \left(s^2\beta_z{}^2\mathbf{I}_{\text{n}} - (\mathbf{G}+s\mathbf{C})(\mathbf{R}+s\mathbf{L})\right)^{-1} \cdot \left(-(\mathbf{G}+s\mathbf{C})\tilde{\mathbf{V}}_{\text{F}}(s) - s\beta_z\tilde{\mathbf{I}}_{\text{F}}(s)\right) \qquad (5.7)$$

and $\mathbf{I}_{\text{n}}$ is the unity matrix. The coefficients $\tilde{\mathbf{V}}_{\text{F}}(s)$ and $\tilde{\mathbf{I}}_{\text{F}}(s)$ are defined as

$$\tilde{\mathbf{V}}_{\text{F}}(s) = \begin{bmatrix} \vdots \\ -\beta_z(\Phi_i^+ \dfrac{e^{-s\psi_i^+}-1}{\psi_i^+} + \Phi_i^- \dfrac{e^{-s\psi_i^-}-1}{\psi_i^-}) + A_z(e^{-s\psi_i^+} - e^{-s\psi_i^-}) \\ \vdots \end{bmatrix} \qquad (5.8)$$

$$\tilde{\mathbf{I}}_{\text{F}}(s) = (\frac{\mathbf{G}}{s} + \mathbf{C}) \begin{bmatrix} \vdots \\ \Phi_i^+ \dfrac{e^{-s\psi_i^+}-1}{\psi_i^+} + \Phi_i^- \dfrac{e^{-s\psi_i^-}-1}{\psi_i^-} \\ \vdots \end{bmatrix} \qquad (5.9)$$

$$\Phi_i^{\pm} = A_x x_i \pm A_y y_i\,; \quad \psi_i^{\pm} = \beta_y y_i \pm \beta_x x_i \qquad (5.10)$$

The expressions of (5.8)-(5.10) correspond for the case when the transmission line network has a ground plane. For the case when the transmission line network has no ground plane $\Phi_i^- = \psi_i^- = 0$. The derivation of the equations is given in Appendix B.

In the next section, the equivalent near- and far-end voltage and current sources due to the incident field are extracted based on the PMoC macromodel.

5.3 Modeling Incident Fields using PMoC

To include the effects of incident field coupling the solution of (5.4) at the near and far end terminals (i.e. $z = 0$ and $z = l$) can be expressed in a form similar to (3.2) as

$$
\begin{aligned}
(\mathbf{I}_1 - \mathbf{I}_1^{inc}) &= \mathbf{Y}_0(\mathbf{V}_1 - \mathbf{V}_1^{inc}) - \mathbf{J}_1(s) \\
(\mathbf{I}_2 - \mathbf{I}_2^{inc}) &= \mathbf{Y}_0(\mathbf{V}_2 - \mathbf{V}_2^{inc}) - \mathbf{J}_2(s) \\
\mathbf{J}_1(s) &= e^{-\boldsymbol{\Gamma} l}[\mathbf{Y}_0(\mathbf{V}_2 - \mathbf{V}_2^{inc}) + (\mathbf{I}_2 - \mathbf{I}_2^{inc})] \\
\mathbf{J}_2(s) &= e^{-\boldsymbol{\Gamma} l}[\mathbf{Y}_0(\mathbf{V}_1 - \mathbf{V}_1^{inc}) + (\mathbf{I}_1 - \mathbf{I}_1^{inc})]
\end{aligned}
\tag{5.11}
$$

where

$$
\begin{aligned}
\mathbf{V}_1^{inc} &= \mathbf{V}^{inc}(0,s) = E(s)\widetilde{\mathbf{V}}^{inc}(s) \\
\mathbf{I}_1^{inc} &= \mathbf{I}^{inc}(0,s) = E(s)\widetilde{\mathbf{I}}^{inc}(s) \\
\mathbf{V}_2^{inc} &= \mathbf{V}^{inc}(l,s) = E(s)\widetilde{\mathbf{V}}^{inc}(s)e^{-s\beta_z l} = \mathbf{V}_1^{inc}e^{-s\beta_z l} \\
\mathbf{I}_2^{inc} &= \mathbf{I}^{inc}(l,s) = E(s)\widetilde{\mathbf{I}}^{inc}(s)e^{-s\beta_z l} = \mathbf{I}_1^{inc}e^{-s\beta_z l}
\end{aligned}
\tag{5.12}
$$

Equation (5.11) represents the solution of Telegrapher's equations with the incident field coupling. In comparison to (3.2), equation (5.11) has the following additional terms $\mathbf{V}_1^{\text{inc}}$, $\mathbf{V}_2^{\text{inc}}$, $\mathbf{I}_1^{\text{inc}}$ and $\mathbf{I}_2^{\text{inc}}$, which represent the external voltage and current sources used to model the effect of the incident fields.

The circuit realization of (5.11) is shown in Figure 5-2. The time domain representation of the incident field coupling is obtained by approximating $\widetilde{\mathbf{V}}^{\text{inc}}(s)$ and $\widetilde{\mathbf{I}}^{\text{inc}}(s)$ as

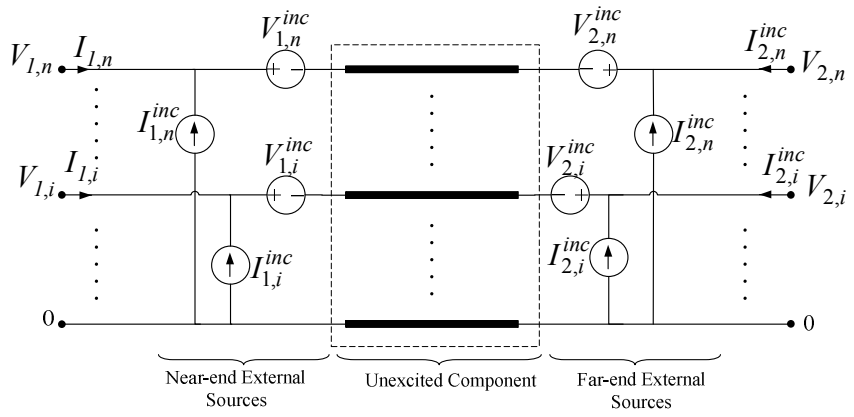

Figure 5-2: Circuit realization of a multiconductor transmission line with incident field coupling.

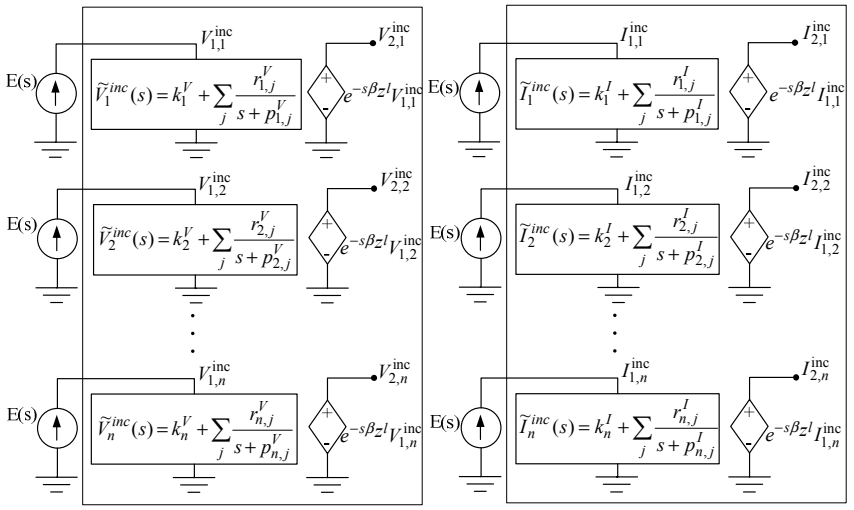

Figure 5-3: Circuit diagram of the incident field equivalent voltage and current sources.

rational functions using the vector fitting algorithm [20]. As illustrated in (5.12), the incident field sources at the far end of the transmission line is derived from the incident field equations at the near end with a $\tau = \beta_z l$ time delay due to the time required by the incident wave to propagate the length of the line. This allows for efficient computation of the incident field coupling of transmission lines in the time domain. In this chapter, once $\mathbf{Q}(s)$, $\hat{\mathbf{Y}}_0(s)$, $\widetilde{\mathbf{V}}^{\text{inc}}(s)$ and $\widetilde{\mathbf{I}}^{\text{inc}}(s)$ are described in terms of rational functions, the

proposed macromodel is realized in HSPICE using Laplace and delay elements to obtain the time-domain response of transmission lines exposed to incident fields [64].

The detailed circuit realization of the unexcited transmission line using the PMoC is described in [73], while the circuit diagram of the incident field coupling sources is provided in Figure 5-3. In this circuit representation, the electric field amplitude $E(s)$ is treated as a current source and the rational approximations of $\widetilde{\mathbf{V}}^{\text{inc}}(s)$ and $\widetilde{\mathbf{I}}^{\text{inc}}(s)$ as impedances to calculate $\mathbf{V}_1^{\text{inc}}$ and $\mathbf{I}_1^{\text{inc}}$ as node voltages. The terms $p_{i,j}^{V}$ and $p_{i,j}^{I}$ represent the poles of the rational approximation; $r_{i,j}^{V}$ and $r_{i,j}^{I}$ are the residues and k_i^{V} and k_i^{I} are the quotient variables. The node vectors of $\mathbf{V}_1^{\text{inc}}$ and $\mathbf{I}_1^{\text{inc}}$ are also time shifted by $\tau = \beta_z l$ to calculate $\mathbf{V}_2^{\text{inc}}$ and $\mathbf{I}_1^{\text{inc}}$. Controlled sources are then used to place $\mathbf{V}_1^{\text{inc}}$, $\mathbf{V}_2^{\text{inc}}$, $\mathbf{I}_1^{\text{inc}}$ and $\mathbf{I}_2^{\text{inc}}$ in Figure 5-2 to model the overall effect of the incident field on transmission lines.

5.4 Numerical Results

Two examples are provided in this section to demonstrate the accuracy and efficiency of the proposed time domain macromodel in the presence of electromagnetic fields. The results of the proposed algorithm are also compared with other passive macromodels such as the matrix rational approximation [53] and DEPACT [54] algorithms.

Example 1) Fig 5-4 shows the cross sectional view of a microstrip structure. The per-unit-length parameters of the structure are obtained using HSPICE field solver, and includes

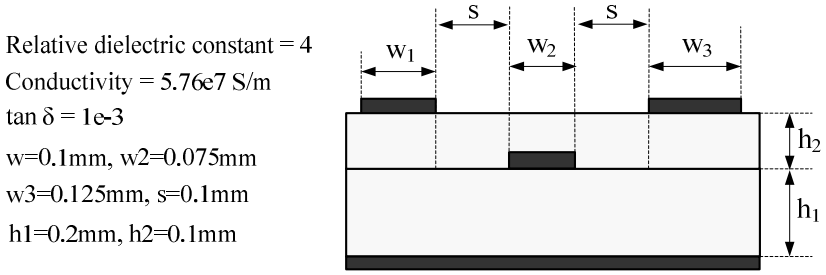

Figure 5-4: Cross-sectional view of the multiconductor transmission line (example 1).

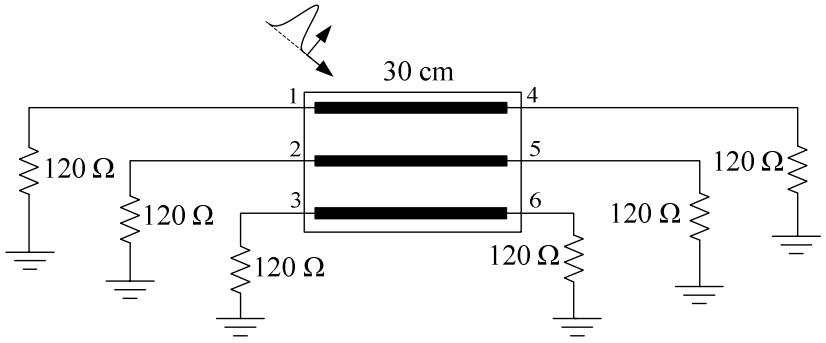

Figure 5-5: Transmission line network with linear termination (example 1).

skin effect losses. The length of the line is 30 cm. The first analysis terminates the interconnect network with 120Ω resistors as shown in Figure 5-5, and the network is exposed to an incident electric field of double exponential waveform $E(t) = E_0\left(\exp(-\alpha t) - \exp(-\beta t)\right)$ with $\alpha = 4\times10^8$ and $\beta = 10^9$, the peak amplitude E_0 =1kV/m, an elevation angle of θ_p = 60° , an azimuthal angle of φ_p = −60° and a polarized angle of θ_E = −90°. The time domain responses of nodes 1, 2, 4 and 5 are shown in Figure 5-6. To verify the accuracy of the proposed macromodel, the results are also compared with the inverse discrete Fourier transform (IDFT) of the exact frequency-domain solution [1]. Both methodologies give similar time domain responses.

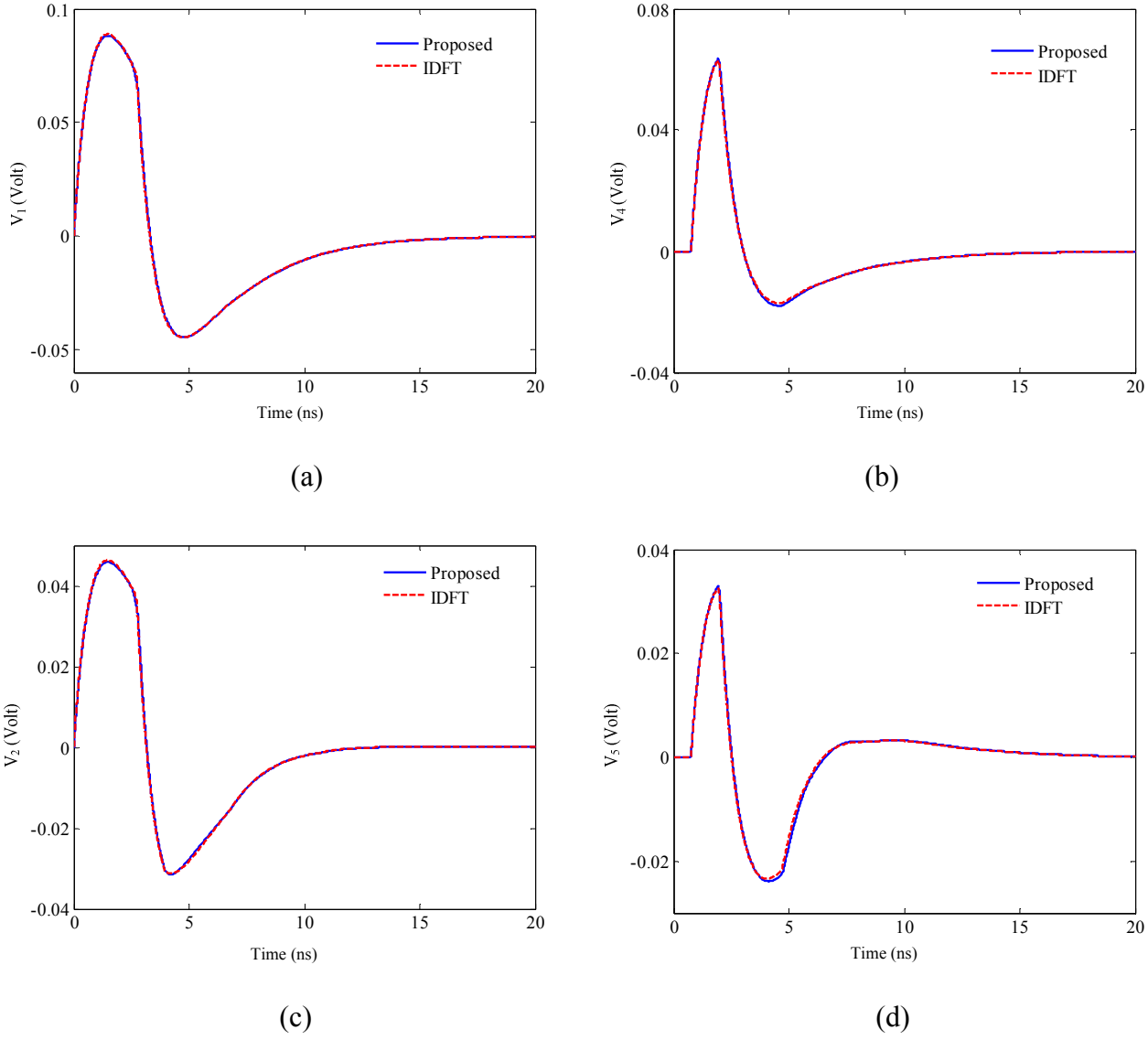

Figure 5-6: Transient response comparison for the network in Figure 5-5 (Example 1).

Next, the interconnect structure is connected to nonlinear CMOS inverters as shown in Figure 5-7. The input of the circuit is a trapezoidal voltage source with the amplitude of 1.8 volt, rise time of 0.1ns and pulse width of 10ns. The transmission line network is

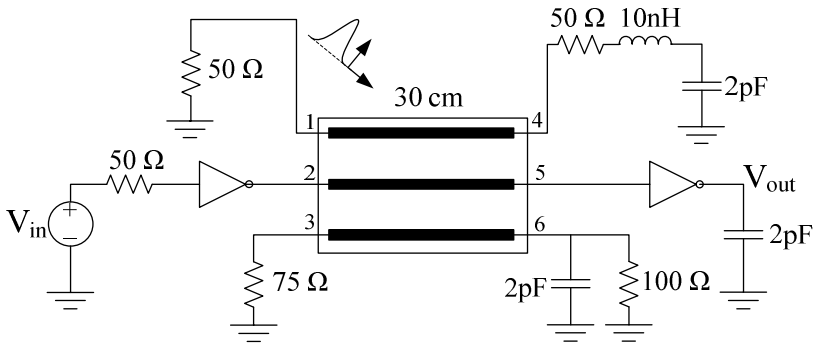

Figure 5-7: Transmission line network with nonlinear elements (example1).

Table 5-1: Computational Cost Comparison (Example 1)

Line length		10 cm	30 cm	50 cm
Proposed	CPU time (s)	4.3	5.1	5.1
DEPACT [54]	CPU time (s)	26.1	68.2	127.7
	# of sections	14	40	70

exposed to an incident field of trapezoidal waveform with rise time of 0.1ns and pulse width of 3ns, E_0 =4kV/m, and the same angular parameters provided above.

In Figure 5-8, the near and far-end responses at nodes 1, 2, 4 and 5 are compared with the DEPACT macromodel [54]. Figure 5-9 shows the response of the output of the inverter at V_{out}, illustrating that the electromagnetic interference may induce false switching since the voltage level of the output pulse drops significantly. For their respective orders all algorithms give similar responses. The computational costs of the simulations are listed in Table 5-1 for different line lengths (on an Intel 1.6 GHz machine with 1 GB memory). For this example, as the length of the line increases the efficiency of the PMoC is greater

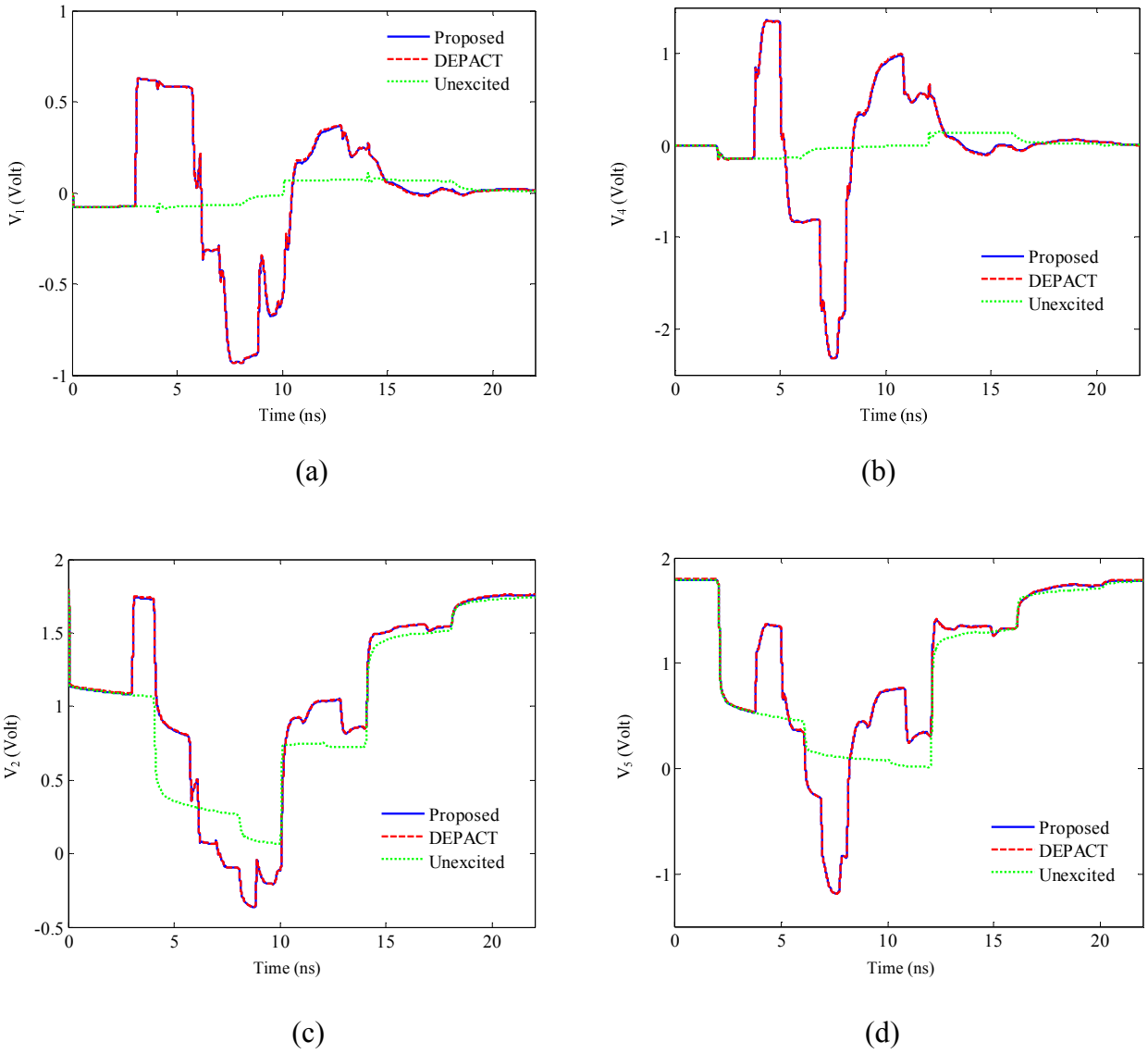

Figure 5-8: Transient response comparison for the nonlinear network in Figure 5-7 (Example 1).

when compared to DEPACT. This is due to the fact that the PMoC uses delay extraction without segmentation to model long interconnects while DEPACT requires more segments for longer lines.

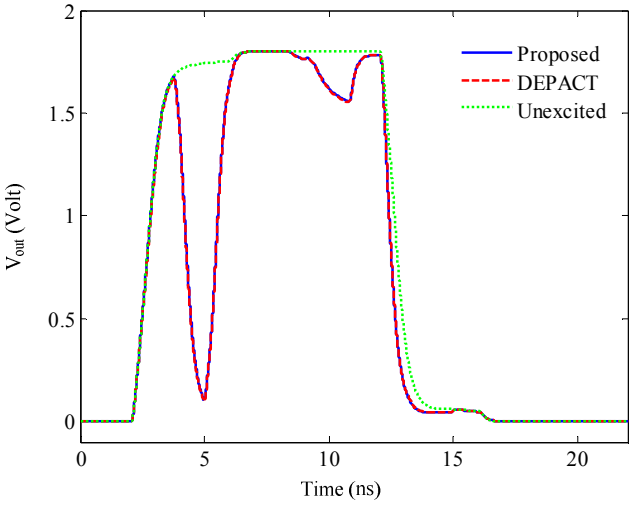

Figure 5-9: Output waveform of the nonlinear network in Figure 5-7 (Example 1).

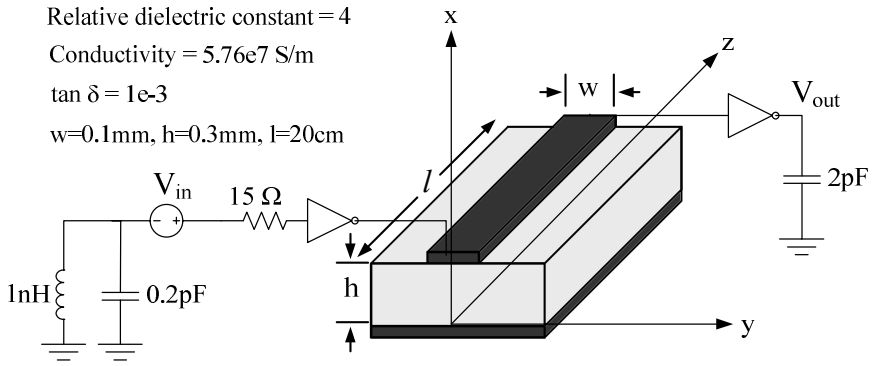

Figure 5-10: Transmission line network with nonlinear elements (Example 2).

Example 2) Figure 5-10 shows a microstrip structure which is connected to nonlinear CMOS inverters. The circuit is derived using a trapezoidal voltage source with the amplitude of 1.8 volts, rise time of 0.1ns and pulse width of 4ns. The test structure is exposed to an incident field of Gaussian waveform $E(t) = E_0(\exp((t-t_0)^2/T^2))$, with t_0=2ns, T=300ps, E_0=3kV/m, and angular parameters of $\theta_E = -90^o$, $\theta_p = 60^o$, and φ_p =

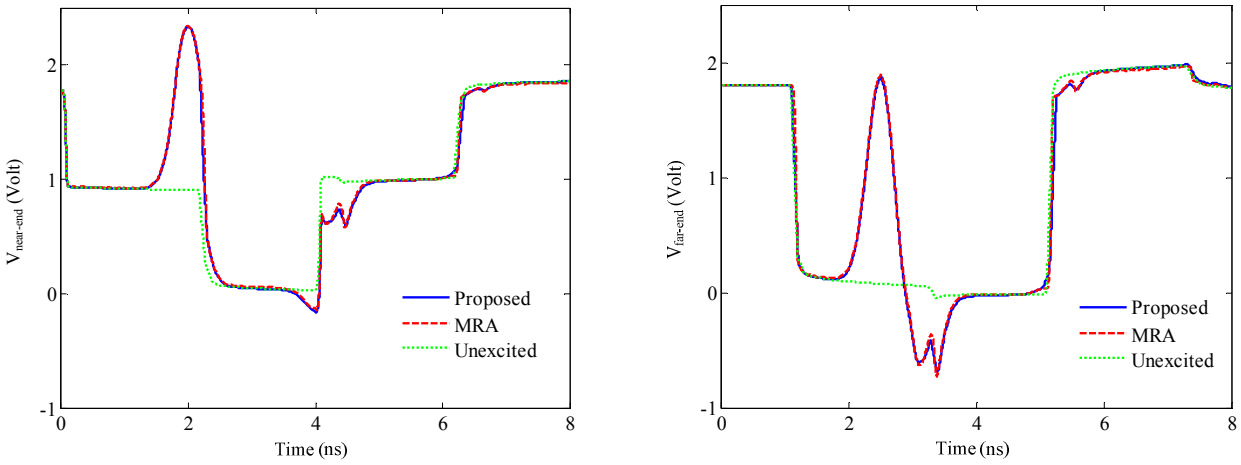

(a) (b)

Figure 5-11: Transient response comparison for the nonlinear network in Figure 5-10 (a) near-end and (b) far-end (Example2).

Table 5-2: Computational Cost Comparison (Example 2)

Line length		10 cm	20 cm
Proposed	CPU time (s)	0.5	0.5
MRA [53]	CPU time (s)	9.2	17.8
	Padé order	32	64

-60^{o}. The near- and far-end responses of the circuit are compared with the matrix rational approximation macromodel [53] in Figure 5-11.

The responses of the circuit with and without external field coupling at the output of the inverter V_{out} are plotted in Figure 5-12, illustrating the false switching due to the electromagnetic interference. For their respective orders both algorithms give similar responses. The transient simulation of the PMoC on a (Intel 1.6 GHz CPU with 1 GB

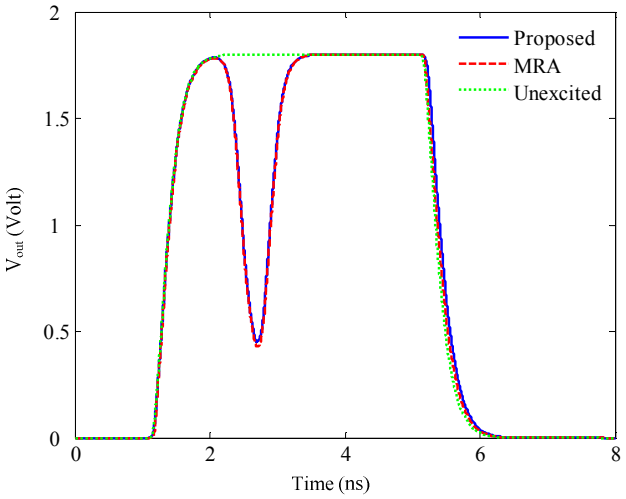

Figure 5-12: Output waveform of the nonlinear network in Figure 5-10 (Example 2).

memory) machine is shown in Table 5-2. PMoC required 0.5 seconds of CPU time, while the matrix rational approximation macromodel required 17.8 seconds on the same machine. For this example, the proposed method is 35 times faster compared to the matrix rational approximation macromodel due to the fact that the PMoC uses delay extract to model electrically long transmission lines.

5.5 Conclusion

In this chapter, an efficient approach to evaluate the effect of electromagnetic field coupling to multiconductor transmission lines is presented. The external sources due to the incident field coupling are approximated as rational functions and the unexcited component is implemented using the PMoC macromodel. This provides significant

computational savings in modeling electrically long transmission lines exposed to incident fields since the PMoC uses delay extraction without segmentation to reduce the complexity of the transfer function of transmission lines.

Chapter 6

6 Improving Vector Fitting Convergence for Noisy Frequency Responses Using Instrumental Variables

6.1 Introduction

System identification has become a critical problem for analysis of high speed packages and microwave devices and structures. Among the various methodologies available, vector fitting (VF) [20] has emerged as one of the most convenient and popular tools for system identification. It approximates the broadband terminal response of any chosen device as a rational function and allows the integration of the device into traditional circuit simulators with IC emphasis like SPICE. It has recently found extensive application in analysis of power transmission lines and systems [79], characterization of electromagnetic devices [80]-[81] and signal integrity analysis of high speed interconnect network [14],[58],[82]-[84] to name a few. VF algorithm uses an iterative approach to improve the accuracy of a set of given initial poles. In [85], an orthonormal VF algorithm

is proposed which leads to better conditioned equations, reduction in the numerical sensitivity of the model parameterization to the choice of starting poles, and consequently better convergence. In [86], a Z-domain vector fitting algorithm is proposed which has less sensitivity to the selection of starting poles. A time domain vector fitting algorithm is also proposed [57] in order to identify the rational function based on time-domain measurements.

Although VF algorithm usually converges to the final poles after a few iterations, it has been observed that VF will not produce accurate results for noisy data and will introduce a bias at the corners even after many iterations [20],[65]-[69]. This is due to the fact that, using a least-squares solver for pole identification during vector fitting, the error due to the noise will also become squared.

A different modification of standard VF, referred as vector fitting with adding and skimming (VF-AS) is reviewed in Chapter 2, which addresses the convergence issues of VF when the frequency data samples are contaminated with noise. The algorithm is based on the identification and removal of spurious poles, an incremental pole addition, and relocation process in order to provide automatic order estimation even in the presence of significant noise. However, the process of identification of the spurious poles and selecting the new position of the poles increases the complexity of the algorithm.

Relaxed vector fitting (RVF) [67], on the other hand, introduces a relaxed constraint to relocate poles to better positions, and hence, to improve the convergence sensitivity to the choice of the initial poles.

In this chapter, a methodology using instrumental variables is proposed which improves the accuracy and convergence of rational approximation of measured data in a noisy environment while it does not increase the computational complexity. This will be illustrated by numerical examples.

6.2 Problem Description

To review the problems of the vector fitting algorithm in the presence of noise, consider $Y(s)$ as a one-port structure with a rational approximation for the transfer function, as

$$Y(s) = \sum_{k=1} \frac{r_k}{s - p_k} + d + se \tag{6.1}$$

where p_k and r_k correspond to real or complex conjugate poles and residues respectively; d and e are optional quotient variables and s is the Laplace variable. As described in Chapter 2, the coefficients of the rational function are determined by choosing N_s frequency points s_i over the frequency range of interest to obtain an overdetermined linear system of

$$\mathbf{A}_i \mathbf{X} = \mathbf{B}_i \tag{6.2}$$

where $\mathbf{A}_i$, $\mathbf{X}$, and $\mathbf{B}_i$ are defined as

$$\mathbf{A}_i = \begin{bmatrix} \mathrm{Re}(a_1^i) \ldots \mathrm{Re}(a_N^i) & 1 & 0 & \mathrm{Re}(\tilde{a}_1^i) \ldots \mathrm{Re}(\tilde{a}_N^i) \\ \mathrm{Im}(a_1^i) \ldots \mathrm{Im}(a_N^i) & 0 & \mathrm{Im}(s_i) & \mathrm{Im}(\tilde{a}_1^i) \ldots \mathrm{Im}(\tilde{a}_N^i) \end{bmatrix}$$

$$\mathbf{X} = [r_1 \quad \cdots \quad r_n \quad d \quad e \quad \tilde{r}_1 \quad \cdots \quad \tilde{r}_n]^{\mathrm{T}}$$

$$\mathbf{B}_i = \begin{bmatrix} \mathrm{Re}(Y(s_i)) \\ \mathrm{Im}(Y(s_i)) \end{bmatrix} \tag{6.3}$$

for the original vector fitting algorithm and

$$\boldsymbol{A}_i = \begin{bmatrix} \mathrm{Re}(a_1^i) \ldots \mathrm{Re}(a_N^i) & 1 & 0 & \mathrm{Re}(\tilde{a}_0^i) \ldots \mathrm{Re}(\tilde{a}_N^i) \\ \mathrm{Im}(a_1^i) \ldots \mathrm{Im}(a_N^i) & 0 & \mathrm{Im}(s_i) & \mathrm{Im}(\tilde{a}_0^i) \ldots \mathrm{Im}(\tilde{a}_N^i) \end{bmatrix}$$

$$\mathbf{X} = [r_1 \quad \cdots \quad r_n \quad d \quad e \quad \tilde{c}_0 \quad \tilde{r}_1 \quad \cdots \quad \tilde{r}_n]^{\mathrm{T}}$$

$$\boldsymbol{B}_i = \begin{bmatrix} 0 \\ 0 \end{bmatrix} \tag{6.4}$$

for the relaxed vector fitting algorithm. For real poles and residues, the coefficients of (6.3) and (6.4) are

$$a_k^i = \frac{1}{s_i - q_k}$$

$$\tilde{a}_k^i = \frac{-Y(s_i)}{s_i - q_k}$$

$$r_k = c_k; \quad \tilde{r}_k = \tilde{c}_k \tag{6.5}$$

For complex conjugate pole and residue pairs (i.e. $q_{k,k+1} = q_{re} \pm jq_{im}$, $c_{k,k+1} = c_{re} \pm jc_{im}$, $\tilde{c}_{k,k+1} = \tilde{c}_{re} \pm j\tilde{c}_{im}$) the coefficients of (6.3) and (6.4) are

$$a_k^i = \frac{1}{s_i - q_k} + \frac{1}{s_i - q_{k+1}}$$

$$a_{k+1}^{i} = \frac{j}{s_i - q_k} - \frac{j}{s_i - q_{k+1}}$$

$$\tilde{a}_{k}^{i} = \frac{-Y(s_i)}{s_i - q_k} + \frac{-Y(s_i)}{s_i - q_{k+1}}$$

$$\tilde{a}_{k+1}^{i} = \frac{-j \cdot Y(s_i)}{s_i - q_k} + \frac{j \cdot Y(s_i)}{s_i - q_{k+1}}$$

$$r_k = c_{re}, \quad r_{k+1} = c_{im}$$

$$\tilde{r}_k = \tilde{c}_{re}; \quad \tilde{r}_{k+1} = \tilde{c}_{im} \tag{6.6}$$

and $\tilde{a}_0^i = Y(s_i)$. To avoid the null solution for the case of relaxed vector fitting algorithm an additional equation is added to the least square problem

$$\mathrm{Re}\left\{\sum_{i=1}^{N_s}\left(\sum_{k=1}^{N}\frac{\tilde{c}_k}{s_i - q_k} + \tilde{c}_0\right)\right\} = N_s \tag{6.7}$$

The equations of (6.2) at N_s different frequency points are assembled to obtain an over determined linear system of equations

$$\mathbf{AX} = \mathbf{B}. \tag{6.8}$$

Next, consider the tabulated data from measurement is perturbed with a zero-mean complex random noise ε as

$$\hat{Y}(s) = Y(s) + \varepsilon \tag{6.9}$$

where $Y(s)$ is the exact theoretical transfer function in the absence of noise. Even though the noise of the data is assumed to be zero-mean, this section will illustrate that the solution of the least squares problem of (6.8) will be biased which may lead to less accurate results.

To investigate the biasing effects of the original vector fitting algorithm in the presence of zero-mean noise, (6.9) at sample frequency s_i (i.e. $\hat{Y}(s_i) = Y(s_i) + \varepsilon_i$) is substituted into (6.2)-(6.6) to obtain

$$\hat{\boldsymbol{A}}_i = \boldsymbol{A}_i + \boldsymbol{H}_i^A$$

$$\hat{\boldsymbol{B}}_i = \boldsymbol{B}_i + \boldsymbol{H}_i^B \tag{6.10}$$

where

$$\boldsymbol{H}_i^A = \begin{bmatrix} 0 & \dots & 0 & \mathrm{Re}(\tilde{e}_1^i) \dots \mathrm{Re}(\tilde{e}_N^i) \\ 0 & \dots & 0 & \mathrm{Im}(\tilde{e}_1^i) \dots \mathrm{Im}(\tilde{e}_N^i) \end{bmatrix}$$

$$\boldsymbol{H}_i^B = \begin{bmatrix} \mathrm{Re}(\varepsilon_i) \\ \mathrm{Im}(\varepsilon_i) \end{bmatrix} \tag{6.11}$$

For real poles and residues, $\tilde{e}_k^i$ is defined as

$$\tilde{e}_k^i = \frac{-\varepsilon_i}{s_i - q_k} \tag{6.12}$$

For complex conjugate pole and residue pairs, $\tilde{e}_k^i$ and $\tilde{e}_{k+1}^i$ are defined as

$$\tilde{e}_k^i = \frac{-\varepsilon_i}{s_i - q_k} + \frac{-\varepsilon_i}{s_i - q_{k+1}}$$

$$\tilde{e}_{k+1}^i = \frac{-j\varepsilon_i}{s_i - q_k} + \frac{j\varepsilon_i}{s_i - q_{k+1}} \tag{6.13}$$

and q_k are the staring poles. The least square solution of (6.8) in the presence of noise can be expressed as

$$\mathbf{X} = \left[\sum_{i=1}^{N_s} \hat{\mathbf{A}}_i^{\mathrm{T}} \hat{\mathbf{A}}_i\right]^{-1} \left[\sum_{i=1}^{N_s} \hat{\mathbf{A}}_i^{\mathrm{T}} \hat{\boldsymbol{B}}_i\right] \tag{6.14}$$

where

$$\hat{\mathbf{A}}_i^{\mathrm{T}} \hat{\mathbf{A}}_i = \mathbf{A}_i^{\mathrm{T}} \mathbf{A}_i + \mathbf{A}_i^{\mathrm{T}} \boldsymbol{H}_i^A + (\boldsymbol{H}_i^A)^T \mathbf{A}_i + (\boldsymbol{H}_i^A)^T \boldsymbol{H}_i^A$$

$$\hat{\mathbf{A}}_i^{\mathrm{T}} \hat{\boldsymbol{B}}_i = \mathbf{A}_i^{\mathrm{T}} \boldsymbol{B}_i + \mathbf{A}_i^{\mathrm{T}} \boldsymbol{H}_i^B + (\boldsymbol{H}_i^A)^T \boldsymbol{B}_i + (\boldsymbol{H}_i^A)^T \boldsymbol{H}_i^B \tag{6.15}$$

Note that $\mathbf{A}_i^{\mathrm{T}} \mathbf{A}_i$ and $\mathbf{A}_i^{\mathrm{T}} \boldsymbol{B}_i$ of (6.15) are the matrices obtained in the absence of noise. Since it is assumed that the biasing of the noise ε is zero (i.e. expected value $E[\varepsilon] = 0$), the expected values of the second and third terms of (6.15) are also zero

$$E[\mathbf{A}_i^{\mathrm{T}} \boldsymbol{H}_i^A] = E[(\boldsymbol{H}_i^A)^T \mathbf{A}_i] = \boldsymbol{0}$$

$$E[\mathbf{A}_i^{\mathrm{T}} \boldsymbol{H}_i^B] = E[(\boldsymbol{H}_i^A)^T \boldsymbol{B}_i] = \boldsymbol{0} \tag{6.16}$$

Thus, the matrices of (6.16) do not statistically bias the results of the least square approximation. The forth terms of (6.15) are defined as

$$(\boldsymbol{H}_i^A)^T \boldsymbol{H}_i^A = \left[h_{m,n}^a\right]$$

$$(\boldsymbol{H}_i^A)^T \boldsymbol{H}_i^B = \left[h_m^b\right] \tag{6.17}$$

where

$$h_{m,n}^a = \begin{cases} \mathrm{Re}(\tilde{e}_{m'}^i).\mathrm{Re}(\tilde{e}_{n'}^i) + \mathrm{Im}(\tilde{e}_{m'}^i).\mathrm{Im}(\tilde{e}_{n'}^i) & m,n > N+2 \\ 0 & otherwise \end{cases}$$

$$h_m^b = \begin{cases} \mathrm{Re}(\tilde{e}_{m'}^i).\mathrm{Re}(\varepsilon_i) + \mathrm{Im}(\tilde{e}_{m'}^i).\mathrm{Im}(\varepsilon_i) & m > N+2 \\ 0 & otherwise \end{cases} \tag{6.18}$$

and $m' = m-(N+2)$ and $n' = n-(N+2)$. Note that the expected value of $E[\mathrm{Re}(\varepsilon)^2] \neq 0$ and $E[\mathrm{Im}(\varepsilon)^2] \neq 0$. This causes the non-zero terms of $h_{m,n}^a$ and h_m^b to statistically bias the least square approximation of (6.14),

$$E[(\boldsymbol{H}_i^A)^T \boldsymbol{H}_i^A] \neq \boldsymbol{0}$$

$$E[(\boldsymbol{H}_i^A)^T \boldsymbol{H}_i^B] \neq \boldsymbol{0} \tag{6.19}$$

The nonzero $h_{m,n}^a$ terms bias the $\hat{\mathbf{A}}_i^{\mathrm{T}}\hat{\mathbf{A}}_i$ matrices which affect the solution of all unknown variables in (6.14). The nonzero h_m^b terms bias the $\tilde{c}_k$ residues, which are used to determine the poles of $Y(s)$. It is the biasing effect of h_m^b which is mainly responsible for the failure of vector fitting to capture the actual poles of the system in the presence of zero-mean noise.

To investigate the biasing effects of relaxed vector fitting algorithm in the presence of zero-mean noise, (6.9) at sample frequency s_i (i.e. $\hat{y}(s_i) = y(s_i) + \varepsilon_i$) is substituted into (6.4) -(6.7) to obtain

$$\hat{\boldsymbol{A}}_i = \boldsymbol{A}_i + \boldsymbol{H}_i^A$$

$$\hat{\boldsymbol{B}}_i = \boldsymbol{B}_i \tag{6.20}$$

where

$$\boldsymbol{H}_i^A = \begin{bmatrix} 0 & \dots & 0 & \mathrm{Re}(\tilde{e}_0^i) \dots \mathrm{Re}(\tilde{e}_N^i) \\ 0 & \dots & 0 & \mathrm{Im}(\tilde{e}_0^i) \dots \mathrm{Im}(\tilde{e}_N^i) \end{bmatrix} \tag{6.21}$$

For $k \geq 1$, the coefficients $\tilde{e}_k^i$ are defined by (6.12) and (6.13) for real and complex conjugate poles, respectively and $\tilde{e}_0^i = \varepsilon_i$. The least square solution of the relaxed vector fitting algorithm can be expressed as (6.14), where

$$\hat{\mathbf{A}}_i^{\mathrm{T}} \hat{\mathbf{A}}_i = \mathbf{A}_i^{\mathrm{T}} \mathbf{A}_i + \mathbf{A}_i^{\mathrm{T}} \boldsymbol{H}_i^A + (\boldsymbol{H}_i^A)^T \mathbf{A}_i + (\boldsymbol{H}_i^A)^T \boldsymbol{H}_i^A$$

$$\hat{\mathbf{A}}_i^{\mathrm{T}} \hat{\boldsymbol{B}}_i = \mathbf{A}_i^{\mathrm{T}} \boldsymbol{B}_i + (\boldsymbol{H}_i^A)^T \boldsymbol{B}_i \tag{6.22}$$

Making the assumption that the biasing of the noise ε is zero, the expected values of the second and third terms of (6.22) are

$$E[\mathbf{A}_i^{\mathrm{T}} \boldsymbol{H}_i^A] = E[(\boldsymbol{H}_i^A)^T \mathbf{A}_i] = \boldsymbol{0}$$

$$E[(\boldsymbol{H}_i^A)^T \boldsymbol{B}_i] = \boldsymbol{0} \tag{6.23}$$

Similarly, the matrix $(\boldsymbol{H}_i^A)^T \boldsymbol{H}_i^A$ is defined by (6.17)-(6.18), where $m' = m - (N+3)$ and $n' = n - (N+3)$. Since $E[\mathrm{Re}(\varepsilon)^2] \neq 0$ and $E[\mathrm{Im}(\varepsilon)^2] \neq 0$, the matrix $(\boldsymbol{H}_i^A)^T \boldsymbol{H}_i^A$ will bias the least square approximation of (6.14).

$$E[(\boldsymbol{H}_i^A)^T \boldsymbol{H}_i^A] \neq \boldsymbol{0} \tag{6.24}$$

In comparison with the traditional vector fitting algorithm, the biasing effect of relaxed vector fitting is less pronounced since formulation moves the h_m^b terms of (6.18) to (6.24). As a result, the matrix inversion of (6.14) distributes the biasing effects of (6.24) among all unknown variables of **X**. Thus, relaxed vector fitting is better able to capture the poles of the system in comparison to the traditional vector fitting algorithm.

The next section describes an instrumental variable approach to eliminate the biasing effects of (6.19) and (6.24). Numerical examples will illustrate that combining the vector fitting algorithms with instrumental variable approach will provide more accurate pole estimations with less iteration to converge.

6.3 Proposed Algorithm

The previous section shows that in presence of noise, the least square solution is biased. More precisely, when the measured frequency-domain data is contaminated with noise, the poles are perturbed from their original positions [65] or may require additional iterations to converge. To minimize the biasing effects of the least square solution an instrumental variable approach is proposed.

6.3.1 Description of Instrumental Variable Algorithm

The least squares solution using the instrumental variable approach can be defined as

$$\mathbf{X} = \left[\sum_{i=1}^{N_s} \mathbf{\Psi}_i^{\mathrm{T}} \hat{\mathbf{A}}_i \right]^{-1} \left[\sum_{i=1}^{N_s} \mathbf{\Psi}_i^{\mathrm{T}} \hat{\boldsymbol{B}}_i \right]. \tag{6.25}$$

where $\boldsymbol{\Psi}_i$ is referred as an instrument of the least squares solution. The objective of the instrumental variable is for $\boldsymbol{\Psi}_i$ to match $\boldsymbol{A}_i$ where the errors of $\boldsymbol{\Psi}_i$ are zero mean and uncorrelated with the noise of $\hat{\boldsymbol{A}}_i$ and $\hat{\boldsymbol{B}}_i$. This leads to an unbiased solution for $\boldsymbol{X}$ in (6.25) [87]-[90]. The construction of $\boldsymbol{\Psi}_i$ can be generated from different estimates of $Y(s)$, defined as

$$\hat{Y}(s) = Y(s) + \eta \tag{6.26}$$

where η is the error of the approximation of $Y(s)$ and is assumed to be zero-mean and uncorrelated with ε. Substituting the sample frequency s_i (i.e. $\hat{Y}(s_i) = Y(s_i) + \eta_i$) into (6.2), generates the instrument $\boldsymbol{\Psi}_i$ defined as

$$\boldsymbol{\Psi}_i = \boldsymbol{A}_i + \boldsymbol{H}_i^{\Psi} \tag{6.27}$$

where $\boldsymbol{H}_i^{\Psi}$ is the error of the instrument and it is similar to $\boldsymbol{H}_i^{A}$ as defined by (6.11) and (6.21) where ε is replaced by η. To investigate the biasing effects of the instrumental variable approach the matrices of (6.25) are expressed as

$$\mathbf{\Psi}_i^{\mathrm{T}} \hat{\mathbf{A}}_i = \mathbf{A}_i^{\mathrm{T}} \mathbf{A}_i + \mathbf{A}_i^{\mathrm{T}} \boldsymbol{H}_i^{A} + (\boldsymbol{H}_i^{\Psi})^{T} \mathbf{A}_i + (\boldsymbol{H}_i^{\Psi})^{T} \boldsymbol{H}_i^{A}$$

$$\boldsymbol{\Psi}_i^{\mathrm{T}} \hat{\boldsymbol{B}}_i = \mathbf{A}_i^{\mathrm{T}} \boldsymbol{B}_i + \mathbf{A}_i^{\mathrm{T}} \boldsymbol{H}_i^{B} + (\boldsymbol{H}_i^{\Psi})^{T} \boldsymbol{B}_i + (\boldsymbol{H}_i^{\Psi})^{T} \boldsymbol{H}_i^{B} \tag{6.28}$$

Since it is assumed that the biasing of ε and η are zero, the expected values of the second and third terms of (6.28) are also zero. Furthermore, ε and η are assumed to be uncorrelated (i.e. $E[\eta_i \varepsilon_i] \approx 0$) which causes the expected values of the forth terms in (6.28) to be zero.

$$E[(\boldsymbol{H}_i^{\Psi})^{T} \boldsymbol{H}_i^{A}] \approx \boldsymbol{0}$$

$$E[(\boldsymbol{H}_i^{\Psi})^{T} \boldsymbol{H}_i^{B}] \approx \boldsymbol{0} \tag{6.29}$$

The next section describes techniques for constructing the instrument variables for $\boldsymbol{H}_i^{\Psi}$.

6.3.2 Methodology to Construct Instrument $\boldsymbol{\Psi}_i$

A simple way to create $\boldsymbol{\Psi}_i$ is to use two sets of measurements that are uncorrelated. For the case when additional uncorrelated data samples are not available, the vector fitting algorithm can construct the instrumental variables by using the previous rational approximation for each of the iterations. Since the previous rational approximation is less correlated with the noise of the data, the biasing effect of the least squares solution is minimized. The proposed vector fitting instrumental variable algorithm is summarized in the form of pseudo-code of *Algorithm 1*.

Algorithm 1: Vector fitting algorithm using the instrumental variable technique.

Require: Obtain tabulated data of the frequency response.

Require: Select maximum number of iterations $N_{\max}$ and stopping accuracy ε_y.

Require: Select starting poles over the frequency range of interest such that they are highly resonant.

Step 1: Generate $\boldsymbol{A}$ and $\boldsymbol{B}$ matrices using the tabulated data $\hat{Y}(s)$ and the starting poles and solve the least squares problem of (6.8).

Step 2: Compute the residues by solving the second least squares problem performed on (6.1).

Step 3: Obtain $Y_{app}(s)$, the estimate of $Y(s)$ for different frequency point using the computed sets of poles and residues.

Step 4: Check error criteria.

if error tolerance of $\| \hat{Y}(s) - Y_{app}(s) \| < \varepsilon_y$ is satisfied or the number of iterations equals $N_{\max}$ finish the algorithm.

end

Step 5: Generate $\boldsymbol{A}$ and $\boldsymbol{B}$ matrices using the tabulated data $\hat{Y}(s)$ and the new set of calculated poles.

Step 6: Generate the instrument $\boldsymbol{\Psi}$ using the estimate $Y_{app}(s)$ (computed in Step 2) and the new set of calculated poles.

Step 7: Solve the least squares problem of (6.25) using the instrumental variable technique and go Step 2.

6.4 Numerical Results

Three examples are provided in this section to demonstrate the accuracy and efficiency of the proposed vector fitting algorithm in the presence of noise.

Example 1) The first example is a synthetic transfer function with 18 poles [65] as demonstrated in Table 1. Several Gaussian noises with different RMS values are added to the frequency response of the system and the algorithms of vector fitting, relaxed vector fitting, vector fitting algorithm with the instrumental variable technique and relaxed vector fitting algorithm with the instrumental variable techniques are examined for the rational approximation of the noisy frequency response . Figure 6-1 shows the fitting of the noisy frequency response with signal to noise ratios (SNR) of 30dB and 20dB. As illustrated in the figure the conventional vector fitting algorithm is not able to catch all the poles and it has biasing at the convex areas, while vector fitting with the instrumental variable technique shows a good agreement with the original data.

Due to the random nature of the noise, the frequency characteristics of the noise signal for the same SNR will be different for each simulation. As a result, the number of iterations required for the proposed algorithm to converge for each simulation will vary as well. Taking this into account, the results shown below are the average achieved for 20 simulations that have been conducted with the same SNR value.

Table 6-1: Poles and Residues of the Transfer Function [65]

Poles (GHz)	Residues (GHz)
-0.6930 $\pm j$ 2.3198	-0.9260 $\mp j$ 0.0855
-0.3110 $\pm j$ 5.9866	-0.2029 $\mp j$ 0.0146
-0.1175 $\pm j$ 1.2123	-0.0832 $\mp j$ 0.0150
-0.3550 $\pm j$ 14.0473	-0.1932 $\mp j$ 0.0137
-0.5322 $\pm j$ 19.8046	-0.7199 $\pm j$ 0.0580
-0.3091 $\pm j$ 22.7294	-0.5464 $\mp j$ 0.1157
-1.1285 $\pm j$ 28.6601	-0.6624 $\mp j$ 0.2276
-0.3179 $\pm j$ 38.2834	-0.4653 $\mp j$ 0.0417
-0.5498 $\pm j$ 47.9715	-0.7635 $\mp j$ 0.1634

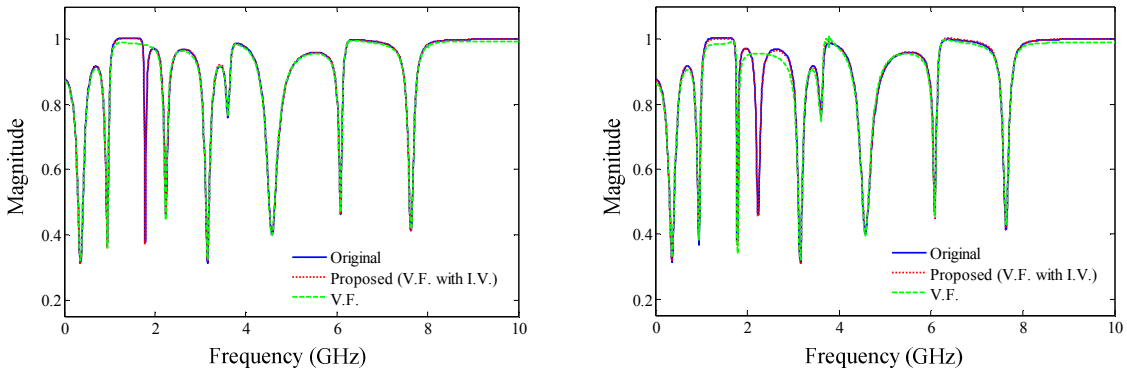

Figure 6-1: Vector fitting for the transfer function of example 1 (a) SNR=30dB (b) SNR=20dB (Example 1).

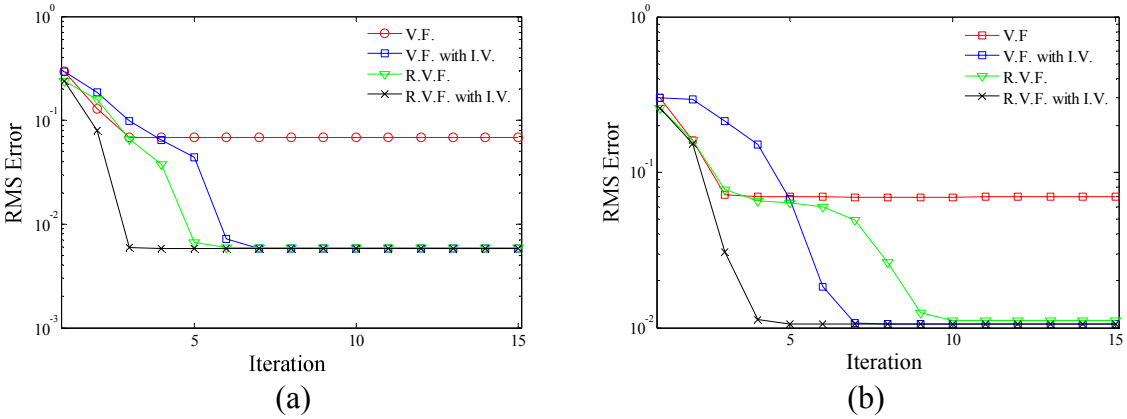

Figure 6-2: RMS error vs. iteration count (a) SNR=20dB and (b) SNR=20dB (Example 1).

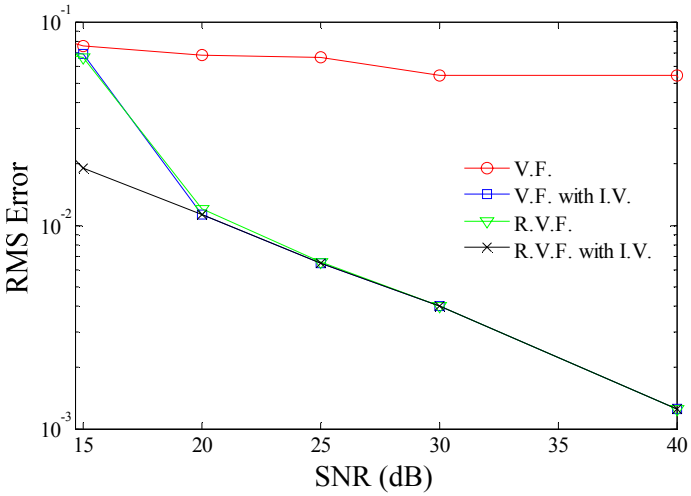

Figure 6-3: RMS Error after 15th iteration for different SNRs (Example 1).

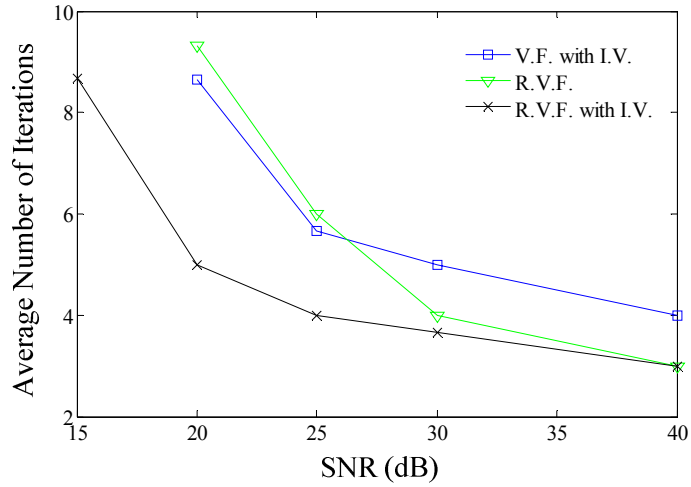

Figure 6-4: Average number of iterations to converge for different SNRs (Example 1).

Figure 6-2 shows the RMS error values versus iteration count for SNR=20dB and SNR=20dB. Figure 6-3 shows the RMS error after the 15th iteration for different SNRs. For SNR=10 dB none of the algorithms were able to converge before 15th iterations, while for SNR=15dB relaxed vector fitting with instrumental variable was the only

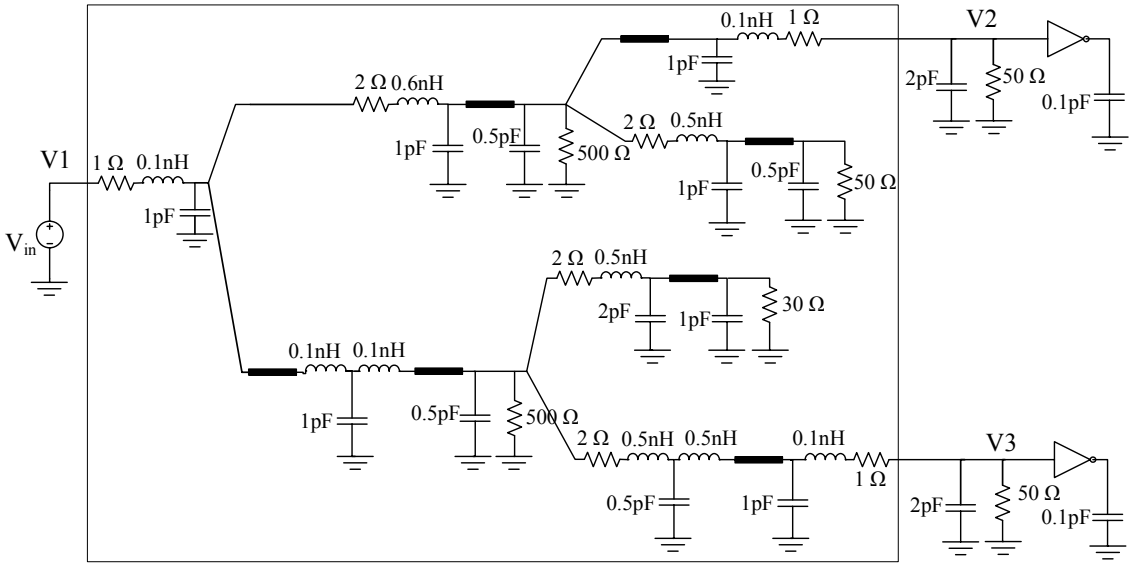

Figure 6-5:Transmission line network with nonlinear termination (Example 2)

algorithm to obtain the appropriate accuracy. One can see that all three algorithms except the conventional vector fitting are showing good results for the remaining noisy data, while the algorithms with instrumental variable benefit the best accuracy.

Figure 6-4 shows the average required number of iterations versus the SNR. As illustrated in the figure, instrumental variable technique can accelerate the convergence of the vector fitting algorithm. It is to be noted that for the example, relaxed vector fitting algorithm with instrumental variable requires less number of iterations to converge and original vector fitting algorithm has sever issues in terms of convergence and accuracy. Moreover, depending on the noise, vector fitting algorithm with instrumental variable is usually superior to the relaxed vector fitting.

Example2) A seven transmission line network with nonlinear CMOS inverters is shown in Figure 6-5. The p.u.l. parameters of each line are R=8.26Ω/m, L=361nH/m,

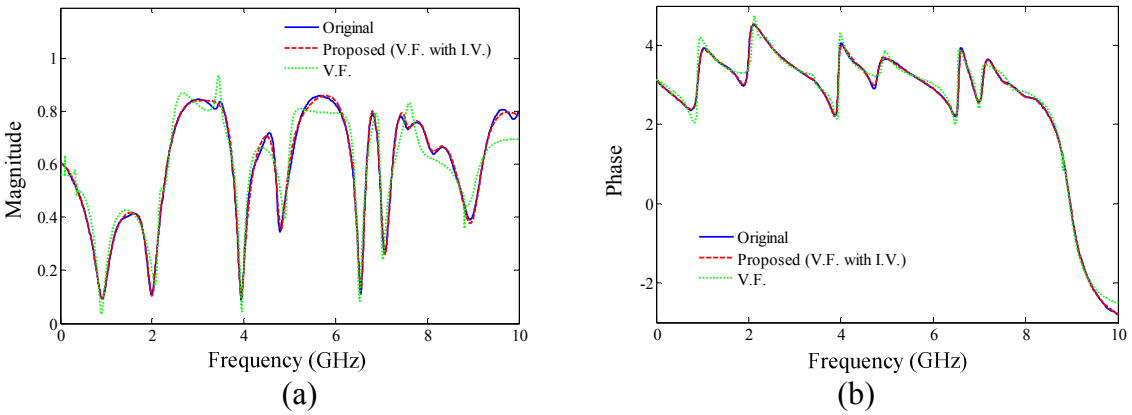

(a) (b)

Figure 6-6: Vector fitting for S(1,1) of the network in Figure 6-5 with SNR=20dB (a) magnitude and (b) phase plots (Example 2).

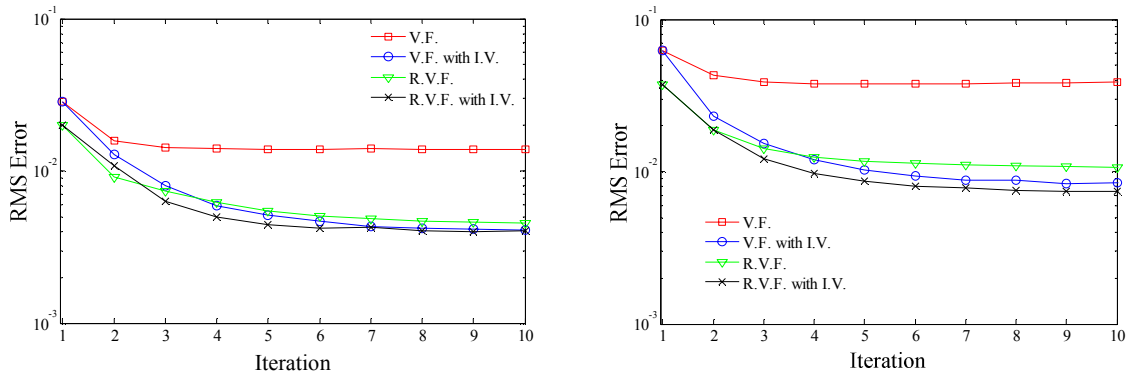

(a) (b)

Figure 6-7: RMS Error for (a) SNR=30dB and (b) SNR=20dB (Example 2).

C=140pF/m, G=0.0 and the length of each line is 2cm. The input voltage is a step source of amplitude 1.8V with rise time of 0.2ns. The S-parameters of the three port circuit which is included in the box have been obtained using SPICE. In this example, different values of noises have been added to the computed S-parameters and different vector fitting algorithms have been applied. Figure 6-6 shows vector fitting for S(1,1) parameter with SNR=20dB using 30 poles. The results of the proposed method illustrate significant

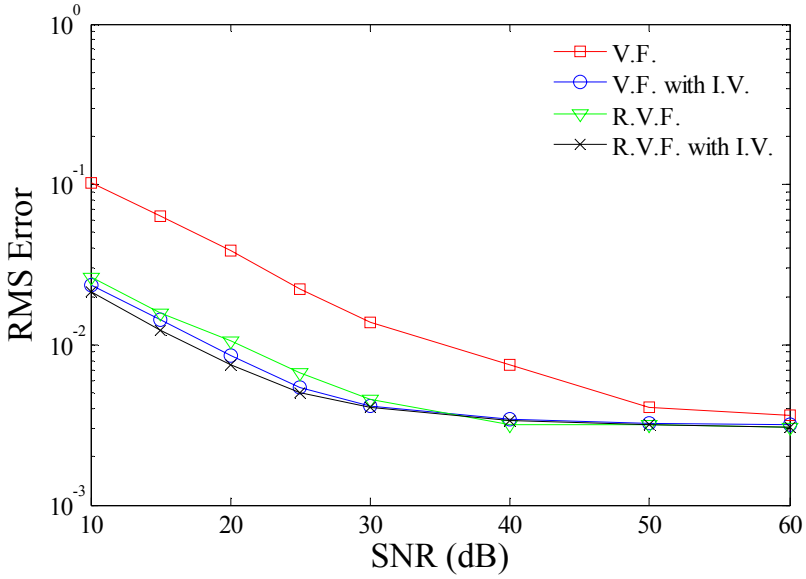

Figure 6-8: RMS Error after 10th iteration for different SNRs (Example 2).

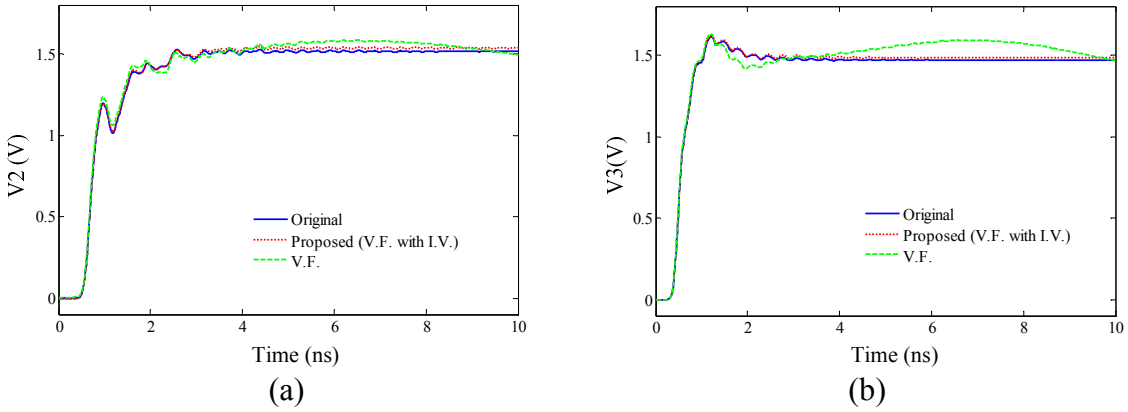

Figure 6-9: Transient response of nodes V2 and V3 using vector fitting for noisy data with and without instrumental variables (SNR=20dB) (Example 2).

improvement in capturing the data compared to the results of the original vector fitting which lead to considerably inaccurate fitting and biasing.

Figure 6-7 shows the RMS errors of S(1,1) of the noisy data with two SNRs of 30 and 20 dB versus the iteration count. Figure 6-8 shows the overall RMS Error after 10th iteration for different SNRs. The results of the proposed method are compared with the

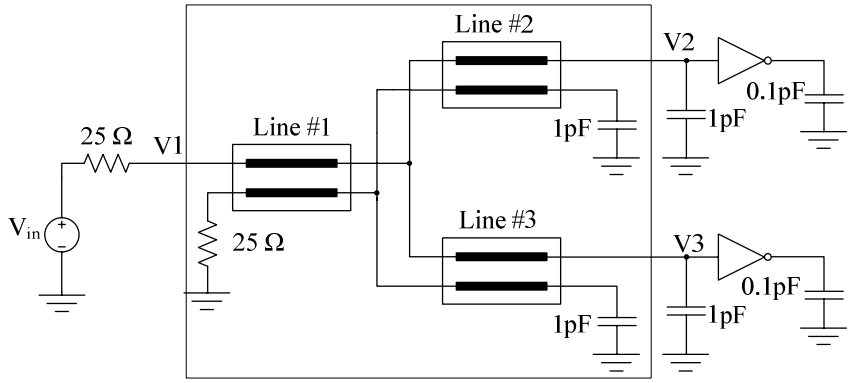

(a)

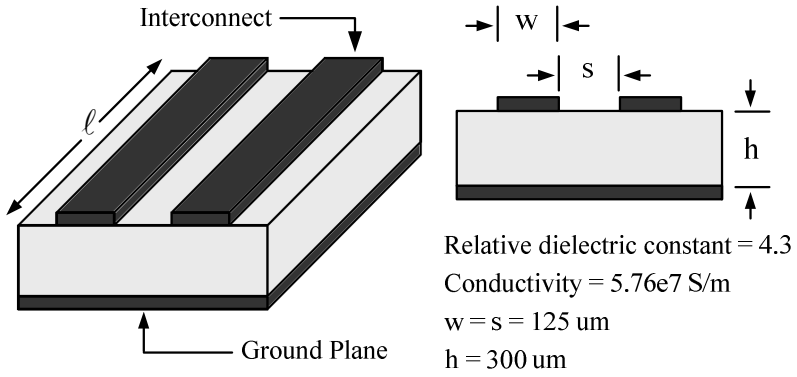

(b)

Figure 6-10: (a) Multiconductor transmission line network with nonlinear CMOS inverter and (b) physical/geometrical parameters for the MTL sub-networks (Example 3).

vector fitting and relaxed vector fitting algorithm. As demonstrated in Figure 6-7 and 8, the proposed instrumental variables can assist vector fitting algorithms with faster convergence and better accuracy. The transient response at nodes V2 and V3 using the proposed vector fitting algorithm and the conventional method is shown in Fig 9.

Example 3) Figure 6-10 (a) shows a multi-conductor transmission line network, terminated with two nonlinear CMOS inverters. The physical description of the interconnect networks are depicted in Figure 6-10 (b) and the lengths of the lines are as following: l_1 = 5cm, l_2 = 3cm and l_3 = 4cm. The p.u.l parameters are computed from the

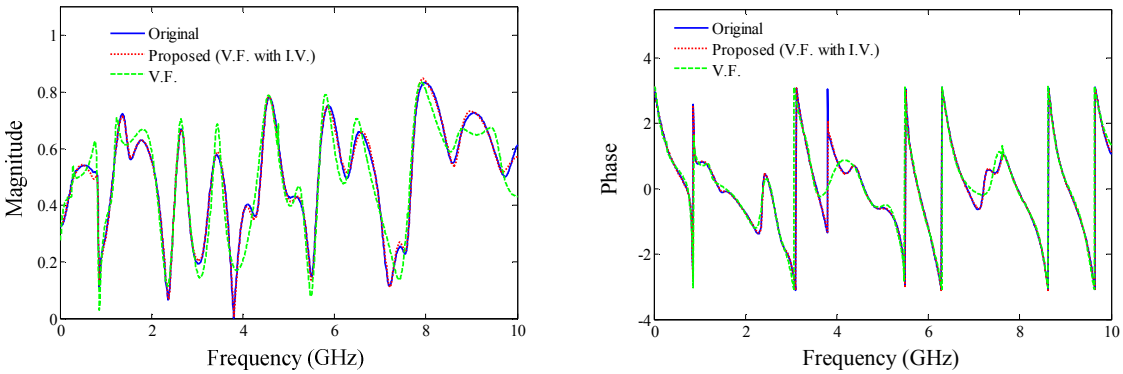

(a) (b)

Figure 6-11: Vector fitting for S(2,2) of the network in Figure 6-10 with SNR=20dB (a) magnitude and (b) phase plots (Example 3).

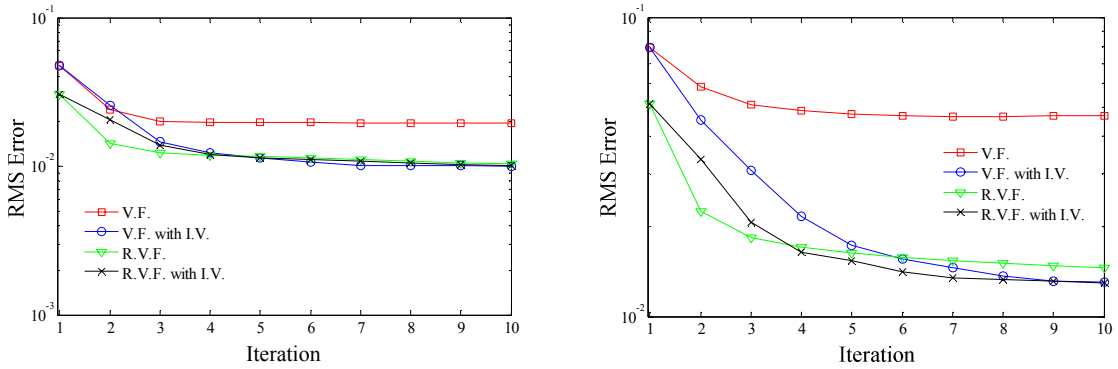

(a) (b)

Figure 6-12: RMS Error (a) SNR=30dB and (b) SNR=20dB (Example 3).

physical description using HSPICE field solver. The input voltage of the circuit is a 1.8 V step response with a time rise of 0.2 ns.

The S-parameters of the three port circuit which is surrounded by the box have been calculated using the similar method as example 2. Then, different values of Gaussian noises have been added to the computed S-parameters and different vector fitting algorithms have been applied.

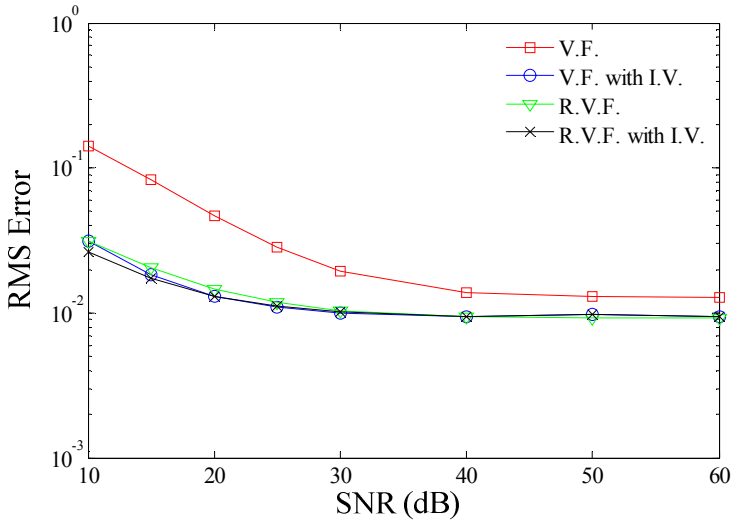

Figure 6-13: RMS Error after 10th iteration for different SNRs (Example 3).

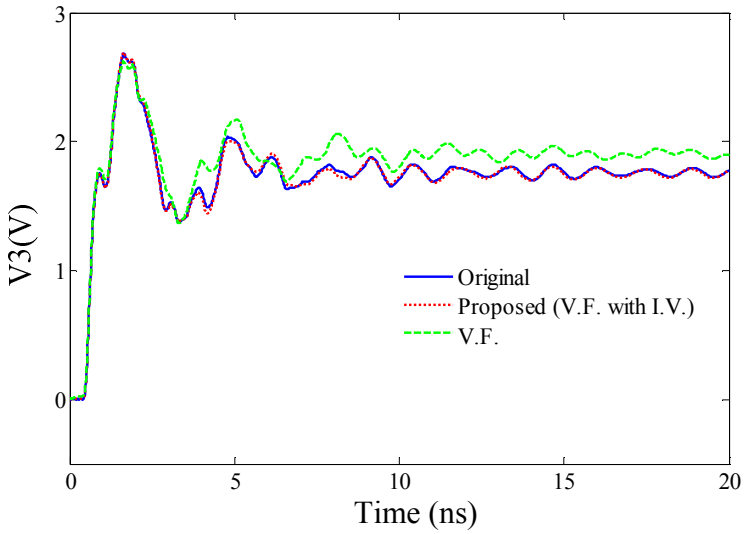

Figure 6-14: Transient response of nodes V3 using vector fitting for noisy data with and without instrumental variables (SNR=20dB) (Example 3).

Figure 6-11 shows vector fitting for S(2,2) parameter with SNR=20dB using 36 poles. The results of the proposed method illustrate significant improvement compared to the conventional vector fitting algorithm. Figure 6-12 shows the RMS errors of S(1,1) as the

iterations continue. Figure 6-13 shows the overall RMS Error after 10th iteration for different SNRs. The results of the proposed method are compared with the vector fitting and relaxed vector fitting algorithm. The transient response at node V3 using the proposed vector fitting algorithm has been compared to the conventional vector fitting in Figure 6-14.

6.5 Conclusion

In this chapter, an efficient approach to increase the accuracy and convergence of VF algorithm for noisy frequency responses is presented which is based on instrumental variables technique. Using instrumental variable approach will not affect the computational complexity of VF, while it provides significant improvement in convergence and reduction of biasing.

Chapter 7

7 Summary and Future Work

7.1 Summary

The objective of this thesis is to develop efficient algorithms to model high-speed interconnects in a circuit simulation environment. This thesis addresses both macromodels where the physical dimensions and characteristics of the structure are known and when the macromodels are derived based on the tabulated data. This work includes the following contributions.

Firstly, a passive closed-form macromodeling technique based on method of characteristics is developed for multiconductor transmission lines. This algorithm is based on extracting the significant propagation delay of the transmission line followed by a low order rational approximation to capture the attenuation effects. The key advantage of the algorithm is that the curve fitting to realize the macromodel depends only on per-unit-length (p.u.l.) parameters and not on the length of the transmission line. This avoids

computationally expensive and sometimes unreliable numerical fitting algorithms that are on occasion associated with the MoC-based algorithms.

An efficient approach to perform sensitivity analysis of lossy transmission lines in the presence of nonlinear terminations is also presented where the sensitivity information is derived using the PMoC macromodel. An important feature of the proposed method is that the sensitivities are calculated from the solution of the original system resulting in significant computational advantages when compared to perturbation methods. Perturbation based techniques can also lead to inaccurate results depending on the magnitude of the perturbation. In addition the perturbed network must be solved separately for every parameter of interest. However, in the proposed approach, the sensitivity information with respect to all the parameters can be essentially obtained from the solution of the original network, since both the original and sensitivity networks have the same MNA matrices and additional LU decompositions to invert the sensitivity network matrices are not required. The sensitivity analysis is also included in an optimization process to obtain the appropriate physical parameters of the network to satisfy the required design constraints.

A time-domain macromodel for lossy multiconductor transmission lines exposed to electromagnetic interference is described in this thesis based on PMoC. The algorithm provides an efficient mechanism to ensure the passivity of the macromodel for different line lengths. The proposed method is efficient in modeling electrically long interconnects since delay extraction without segmentation is used to capture the frequency response.

An efficient approach to increase the accuracy and convergence of vector fitting for noisy frequency responses is described in this thesis. The proposed technique uses instrumental variables in order to solve the least square problem and hence, it provides better convergence and reduced biasing. The proposed approach will not affect the computational complexity of VF algorithms, while it provides a faster convergence compared to the original VF.

Several numerical examples are provided in this thesis to demonstrate the validity and efficiency of the proposed algorithms.

7.2 Future Work

This section provides some suggestions for future research based on the work presented in this thesis:

1. The analysis of excited MTLs is extended to analysis of shielding capability of shielded cables in [91]-[95]. The problem is formulated by considering an external transmission line having currents flowing on the exterior of the cable together with a ground plane return and an internal multiconductor transmission line consisting of internal conductors referenced to the interior part of the shield. Time-domain analysis of electromagnetic field coupling to shielded cables can be performed based on PMoC in order to achieve faster simulation times while ensuring the passivity.

2. The waveform relaxation algorithm [69]-[100] reduces the simulation costs of large networks. This technique attempts to break a large circuit into smaller subcircuits which can be solved iteratively in sequence or in parallel. PMoC macromodel of multiconductor transmission lines with several conductors can be partitioned into two-conductor transmission lines using with waveform relaxation techniques. Since each section is considered as a two-conductor transmission line, the enforcement of passivity conditions is also expected to be faster.
3. Applications of PMoC for the optimization of power transmission line issues such as corona discharge, lightening discharge, and overvoltage analysis, can be examined.
4. Providing an automatic optimization routine for ensuring passivity conditions of PMoC based on Hamiltonian matrix approach presented in [61]-[62]. This method improves computation complexity of the passivity enforcement techniques proposed in [19] for traditional MoC. This is due to the fact that the complexity of eigenvalue calculation of a network admittance matrix increases rapidly as the order increases and thus, it requires more time compared to the half-sized characteristic admittance $\boldsymbol{Y}_0(s)$, propagation function $\boldsymbol{\Gamma}(s)$ and their products.

References

[1] C. R. Paul, *Analysis of multiconductor transmission lines*, 2nd ed. New Jersey, NY: John Wiely and Sons, 2008.

[2] R. Achar and M. Nakhla, "Simulation of high-speed interconnects," *Proc. IEEE*, vol. 89, no. 5, pp. 693-728, May 2001.

[3] A. Ruehli and A. Cangellaris, "Progress in the methodologies for the electrical modeling of interconnects and electronic packages," *Proc. IEEE*, vol. 89, no. 5, pp. 740–771, May 2001.

[4] C. D. Taylor, R. S. Satterwhite, and and C. W. Harrison, "The response of a terminated two-wire transmission line excited by a nonuniform electromagnetic field," *IEEE Trans. Antennas Propagat.*, vol. 13, no. 6, pp. 987–989, November 1965.

[5] C. R. Paul, "Frequency response of multiconductor transmission lines illuminated by an incident electromagnetic field," *IEEE Trans. Microwave Theory Tech.*, vol. 22, pp. 454–457, April 1967.

[6] C. R. Paul, "A SPICE model for multiconductor transmission lines excited by an incident electromagnetic field," *IEEE Trans. Electromagn. Compat.*, vol. 36, pp. 342–354, November 1994.

[7] C. R. Paul, "Literal solutions for the time-domain response of a two-conductor transmission line excited by an incident electromagnetic field," *IEEE Trans. Electromagn. Compat.*, p. 37, May 1995.

[8] A. Odabasioglu, M. Celik, and L. T. Pilleggi, "PRIMA: Passive Reduced-Order Interconnect Macromodeling Algorithm," *IEEE Trans. on CAD*, vol. 17, no. 8, pp. 645-653, August 1998.

[9] A. Dounavis, R. Achar, and M. Nakhla, "Efficient passive circuit models for distributed networks with frequency-dependent parameters," *IEEE Trans. on Adv. Packag.*, vol. 23, pp. 382-392, August 2000.

[10] A. Dounavis, R. Achar, and M. Nakhla, "A general class of passive macromodels for lossy multiconductor transmission lines," *IEEE Trans. on MTT*, vol. 49, pp. 1686-1696, October 2001.

[11] A. Cangellaris, S. Pasha, J. Prince, and M. Celik, "A new discrete time-domain model for passive model order reduction and macromodeling of high-speed interconnections," *IEEE Trans. Comp. Packag. Manf. Tech.*, pp. 356-364, August 1999.

[12] Q. Yu, J. M. L. Wang, and E. S. Kuh, "Passive multipoint moment matching model order reduction algorithm on multiport distributed interconnect networks," *IEEE Trans. Circuits Syst. I*, vol. 46, no. 1, pp. 140-160, January 1999.

[13] E. Gad and M. Nakhla, "Efficient simulation of nonuniform transmission lines using integrated congruence transform," *IEEE Trans. on VLSI*, vol. 12, pp. 1307-1320, 2004.

[14] I.M. Elfadel, H-M. Huang, A. E. Ruehli, A. Dounavis, and M. S. Nakhla, "A Comparative Study of Two Transient Analysis Algorithms for Lossy Transmission Lines With Frequency-Dependent Data," *IEEE Trans. On Adv. Packaging*, vol. 25,

pp. 143-153, May 2002.

[15] Jr. F. H. Branin, "Transient analysis of lossless transmission lines," *Proc. IEEE*, vol. 55, no. 11, pp. 2012-2013, 1967.

[16] N. M. Nakhla, A. Dounavis., R. Achar, and M. S. Nakhla, "DEPACT: delay extraction-macromodels of electrical interconnects," *IEEE Trans.on Adv. Packaging*, vol. 28, no. 1, pp. 13-23, February 2005.

[17] E. Gad, C. Chen, M. Nakhla, and R. Achar, "Passivity verification in delay-based macromodels of electrical interconnects," *IEEE Trans. on Circuit and Systems I*, vol. 52, no. 10, pp. 2173-2187, Oct. 2005.

[18] C. Chen, E. Gad, M. Nakhla, and R. Achar, "Passivity Verification in Delay-Based Macromodels of Multiconductor Electrical Interconnects," *IEEE Trans. on Adv. Packag.*, vol. 30, pp. 246-256, May 2007.

[19] A. Chinea and S. Grivet-Talocia, "A Passivity Enforcement Scheme for Delay-Based Transmission Line Macromodels," *IEEE Microwave and Wireless Components Letters*, vol. 17, pp. 562-564, Aug. 2007.

[20] B. Gustavsen and A. Semlyen, "Rational approximation of frequency domain responses by vector fitting," *IEEE Trans. Power Del.*, vol. 14, no. 3, pp. 1052–1061, July 1999.

[21] M.J. Manyahi and R. Thotappillil, "Transfer of lightning transients through distribution transformer circuits," in *Proc. Internat. Conf. Lightning Protection*, Cracow, Poland, 2002, pp. 435-440.

[22] A. Antonini, "Equivalent network synthesis for via holes discontinuities," *IEEE*

Trans. Adv. Packag., vol. 25, no. 4, pp. 528-536, Nov. 2002.

[23] A. Antonini, "SPICE equivalent circuits of frequency-domain responses," *IEEE Trans. Electromagn. Compatibilty*, vol. 45, no. 3, pp. 502-512, Aug. 2003.

[24] M. Abdel-Rahman, A. Semlyen, and M.R. Iravani, "Two-layer network equivalent for electromagnetic transients," *IEEE Trans. Power Del.*, vol. 18, no. 4, pp. 1328-1335, Oct. 2003.

[25] D. Saraswat, R. Achar, and M. Nakhla, "Passive macromodels of microwave subnetworks characterized by measured/simulated data," in *Proc. Int. Microwave Symposium, IEEE MTT-S*, vol. 2, Jun. 2003, pp. 999-1002.

[26] S. Grivet-Talocia, "Time-domain and frequency-domain macromodeling: application to package structures," in *Proc. IEEE Int. Symp. EMC*, Boston MA, 2003, pp. 570-574.

[27] B. Gustavsen, "Application of vector fitting to high frequency transformer modeling," in *Proc. International Conference on Power System Transients*, New Orleans, 2003, pp. 1-5.

[28] B. Gustavsen, "Wide band modeling of power transformers," *IEEE Trans. Power Del.*, vol. 19, no. 1, pp. 414-422, Jan. 2004.

[29] B. Gustavsen, "Frequency dependent modeling of power transformers with ungrounded windings," *IEEE Trans. Power Del.*, vol. 19, no. 3, pp. 1328-1334, Jul. 2004.

[30] J.M. Griffith and M. Toupikov, "Time-domain modeling from S-parameters: applicable to hard-disk drives," *IEEE Trans. Magnetics*, vol. 39, no. 6, pp. 3581-

3586, Nov. 2003.

[31] V.I. Okhmatovski and A.C. Cangellaris, "Evaluation of layered media Green's functions via rational function fitting," *IEEE Microwave Components Letters*, vol. 14, no. 1, pp. 22-24, Jan. 2004.

[32] Z. Zhang, X. Cui G. Liang, and M. Wu, "A high frequency transfer function model of potential transformers in GIS," in *Proc Symp. on Electromagnetic Compatibility*, May 2002, pp. 21-24.

[33] A. J. Gruodis and C. S. Chang, "Coupled lossy transmission line characterization and simulation," *IBM Journal of Research and Development*, vol. 25, pp. 25-41, January 1981.

[34] F. Y. Chang, "The generalized method of characteristics for wave-form relaxation analysis of coupled transmission lines," *IEEE Trans. Microwave Theory Tech.*, vol. 37, no. 12, pp. 2028-2038, December 1989.

[35] S. Lin and E.S. Kuh, "Transient simulation of lossy interconnects based on the recursive convolution formulation," *IEEE Trans. Circuits Systems I*, vol. 39, no. 11, pp. 879-892, November 1992.

[36] D.B. Kuznetsov and J.E. Schutt-Aine, "Optimal transient simulation of transmission lines," *IEEE Trans. Circuits Systems I*, vol. 43, pp. 110-121, February 1996.

[37] S. Grivet-Talocia, Hao-Ming Huang, A.E. Ruehli, F. Canavero, and I.M. Elfadel, "Transient analysis of lossy transmission lines: An efficient approach based on the method of characteristics," *IEEE Trans. Adv. Packag.*, vol. 27, no. 1, pp. 45 - 56 ,

February 2004.

[38] *HSPICE U-2003.09-RA*. Synopsys Inc., CA.

[39] M. S. Nakhla, "Analysis of pulse propagation on high-speed VLSI chips," *IEEE Journal of Solid-State Circuits*, vol. 25, pp. 490-494, April 1990.

[40] S. Lum, M. Nakhla, and and Q. Zhang, "Sensitivity analysis of lossy coupled transmission lines," *IEEE Trans. Microw. Theory Tech.*, vol. 39, no. 12, pp. 2089–2099, December 1991.

[41] J. F. Mao and E. S. Kuh, "Fast simulation and sensitivity analysis of lossy transmission lines by the method of characteristics," *IEEE Trans. Circuits Syst. I*, vol. 44, no. 5, pp. 391–401, May 1997.

[42] S. Lum, M. Nakhla, and and Q. Zhang, "Sensitivity analysis of lossy coupled transmission lines with nonlinear terminations," *IEEE Trans. Microw. Theory Tech.*, vol. 42, no. 4, pp. 607–615, April 1994.

[43] C. Jiao, A. C. Cangellaris, A. M.Yaghmour, and and J. L. Prince, "Sensitivity analysis of multiconductor transmission lines and Optimization for high speed interconnect circuit design," *IEEE Trans. Adv. Packag.*, vol. 23, no. 2, pp. 132–141, May 2000.

[44] A. Dounavis, R. Achar, and M. Nakhla, "Efficient sensitivity analysis of lossy multiconductor transmission lines with nonlinear terminations," *IEEE Trans. Microw. Theory Tech.*, vol. 49, no. 12, pp. 2292-2299, December 2001.

[45] N. Nakhla, A. Dounavis, M. Nakhla, and R. Achar, "Delay-extraction-based sensitivity analysis of multiconductor transmission lines with nonlinear

terminations," *IEEE Trans. Microw. Theory Tech.*, vol. 53, no. 11, pp. 3520-3530, November 2005.

[46] A. K. Agrawal, H. J. Price, and S. H. Gurbaxani, "Transient response of multiconductor transmission lines excited by a nonuniform electromagnetic field," *IEEE Trans. Electromagn. Compat.*, vol. EMC-22, no. 2, pp. 119–129, May 1980.

[47] Y. Kami and R. Sato, "Circuit-concept approach to externally excited transmission lines," *IEEE Trans. Electromagn. Compat.*, vol. EMC-27, no. 4, pp. 177–183, Nov. 1985.

[48] P. Bernardi, R. Cicchetti, and C. Pirone, "Transient response of a microstrip line circuit excited by an external electromagnetic source," *IEEE Trans. Electromagn. Compat.*, vol. 34, no. 2, pp. 100–108, May 1992.

[49] I. Wuyts and D. Zutter, "Circuit model for plane-wave incidence on multiconductor transmission lines," *IEEE Trans. Electromagn. Compat.*, vol. 36, no. 3, pp. 206–212, Aug. 1994.

[50] I. Maio and F. Canavero, "Analysis of crosstalk and field coupling to lossy MTLs in a SPICE environment," *IEEE Trans. Electromagn. Compat.*, vol. 38, no. 3, pp. 221–229, Aug. 1996.

[51] R. K. Das and W. T. Smith, "Incident field coupling analysis of multiconductor transmission lines using asymptoticwaveform evaluation," in *Proc. IEEE Int. Symp. Electromagnetic Compatibility*, Aug. 1996, pp. 265–270.

[52] I. Erdin, R. Khazaka, and and M. Nakhla, "Simulation of high-speed interconnects in a multilayered medium in the presence of incident field," *IEEE Trans.*

Microwave Theory Tech., vol. 46, no. 12, pp. 2251–2257, December 1998.

[53] I. Erdin, A. Dounavis, R. Achar, and and M. Nakhla, "A SPICE model for incident field coupling to lossy multiconductor transmission lines," *IEEE Trans. Electromagn. Compat.*, vol. 43, no. 4, pp. 485–494, November 2001.

[54] G. S. Shinh et al., "Fast transient analysis of incident field coupling to multiconductor transmission lines," *IEEE Trans. Electromagn. Compat.*, vol. 48, no. 1, pp. 57–73, February 2006.

[55] G.S. Shinh, R. Achar, N.M. Nakhla, M.S. Nakhla, and I. Erdin, "Simplified macromodel of MTLs with incident fields (SiMMIF)," *IEEE Trans. on Electromagnetic Compatibility*, vol. 50, no. 2, pp. 375 - 389, May 2008.

[56] W.T. Beyene and J.E. Schutt-Aine, "Efficient transient simulation of high-speed interconnects characterized by sampled data," *IEEE Transactions on Components, Packaging, and Manufacturing Technology*, vol. 21, no. 1, pp. 105 - 114 , Feb. 1998.

[57] S. Grivet-Talocia, "Package macromodeling via time-domain vector fitting," *IEEE Microwave and Wireless Components Letters*, vol. 13, no. 11, pp. 472-474, Nov. 2003.

[58] D. Saraswat, R. Achar, and M. Nakhla, "A Fast Algorithm and Practical Considerations for Passive Macromodeling of Measured/Simulated Data," *IEEE Trans. Adv. Packag.*, vol. 27, no. 1, pp. 57-70, Feb. 2004.

[59] D. loan, G. Ciuprina, M. Radulescu, and E. Seebacher, "Compact modeling and fast simulation of on-chip interconnect lines," *IEEE Trans. Magn.*, vol. 42, no. 4, pp.

547-550, April 2006.

[60] C.P. Coelho, J. Phillips, and L.M. Silveira, "A convex programming approach for generating guaranteed passive approximations to tabulated frequency-data," *IEEE Transactions on Computer-Aided Design of Integrated Circuits and Systems*, vol. 23, no. 2, pp. 293 - 301 , Feb. 2004.

[61] S. Grivet-Talocia, "Passivity enforcement via perturbation of Hamiltonian matrices," *IEEE Trans. Circuits Syst. I*, vol. 51, no. 9, pp. 1755–1769, Sep. 2004.

[62] B. Gustavsen, "Computer code for passivity enforcement of rational macromodels," in *Proc. IEEE Workshop on Signal Propagation on Interconnects*, 2005, pp. 115-118.

[63] D. Saraswat, R. Achar, and M.S. Nakhla, "Global passivity enforcement algorithm for macromodels of interconnect subnetworks characterized by tabulated data," *IEEE Transactions on Very Large Scale Integration (VLSI) Systems,* , vol. 13, no. 7, pp. 819 - 832, Jul. 2005.

[64] *HSPICE Signal Integrity User Guide*. Release U-2003.09-RA: Synopsys, Inc., Sep. 2003.

[65] S. Grivet-Talocia and M. Bandinu, "Improving the convergence of vector fitting for equivalent circuit extraction from noisy frequency responses," *IEEE Transactions on Electromagnetic Compatibility*, vol. 48, no. 1, pp. 104 - 120 , February 2006.

[66] F. Ferranti, Y. Rolain, L. Knockaert, and T. Dhaene, "Variance weighted vector fitting for noisy frequency responses," *IEEE Microwave and Wireless Components Letters*, vol. 20, no. 4, pp. 187-189, April 2010.

[67] B. Gustavsen, "Improving the pole relocating properties of vector fitting," *IEEE Trans. Power Del.*, vol. 21, no. 3, pp. 1587-1592, Jul. 2006.

[68] B. Gustavsen, "Relaxed Vector Fitting Algorithm for rational approximation of frequency domain responses," in *IEEE Workshop on Signal Propagation on Interconnects*, 2006, pp. 97 - 100.

[69] D. Deschrijver, B. Gustavsen, and T. Dhaene, "Advancements in iterative methods for rational approximation in the frequency domain," *IEEE Trans. Power Del.* , vol. 22, no. 3, pp. 1633 - 1642 , Jul. 2007.

[70] A. Dounavis and V. A. Pothiwala, "Passive closed from transmission line macromodel using method of characteristics," *IEEE Trans. Advanced Packag.*, vol. 31, pp. 190-202, Feb. 2008.

[71] V. A. Pothiwala and A. Dounavi, "Efficient passive transmission line macromodeling algorithm using method of characteristics," in *International Symposium on Circuits and Systems*, Island of Kos, May 2006, pp. 1780-1783.

[72] V. A. Pothiwala and A. Dounavis, "An Efficient Closed Form Macromodeling Algorithm using Method of Characteristics for Lossy Multiconductor Transmission Lines," in *Proceeding of IEEE Conf. on Electrical Performance of Electronic Packag. and Syst.*, Scottsdale, AZ, Oct. 2006, pp. 203-206.

[73] A. Dounavis, V. A. Pothiwala, and A. Beygi, "Passive macromodeling of lossy multiconductor transmission lines based on the method of characteristics," *IEEE Trans. Adv. Packag.*, vol. 32, pp. 184-198, Feb. 2009.

[74] E. S. Kuh and R. Rohrer, *Theory of Active Linear Networks*. San Francisco:

Holden-Day Inc., 1967.

[75] R. W. Newcomb, *Linear Multiport Synthesis*. New York: McGraw-Hill, 1966.

[76] D. A. Harville, *Matrix Algebra from a Statistician's Perspective*. New York: Springer, 1997.

[77] N. P. Van Der, H. G. Ter Morsche, and R. R. M. Mattheij, "Computation of eigenvalue and eigenvector derivatives for a general complex-valued eigensystem," *Electronic Journal of Linear Algebra*, vol. 16, pp. 300-314, October 2007.

[78] (2007) MATLAB Optimization Toolbox User Guide. MATLAB.

[79] B. Gustavsen and A. Semlyen, "Combined phase and modal domain calculation of transmission line transients based on vector fitting," *IEEE Trans. Power Del.*, vol. 13, no. 2, pp. 596-604, Apr. 1998.

[80] Er-Ping Li, En-Xiao Liu, Le-Wei Li, and Mook-Seng Leong, "A coupled efficient and systematic full-wave time-domain macromodeling and circuit simulation method for signal integrity analysis of high-speed interconnects," *IEEE Trans. Advanced Packaging*, vol. 27, no. 1, pp. 213-223, Feb. 2004.

[81] E.-X. Liu, E.-P Liu, and L.-W. Li, "Analysis of signal propagation on high-speed planar interconnect systems based on full-wave and macromodelling techniques," *Microwave and Optical Technology Letters*, vol. 39, no. 3, pp. 183-187, Nov. 2003.

[82] M.S. Sarto, A. Scarlatti, and C.L. Holloway, "On the use of fitting models for the time-domain analysis of problems with frequency-dependent parameters," in *Proc. IEEE Int. Symp. EMC*, 2001, pp. 588-593.

[83] K.M. Coperich, J. Morsey, V.I. Okhmatovski, A.C. Cangellaris, and S.E. Ruehli,

"Systematic development of transmission-line models for interconnects with frequency-dependent losses," *IEEE Trans. Microwave Theory Tech.*, vol. 49, no. 10, pp. 1677-1685, Oct. 2001.

[84] K.M. Coperich, J. Morsey, A.C. Cangellaris, and S.E. Ruehli, "Physically consistent transmission line models for high-speed interconnects in lossy dielectrics," *IEEE Trans. Adv. Packag.*, vol. 35, no. 2, pp. 129-135, May 2002.

[85] D. Deschrijver, B. Haegeman, and T. Dhaene, "Orthonormal Vector Fitting: A Robust macromodeling tool for rational approximation of frequency domain responses," *IEEE Trans. Adv. Packag.*, vol. 30, no. 2, pp. 216 - 225 , May 2007.

[86] B. Nouri, R. Achar, and M.S. Nakhla, "Z-Domain orthonormal basis functions for physical system identifications," *IEEE Trans. Adv. Packag.*, vol. 33, no. 1, pp. 293 - 307 , Feb. 2010.

[87] L. Ljung, *System Identification - Theory For the User*, 2nd ed. Upper Saddle River, N.J.: PTR Prentice Hall, 1999.

[88] T. Soderstrom and P. Stoica, *Instrumental Variable Methods for System Identification*. Berlin, Germany: Springer-Verlag, 1983.

[89] T. Soderstrom and P. Stoica., *System Identification*. London, U.K.: Prentice Hall International, 1989.

[90] P. Young, *Recursive Estimation and Time Series Analysis*. Berlin, Germany: Springer-Verlag, 1984.

[91] M. Aguet, M. Ianovici, and C. Lin, "Transient electromagnetic field coupling to long shielded cables," *IEEE Trans. Electromagn. Compat.*, vol. EMC-22, no. 4, pp.

276–282, Nov. 1980.

[92] A. Orlandi, "Circuit model for bulk current injection test on shielded coaxial cables," *IEEE Trans. Electromag. Compat.*, vol. 45, no. 4, pp. 602–615, Nov. 2003.

[93] S. Caniggia and F. Maradei, "Spice-like models for the analysis of the conducted and radiated immunity of shielded cables," *IEEE Trans. Electromag. Compat.*, vol. 46, no. 4, pp. 606–616, Nov. 2004.

[94] G. Antonini and G. Ferri, "A new approach for closed-form transient analysis ofmulticonductor transmission lines," *IEEE Trans. Electromagn. Compat.*, vol. 46, no. 4, pp. 529–543, Nov. 2004.

[95] G. Antonini and A. Orlandi, "Efficient transient analysis of long lossy shielded cables," *IEEE Trans. Electromagn. Compat.*, vol. 48, no. 1, pp. 42–56, Feb. 2006.

[96] N. M. Nakhla, A.E. Ruehli, R. Achar, and M. S. Nakhla, "Simulation of coupled interconnects using waveform relaxation and transverse partitioning," *IEEE Trans. Adv. Packag.*, vol. 29, no. 1, pp. 78-87, Feb. 2006.

[97] N. Nakhla, A. E. Ruehli, M. S. Nakhla, R. Achar, and C. Chen, "Waveform relaxation techniques for simulation of coupled interconnects with frequency-dependent parameters," *IEEE Trans. Adv. Packag.*, vol. 30, no. 2, pp. 257-269, May 2007.

[98] D. Paul, N. M. Nakhla, R. AChar, and M. S. Nakhla, "Parallel simulation of massively coupled interconnect networks," *IEEE Trans. Adv. Packag.*, vol. 33, no. 1, pp. 115-127, Feb. 2010.

[99] Y.-Z. Xie, F. G. Canavero, T. Maestri, and Z.-J. Wang, "Crosstalk analysis of

multiconductor transmission lines based on distributed analytical representation and iterative technique," *IEEE Trans. Electromag. Compatibility*, vol. 52, no. 3, pp. 712-727, Aug 2010.

[100] R. Achar et al., "Parallel and scalable transient simulator for power grids via waveform relaxation (PTS-PWR)," *IEEE Trans. VLSI Systs.*, vol. 19, no. 2, pp. 319-332, Feb. 2011.

Appendices

Appendix A: Formulation of Excited Transmission Lines

The modeling of transmission lines with incident field coupling can be formulated as [1]

$$\frac{\partial}{\partial z}\mathbf{V}(z,s)+\left(\mathbf{R}(s)+s\mathbf{L}(s)\right)\mathbf{I}(z,s)=\mathbf{V}_F(z,s)$$

$$\frac{\partial}{\partial z}\mathbf{I}(z,s)+\left(\mathbf{G}(s)+s\mathbf{C}(s)\right)\mathbf{V}(z,s)=\mathbf{I}_{\mathrm{F}}(z,s) \tag{A.1}$$

where s is Laplace transform variable; z is the position variable; $\mathbf{V}(z,s)$ and $\mathbf{I}(z,s)$ represent the voltages and currents of the transmission line; $\mathbf{R}(s)$, $\mathbf{L}(s)$, $\mathbf{G}(s)$ and $\mathbf{C}(s)$ are p.u.l. resistance, inductance, conductance and capacitance parameters, respectively; $\mathbf{V}_F(z,s)$ and $\mathbf{I}_F(z,s)$ are the distributed forcing functions due to the incident field and can be expressed as

$$\mathbf{V}_F(z,s)=-\frac{\partial}{\partial z}\mathbf{E}_T(z,s)+\mathbf{E}_L(z,s)$$

$$\mathbf{I}_F(z,s)=-\left(\mathbf{G}(s)+s\mathbf{C}(s)\right)\mathbf{E}_{\mathrm{T}}(z,s) \tag{A.2}$$

where

$$\mathbf{E}_L(z,s)=\left(\varepsilon_z(x_i,y_i,z)-\varepsilon_z(x_0,y_0,z)\right)$$

$$\mathbf{E}_T(z,s)=\int_{\rho(x,y)}\vec{\varepsilon}_t(\rho,z)\cdot d\vec{l} \tag{A.3}$$

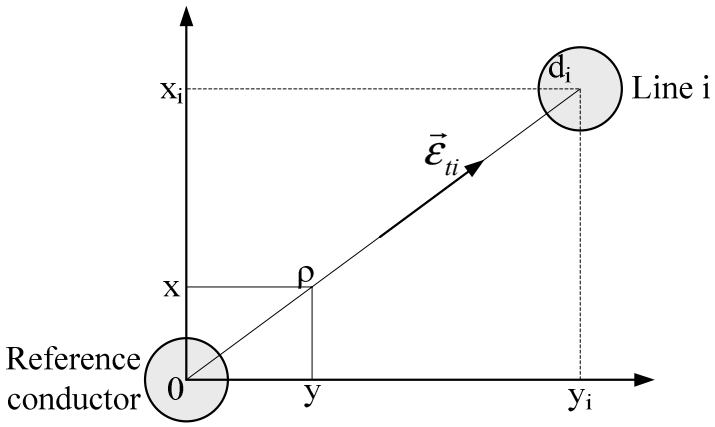

Figure A-1: Derivation of the contributions to the equivalent sources due to the transverse component of incident electric field for a multiconductor transmission line.

and ε_z and ε_t are longitudinal and transverse components of the incident electric field; (x_i, y_i) and (x_0, y_0) refer to the coordinates of the signal corresponding to the ith conductor; ρ is a parameter of x and y in the transverse plane (Figure A-1).

For the case when incident electric field is a uniform plane wave

$$\vec{E}^i(x,y,z) = E_0(s)(A_x\vec{a}_x + A_y\vec{a}_y + A_z\vec{a}_z)e^{-s\beta_x x}e^{-s\beta_y y}e^{-s\beta_z z} \tag{A.4}$$

where $E_0(s)$ is the amplitude; A_x, A_y, and A_z are the direction cosines of the incoming wave; $\beta = [\beta_x\ \beta_y\ \beta_z]^T$ is the propagation vector. If the reference conductor is placed at the origin of the coordinate system, x=0, y=0, the transverse and longitudinal contributions of the incident electric field (A.3) for the case when there is no ground plane can be written as

$$E_{Li}(z,s) = E_0(s) A_z e^{-s\beta_z z}(e^{-s(\beta_x x_i + \beta_y y_i)} - 1) = E_0(s) A_z e^{-s\beta_z z}(e^{-s\psi_i^+} - 1) \tag{A.5}$$

$$E_{Ti}(z,s) = E_0(s) \int_0^{d_i} (A_x \frac{x_i}{d_i} + A_y \frac{y_i}{d_i}) e^{-s\beta_z z} e^{-s(\beta_x \frac{x_i}{d_i} + \beta_y \frac{y_i}{d_i})\rho} d\rho$$

$$= E_0(s)(A_x x_i + A_y y_i) e^{-s\beta_z z} \frac{e^{-s(\beta_x x_i + \beta_y y_i)} - 1}{-s(\beta_x x_i + \beta_y y_i)} = -E_0 \Phi_i^+ e^{-s\beta_z z} \frac{e^{-s\psi_i^+} - 1}{s\psi_i^+} \tag{A.6}$$

where $d\vec{l} = (\vec{a}_x \frac{x_i}{d_i} + \vec{a}_y \frac{y_i}{d_i}) d\rho$, $x = \frac{x_i}{d_i}\rho$, $y = \frac{y_i}{d_i}\rho$, $d_i = \sqrt{x_i^2 + y_i^2}$, $\rho = \sqrt{x^2 + y^2}$ as shown in Figure A-1 and

$$\Phi_i^{\pm} = A_x x_i \pm A_y y_i; \quad \psi_i^{\pm} = \beta_x x_i \pm \beta_y y_i . \tag{A.7}$$

Subsequently, the distributed forcing functions $\mathbf{V}_F(z,s)$ and $\mathbf{I}_F(z,s)$ can be expressed as

$$\mathbf{V}_F(z,s) = E_0(s) \begin{bmatrix} \vdots \\ -s\beta_z \Phi_i^+ \frac{e^{-s\psi_i^+} - 1}{s\psi_i^+} + A_z(e^{-s\psi_i^+} - 1) \\ \vdots \end{bmatrix} e^{-s\beta_z z} \tag{A.8}$$

$$\mathbf{I}_F(z,s) = \big(\mathbf{G}(s) + s\mathbf{C}(s)\big) E_0(s) \begin{bmatrix} \vdots \\ \Phi_i^+ \frac{e^{-s\psi_i^+} - 1}{s\psi_i^+} \\ \vdots \end{bmatrix} e^{-s\beta_z z} \tag{A.9}$$

For the case when the transmission line has a plane ground located on y-z plane, the ground plane can be replaced with the image of the incident source as

$$\vec{E}^{ref}(x,y,z) = E_0(s)(A_x\vec{a}_x - A_y\vec{a}_y - A_z\vec{a}_z)e^{s\beta_x x}e^{-s\beta_y y}e^{-s\beta_z z}. \tag{A.10}$$

Therefore, the equations (A.5)-(A.9) can be substituted by (A.11)-(A.13) for the case when there is a ground plane, which results from the incident electric field $\vec{E}^{i}$ and the image of the incident electric field $\vec{E}^{ref}$.

$$\begin{aligned} E_{Li}(z,s) &= E_0(s)A_z e^{-s\beta_z z}(e^{-s(\beta_x x_i+\beta_y y_i)} - e^{-s(-\beta_x x_i+\beta_y y_i)}) \\ &= E_0(s)A_z e^{-s\beta_z z}(e^{-s\psi_i^+} - e^{-s\psi_i^-}) \end{aligned} \tag{A.11}$$

$$\begin{aligned} E_{Ti}(z,s) &= E_0(s)e^{-s\beta_z z}\int_0^{d_i}\left((A_x\frac{x_i}{d_i} + A_y\frac{y_i}{d_i})e^{-s(\beta_x\frac{x_i}{d_i}+\beta_y\frac{y_i}{d_i})\rho} + (A_x\frac{x_i}{d_i} - A_y\frac{y_i}{d_i})e^{-s(-\beta_x\frac{x_i}{d_i}+\beta_y\frac{y_i}{d_i})\rho}\right)d\rho \\ &= E_0(s)e^{-s\beta_z z}\left((A_x x_i + A_y y_i)\frac{e^{-s(\beta_x x_i+\beta_y y_i)}-1}{-s(\beta_x x_i+\beta_y y_i)} + (A_x x_i - A_y y_i)\frac{e^{-s(-\beta_x x_i+\beta_y y_i)}-1}{-s(-\beta_x x_i+\beta_y y_i)}\right) \\ &= -E_0 e^{-s\beta_z z}\left(\Phi_i^+\frac{e^{-s\psi_i^+}-1}{s\psi_i^+} - \Phi_i^-\frac{e^{-s\psi_i^-}-1}{s\psi_i^-}\right) \end{aligned} \tag{A.12}$$

$$\mathbf{V}_F(z,s) = E_0(s)\begin{bmatrix} \vdots \\ -\beta_z(\Phi_i^+\frac{e^{-s\psi_i^+}-1}{\psi_i^+} - \Phi_i^-\frac{e^{-s\psi_i^-}-1}{\psi_i^-}) + A_z(e^{-s\psi_i^+} - e^{-s\psi_i^-}) \\ \vdots \end{bmatrix} e^{-s\beta_z z} \tag{A.12}$$

$$\begin{aligned} \mathbf{I}_F(z,s) &= \big(\mathbf{G}(s) + s\mathbf{C}(s)\big)E_0(s)\begin{bmatrix} \vdots \\ \Phi_i^+\frac{e^{-s\psi_i^+}-1}{s\psi_i^+} - \Phi_i^-\frac{e^{-s\psi_i^-}-1}{s\psi_i^-} \\ \vdots \end{bmatrix} e^{-s\beta_z z} \\ &= \left(\frac{\mathbf{G}(s)}{s} + \mathbf{C}(s)\right)E_0(s)\begin{bmatrix} \vdots \\ \Phi_i^+\frac{e^{-s\psi_i^+}-1}{\psi_i^+} - \Phi_i^-\frac{e^{-s\psi_i^-}-1}{\psi_i^-} \\ \vdots \end{bmatrix} e^{-s\beta_z z} \end{aligned} \tag{A.13}$$

Equations (A.8)-(A.9) and (A.11)-(A.12) are used in Chapter 5 to model the effects of incident electromagnetic field on transmission lines.

Curriculum Vitae

Name: Amir Beygi

Post-secondary Education and Degrees:

K.N. Toosi University of Technology
Tehran, Iran
2000-2004 B.Sc.

Iran University of Science and Technology
Tehran, Iran
2004-2007 M.Sc.

The University of Western Ontario
London, Ontario, Canada
2007-2011 Ph.D.

Related Work Experience

Research Assistant
The University of Western Ontario
2007-2011

Teaching Assistant
The University of Western Ontario
2007-2011

Selected Publications:

A. Beygi, A. Dounavis, "Sensitivity analysis of lossy multiconductor transmission lines based on the passive method of characteristics macromodel," *IEEE Transactions on Computer-Aided Design of Integrated Circuits and Systems*, vol. 29, issue 8, Aug. 2010.

A. Dounavis, V. A. Pothiwala, A. Beygi, "Passive macromodeling of lossy multiconductor transmission lines based on the method of characteristics," *IEEE Transactions on Advanced Packaging* , vol. 32, issue 1, Feb. 2009.

A. Beygi, A. Dounavis, "Analysis of excited transmission lines based on the passive method of characteristics macromodel," *IEEE International Microwave Symposium*, Jun. 2011.

A. Beygi, A. Dounavis, "Sensitivity analysis of lossy transmission lines based on the passive method of characteristics," *IEEE Conference on Electrical Performance of Electronic Packaging and Systems*, Oct. 2010.